THE LIQUEFACTION BEHAVIOR OF SANDS SUBJECTED TO CYCLIC LOADING

by

KARL ROCKER, JR.
B.S., Northeastern University
(1966)

Submitted in partial fulfillment
of the requirements for the degree of

Master of Science

at the
Massachusetts Institute of Technology
(June 1968)

Signature of Author..
Department of Civil Engineering, May 23, 1968

Certified by.....
Thesis Supervisor

Accepted by.....
Chairman, Departmental Committee on Graduate Students

ABSTRACT

THE LIQUEFACTION BEHAVIOR OF SANDS
SUBJECTED TO CYCLIC LOADING

by

Karl Rocker, Jr.

Submitted to the Department of Civil Engineering
on May 23, 1968 in partial fulfillment of the requirements
for the degree of Master of Science in Civil Engineering.

This thesis examines the liquefaction behavior of two medium to fine sands subjected to cyclic reversing deviator stresses in the isotropically consolidated triaxial state. Sand samples were tested over a range of deviator stress and density, and at two effective confining stress levels. Changes in pore pressure, axial strain, and axial stress were precisely measured by electrical recorders.

Equipment for this experimental study was constructed or adapted and proved satisfactory for these liquefaction tests. This equipment included: a modified triaxial cell; a load cell attached above the sample top cap; a pore pressure transducer; a linearsyn differential transducer (strain measurements); an air-pressure operated stress applicator; a cyclic air-pressure application system; and the necessary recording instrumentation.

These tests concluded: a) that there were significant differences in the liquefaction behavior of the two sands tested; b) there are characteristic patterns of effective stress, pore pressure, and strain behavior that may be identified; c) pre-cycling or a small percentage of air-filled voids significantly increased deviator stress required to cause liquefaction; d) the two tested sands required considerably lower deviator stress to cause failure at the same number of cycles as did previous tests on similar sands under slightly different test conditions.

Thesis Supervisor: Robert V. Whitman

Title: Professor of Civil Engineering

ACKNOWLEDGEMENT

The author wishes to acknowledge his gratitude for the assistance of the following persons and organizations:

Professor Robert V. Whitman, who provided guidance and constructive criticism as thesis advisor of the author, and at whose suggestion this area of research was studied.

Ford Foundation, for sponsorship of the M.I.T. Inter-American Program in Civil Engineering.

Professor Anwar Wissa, for numerous suggestions and guidance on equipment design and laboratory testing.

The Soil Mechanics staff, especially Mr. Carl Stahl and Mr. David Driscoll, who provided considerable aid in equipment problems.

TABLE OF CONTENTS

LIST OF FIGURES

Figures in Appendix

CHAPTER I

INTRODUCTION

A. Inter American Program

This thesis is the third in a series of papers under sponsorship of the M.I.T. Inter American Program investigating densification of sands by vibrations.

The first paper, Repeated Load and Vibration Tests Upon Sand, Progress Report No. 1 was published as M.I.T. Soils Publication No. 203 in August, 1967. This covered initial procurement of equipment and reported on first tests with dry, uniform, rounded sand. Key aspects of soil behavior were noted for further investigation.

The second paper, a thesis by Mr. Pedro Ortigosa De Pablo entitled Densification of Sand by Vertical Vibrations with Almost Constant Stresses, was published in February, 1968. Conclusions from test results were: 1) no significant sand densification occurs in vibration tests for acceleration levels below 1.0 g; 2) there is a minimum acceleration at which sand densification is initiated and this is a function function of amount and nature of confining stress and initial relative density; 3) a terminal void ratio, dependent on confining stress, is achieved at accelerations greater than a critical value.

B. Sand Densification

Several aspects of sand densification from dynamic loadings have now been outlined. This loading can occur from a number of sources under

field conditions. Figure 1* illustrates the three most important cases of dynamically induced stress changes.

Vibration of heavy machinery foundations from eccentricity of moving parts causes rapid cycling at low stress levels. Acceleration levels are usually low in these cases, confining stresses are high, and the number of cycles will be extremely large.

Vibratory compaction induces stress levels varying from a few g's near the surface to almost insignificant levels more then several feet below. Confining stress and the number of cyclic applications are relatively small.

Figure 1.c illustrates shearing stresses in a horizontal soil mass during an earthquake. Acceleration levels of 0.3 g are not uncommon in major earthquakes, although the vast majority of quakes are much lower. Confining stress will vary from zero pressure at the surface to a high level produced by overburden at several hundred feet beneath the surface. Densification of sands during this phenomena can readily occur, but is not often measured. It is difficult to observe minor changes in ground surface unless a building is located directly above the area.

Each of these three cases involve densification. The last example of dynamic loading, however, can produce catastrophic results not directly attributable to a density change problem. This occurs through soil liquefaction.

C. Soil Liquefaction and Earthquakes

A soil liquefies when forces normally supported by the structural soil

---

* Figure 1 is a reproduction of Figure 1 from Ortigosa De Pablo Thesis, 1968.

skeleton are transfered to its pore water. Pore pressure builds up until the structure no longer takes any load, and behaves somewhat like a viscous liquid. Two major requirements for this to occur are saturation of the soil and an undrained state in the zone being liquefied. Although liquefaction does not theoretically require water in the soil pores, the high compressability of air-filled pores prevents major pressure buildup. If drainage occurs, this pressure buildup will also be lessened and liquefaction is not likely to take place.

Soil liquefaction can occur after a large number of cycles or from the application of a single load. Point bar stream deposits and loess, both at unstably low density, can liquefy after a shock of relatively low stress magnitude is applied. Other sands existing at low relative densities tend to decrease (Lee and Seed, "Drained ...", ASCE SM6, 1967) in void ratio when loaded. Sands at higher density will not liquefy as easily at the same stress conditions.

Earthquake induced stresses themselves are extremely hard to analyze. Forces producing earthquakes as well as behavior of the massive soil-rock medium are simply not known well enough to predict and backfigure stresses. Few measurements are recorded in areas of interest during earthquakes. When an earthquake area is well instrumented, and the instrumentation functions, record traces reveal a seemingly random velocity or acceleration pattern. Behavior is then oversimplified to a large degree if any analysis is made of the data. This only means that earthquake response in one area is never exactly similar to response in another area, nor is one earthquake like another.

The general characteristics of soil mass behavior, as recorded, are as follows:

1. Largest accelerations and velocities measured occur during the first few seconds of an earthquake.
2. Minor accelerations and velocities are generated for up to several minutes following initial motion.
3. Frequency of motion is in the order of 1/2 or 1 cycles per second.
4. Motion occurs in all three directions of a grid system.

Stresses induced by an earthquake cannot be realistically identified but must instead be defined over a range of what was probably produced. It is for this reason that direct correlation of laboratory testing to earthquake behavior is not too far advanced an art.

Liquefaction may contribute to failure in a soil mass without total liquefying of the mass itself. The initial state of stress in an embankment or sloping soil profile can exist near failure conditions. A large mass of this soil may slide along a liquefied thin seam or strata of cohesionless soil. This liquefaction may be initiated by a blast-induced shock as well as by an earthquake.

In order to determine liquefaction potential in a given problem, behavior of soils under cyclic loading must be analyzed and understood.

D. Scope of the Thesis

This thesis presents the results of a study into reversing cyclic loading tests on cohesionless soils in the isotropic triaxial state of stress. Figure 2 shows applied principal stresses and induced shear stress during testing. Deformation before and after liquefaction are also presented in Figure 2. It is the purpose of the author to accomplish the following:

1. determine the behavior of sands during liquefaction in a triaxial stress condition with respect to pore pressure buildup, axial strain, and state of stress during testing.
2. determine the liquefaction potential of two cohesionless soils tested; specifically to relate deviator stress, number of cycles, relative density, and confining stress to liquefaction behavior in each sand; then to compare the sands to one another in view of different composition and grain characteristics.

CHAPTER II

EQUIPMENT

Required equipment for reversing cyclic loading tests on saturated sands can be categorized into three groups.

1. Loading equipment; stress application device, cyclic pressure control, and pressure source
2. Testing equipment; triaxial cell and connections
3. Measuring equipment; stress, strain, and pore pressure measurement devices, power source and recording instrumentation.

This equipment was collected and assembled to provide the system shown in Figure A.1 and detailed completely in Appendix A. Each piece was either purchased outright, constructed from scratch, or modified from existing equipment. Availability, cost and time decided which method was used.

Requirements for the stress application device included ability for rapid cycling, upward and downward force application, adaptability to triaxial cells, and low friction or "frictionless" movement for several inches of piston travel. An experimental applicator designed by Dr. Anwar Wissa of M.I.T. and built for Geomeasurements, Inc. of Cambridge, Massachusetts was both suitable and readily available. A few minor modifications to the triaxial cell adaption members and to piston connections were made before it could be used. Performance of this device was satisfactory overall, with some problem in piston alignment and resulting friction from binding. The extraordinary care required during assembly is reflected by occasional poor matching of extension and compression

stresses in the preliminary test series (SCS-RU1 to RU11).

Air pressure in two chambers or "pots" controled force applied to a sample. Cycling speeds are theoretically limited only by air flow characteristics. Response at 1 cps, the fastet cycling speed used, indicates a nearly square "wave" of load application. This is measured indirectly and shown by strain measurements amplified in Figure 3.c. (Force measurement is not a good indicator because of slower response in the X-Y recorder used.)

The stress control device is a series of tubing connections for two pressure tanks, two pressure sources, and a solenoid. An electrical timing divice and cycle counter complete the equipment necessary for operation of the stress applicator. Rapid solenoid response to electrical impulse causes cycling limitations again to be measured in terms of air flow. Varying tubing length and diameter can change the wave form of an air pulse from a square to quasi-sinusoidal shape. Only square waves were used in these tests. The two electrical timers used have cycling ranges of 1 to 6 cps and 5 cph to 5 cpm. This system is a modification of the "stress box" used in earlier Inter American Program investigations by the M.I.T. soils laboratory (1966-1967).

A Norwegian (Genor) triaxial cell was used as the pressure chamber for these tests. Adaptations were made for height increase, pore pressure transducer and load cell connections, and for lubrication of the triaxial bushing. Sample specimens 2 inches in diameter by approximately 3.5 inches in height were tested. Each sample was prepared with porous stones at both ends to prevent pumping of soil into the pore pressure lines during testing. Poor pressures and volume measurments were controled by a mercury pot and burette system.

Measuring equipment for pore pressure, strain, and axial stress was required to be electical because of the dynamic testing. Pore pressure was measured by a pressure transducer connected rigidly to the triaxial base plate. Axial strain was recorded by an L.D.T. (Linearsyn Differential Transformer) connected to the triaxial piston and outside frame. Axial stress was measured by a load cell inside the triaxial cell connected directly to the sample top cap. Response time and accuracy in all three instruments were well within tolerable limits.

Output from each was monitored by amplifier-recorders. Pore pressure and strain were traced on a Sanborn 321 dual channel recorder. Amplified records from each instrument are shown in Figure 3.b and 3.c. Response and accuracy at this recorder is also well within tolerable limits. It is considered an excellent piece of equipment for this testing. Load cell output was traced on a vintage X-Y recorder. A typical amplified record is shown in Figure 3.a. The response time of this recorder was slow, and caused some distortion of the load-time record when testing at 1 cps. A calibration over the load cell output range was made prior to each test to eliminate a long-term scale factor drift. This instrument, while less than totally satisfactory, was used because it was available.

Power was supplied to the pressure transducer and L.D.T through an internal source in the Sanborn recorder. 4.5 to 5.0 volts D.C. were used. The load cell was excited by voltages of 6, 20 and 24 volts D.C. depending on what power supply was available, and on amplification limits of the X-Y recorder.

CHAPTER III

SOILS

A. Choice of Soils

Two cohesionless sands were tested in the program. This choice of soil was guided by several factors. Among these are; 1) similarity to soils which have been known to liquify, 2) similarity to soils which have undergone previous liquefaction studies, 3) concern with liquefaction potential of a well graded sand compared to a uniform sand, 4) similar concern with liquefaction porential of angular sands compared to rounded sands, and 5) availability in uniform quantities.

B. Description of Sands

For these reasons a sub-rounded uniform quartz sand (Wing-Beach sand) and an angular to sub-angular well graded quartz sand (Modified A3 sand) were chosen. Gradation curves and miscrospic photographs of these sands are shown in Figure 4 and Figure 5 respectively.

The Wing-Beach sand was the most tested and was used in a prelininary test series (tests SCS-RU1 to SCS-RU11) to check equipment performance. This sand was obtained from a dune deposit along the north-central Massachusetts shoreline at Wingaershiek Beach. Before testing, the sand was washed to remove salts and traces of organic materials. The sand that was tested has D_{50} = 0.2mm, C_u = 1.3 and a measured S.G. = 2.65. Less than 0.1 percent of the material passed the #200 U.S. Standard Sieve (screen opening $\simeq$ 0.075 mm).

The Modified A3 sand is an artificial gradation of crushed quartz aggregate obtained from the Ottawa Silica Company in Mystic, Connecticut. The gradation was "designed" to produce a moderately well graded sand with an average size partical similar to that of the Wing-Beach sand. The composition is as follows:

22.7% .... SAND #45
22.7% .... SAND #65
22.7% .... SAND #100
22.7% .... SAND #160
9.2% .... SAND #20

This sand has D_{50} = 0.21mm, C_u = 3.1 and S.G. = 2.65. Approximately 5 percent of the material was finer than the #200 U.S. Standard Sieve. A good comparison of the two sands is possible through representative photographs (Figure 5) of two tested samples after oven drying. The photographs clearly show differences in angularity, gradation and uniformity.

C. Strength Characteristics

Several tests were run on these two sands for determination of significant strength properties. Results of four stress-controled drained triaxial compression tests are shown in Figure 6 and Figure 7. These tests were run in the saturated state at a confining pressure of 14.2 psi. The same equipment was used in shear and cyclic load tests to minimize differences in testing conditions.

Two differences in shear behavior of these sands are noticeable. The Wing-Beach sand exhibits considerably larger initial stress-strain moduli than does the Modified A3 sand. Dilation tendencies are greater and control volume changes earlier in the Wing-Beach sand. Further testing of

a sand nearly identical to Modified A3 has confirmed this behavior and the computed friction angles. (This data is as yet unpublished. Other testing on this sand currently underway at M.I.T. includes direct shear, high pressure triaxial undrained, plain strain and constant volume direct shear tests.) The use of strength and pore pressure data from the presented tests in direct comparison with rapid undrained cyclic loading tests is limited. It has been shown (Healy, Doctoral Thesis, 1963) that strain rate differences alone can significantly alter these results.

D. Relative Density

Maximum and minimum relative densities for the two sands tested were determined in the following manner. Minimum densities for both sands were obtained by loosely pouring each sand into a mold of known volume. The sand was placed into a funnel held close to the surface as it was brought up. This method was found to be accurately repeatable as witnessed by a maximum difference in unit weight of 0.6 PCF in four tests on Modified A3 sand.

Maximum unit weight was determined by compacting the sands in several ways, with an "extraneous" vibration mode producing highest densities in both sands. This highly non-repeatable method consisted of horizontal and vertical excitation of a sand filled Harvard Miniature Mold by a mechanical vibration tool. Modified and standard AASHO tests, accelerations from 1.0 to 2.5 g's on a shaking table, and other methods were tried on the Wind-Beach sand in an effort to achieve a higher density.

Relative density is the most frequently referred to density parameter in this report. In contrast to void ratio and unit weight it is not a completely definable term. While void ratio and unit weight may be calculated in terms of measureable values, relative density depends on what method is used for determining the range of possible density. The "maximum" and "minimum" values are, then, only maximum and minimum for a particular method of their determination. Once these densities are determined, relative density has a specific one to one correspondance with void ratio and unit weight. The advantage of using relative density is in comparison of one sand with another. Void ratio and unit weight may well lose significance as a basis of comparison, but relative density relates sands in degree of possible compaction.

It is important to note that values of void ratio and relative density reported in this thesis refer to the condition just prior to application of reversing deviaitor stress - after consolidation under all-round effective stress.

CHAPTER IV

TEST RESULTS

A. Preliminary Testing Program

A total of forty-one liquefaction tests were run in five basic series. Each sample measured 2 inches in diameter by approximately 3.5 inches high with little variation from one sample to another. The first eleven tests were run to check out equipment and to determine ambient conditions for future tests. Wing-Beach sand was used and compacted at 80 to 86 of relative density. A confining pressure of 54.2 psi and backpressure of 40.0 psi were applied to produce the initial test effective stress of 14.2 psi, or one kilogram per square centimeter. The first four tests were cycled at .13 cps and the remaining seven at 1 cps.

In each test, and in all subsequent tests run, the samples were isotropically consolidated to the initial state of stress. A check of saturation was made at this stage by increasing confining stress by 10.0 psi. No drainage was allowed and the pore pressure response to this increase noted. The resulting increase in pore pressure for a saturated sample should be close to 10.0 psi, depending on compressability of the soil skelleton. Measured response varied from consistantly near 100 percent (10.0 psi increase) in dense sands to between 88 and 95 percent on most looser samples. A response above 88 percent was arbitrarily considered to indicate complete saturation. Several tests responded at this level, with little increase after attempts at further saturation.

Cyclic stressing began after initial undrained stress-controled loading to the first (compressive) cycle. This step enables stress-strain

data to be collected and allowed uniformity comparison of "like" samples. Data from this comparison is plotted in Figure B-5 and B-6. Cycling was begun and continued, in most cases, until liquefaction and necking of the sample had occured. Pore pressure of the undrained samples built up to within 7 or 8 percent of cell pressure. Drainage of this excess pore pressure was allowed, to return the sample to its initial backpressure. Decrease in sample volume was measured.

The preliminary testing program led to the following conclusions:

1. Triaxial and measuring equipment performed very well during cyclic testing.
2. The stress applicator performed satisfactorily although extreme care would be necessary to accurately produce an equal and opposite deviator stress. Friction from piston binding was the major problem.
3. A larger confining stress of 28.4 psi should be used in subsequent testing. This allows better definition in stress application from current pressure gages with 0.1 psi accuracy.
4. A cycling speed of 1 cps should be used. This strikes an "experimental" medium of being fast enough to prevent long duration tests and slow enough to allow measurement. (This loading is also more within the range of cyclic stress application during an earthquake.)
5. The test proceedure, with a few minor changes, should be followed for all subsequent tests.

The last 30 tests can be divided into four main groups or series. Two series were run on Wing-Beach and Modified A3 sand samples. In each of the sands two relative density ranges (about 20 percent apart) in the

medium to dense category were tested. The same range of investigation was aimed for in both sands, but difficulty in being able to repeat test density exactly caused some difference. Several of these last 30 tests were either not saturated, not liquefied, or not within the average density shown, and are considered separately.

B. Tests on Denser Wing-Beach Sand

The first of these test series was run on Wing-Beach sand with an average relative density of 76%. Eight tests (SCS-RU12 through RU19) are included in the average covering a range of initial liquefaction from 6 to 7,247 cycles. Test RU16 was cycled to 16,800 repetitions with no liquefaction. Stress, stress path, and strain are summarized in Figures 8, 11 and 17 respectively. In addition, deviation stress to cause initial liquefaction and to cause 5 and 10 percent double amplitude strain is shown vs. number of cycles in Figure 21. A complete set of pore pressure data for these tests and for tests which did not liquify is presented in Figure 24.

This test series is the second largest to the preliminary program. In general the samples were consistantly prepared, varying between 73 to 81 percent relative density.

C. Tests on Denser Modified A3 Sand

The denser Modified A3 series had an average relative density of 83 percent with samples prepared from 79 to 86 percent. Six tests (SCS-RU21 through RU32) are included in this average covering a range of initial liquefaction from 8 to 324 cycles. Stress, stress path and strain are summarized in Figures 9, 13, and 19 respectively. Deviator stress to

cause initial liquefaction and to cause 5 and 10 percent strain is shown vs. number of cycles in Figure 22.

D. Tests on Looser Modified A3 Sand

The looser Modified A3 series had an average relative density of 65 percent. Five tests (SCS-RU26 through RU30) are included in this average covering a range of initial liquefaction from 3 to 297 cycles. Test RU31 liquefied at 934 cycles, but has RD = 55 percent and is used only as a lower limit in several figures. Other relative densities ranged from 60 to 71 percent. Test RU27 had a pore pressure response of 77 percent, somewhat below the assumed range for complete saturation. Stress, stress path and strain are summarized in Figures 9, 12, and 18 respectively. In addition, strain during several phases of liquefaction is shown on a $\bar{p}$ - q plot in Figure 15. On this figure double amplitude strain at initial, 5, 10, and 20 percent are contoured from stress paths on Figure 12.

E. Tests on Looser Wing-Beach Sand

The looser Wing-Beach series had an average relative density of 57 percent with samples prepared from 52 to 60 percent. Six tests (SCS-RU33 and RU35 through RU39) are included in this average. Initial Liquefaction began from 0 to 3,724 cycles. Test RU35 was cycled to 26,500 repetitions before liquefaction occurred, the largest number in this testing program. Stress, stress path and strain are summerized in Figures 8, 10, and 16. Contours of double amplitude strain at initial, 5, 10 and 20 percent are plotted on a $\bar{p}$ - q diagram in Figure 14.

F. Other Tests

Effects of saturation were studied with several tests (SCS-RU18, 20, 27, 40, and 41) being run on partially saturated samples. Data from these tests is presented in Figures 31, 32 and 33. Several tests were run at pore pressure responses less than 80 percent, but were not intended to investigate saturation.

The effect of pre-cycling Wing-Beach sand at a low stress level which will not induce initial liquefaction was observed in two tests (SCS-RU17 and RU40). Data from test RU17 and a related test (RU12) are presented in Figures 34 and 35.

G. Presentation of Data

Figures presented in the main body of this thesis are primarily summary plots. Several individual tests are shown to examine saturation and pre-cycling effects. Individual presentation of tests is made in Appendix D with plots of pore pressure and strain versus number of cycles for thirteen tests. Plotted tests are from the four major test series and cover the range of cycling to cause initial liquefaction in each series.

Data shown through figures in the main body is arranged in the following order:

Figures 7 to 9	liquefaction summaries for each sand
Figures 10 to 13	stress paths for each series
Figures 14 to 20	strain summaries
Figures 21 to 23	strain data after liquefaction

Figures 24 to 27 pore pressure summaries

Figures 28 to 30 comparison of sands

Figures 31 to 36 saturation, pre-cycling, volume change

Figures 37 to 39 comparisons with previous tests

Significance of each figure will be discussed in the following two chapters entitled Discussion of Test Results and Comparison with Previous Tests. Before proceeding into the analysis of presented data several frequently mentioned parameters should be defined.

Initial Liquefaction is specifically defined as the first cycle at which "appreciable" strains occur. Appreciable usually meaning 0.2 to 0.4 percent axial strain, and indicates the first strain increase visible on a recorded trace. (Definition in terms of pore pressure would have to be inconsistant as in no test did pore pressure increase above the total confining stress.)

Relative density is based on experimental values of maximum and minimum density, and is used as the basis of comparison in many instances. Section D of Chapter III discusses this reasoning.

Double amplitude strain is defined as the sum of strain in compression and in extension for the cycle mentioned. Following initial liquefaction use of the terms "extension" and "compression" strain becomes somewhat less applicable, being based on the initial sample height.

Necking is the phenomena where a sample elongates and one cross-sectional area of sample becomes considerably less than the average. At this time common analysis assumptions are completely unreliable.

CHAPTER V

DISCUSSION OF TEST RESULTS

The stated purpose of this experimental thesis is to examine the behavior of sands during liquefaction, and to determine the liquefaction potential of the two tested sands. Chapter V presents this behavior by taking a close look at what is happening to stress, strain, and pore pressure during testing. A comparison of liquefaction potential in Wing-Beach and Modified A3 sands is then made. Influence of saturation and pre-cycling will also be discussed. A comparison of this test series with liquefaction studies made primarily by Dr. H. Bolton Seed and Dr. Kenneth L. Lee is included in Chapter VI.

A. Effective Stress During Liquefaction

In undrained reversing-stress cyclic loading tests, deviator stress $(\sigma_1 - \sigma_3)$ is applied alternately in compression and extension. If the initial sample stress is isotropic, shearing forces are also equal in magnitude and reverse with each cycle, as shown in Figure 2. Deviator stress, by definition the difference between the two principal stresses, is not affected by a change in pore pressure. Effective confining stress $(\bar{\sigma}_3)$, on the other hand, decreases with increasing pore pressure. In undrained testing of cohesionless soils effective confining stress controls sample strength. Therefore if pore pressures during cyclic loading are built up in excess of those associated with undrained shear, failure may occur with reversing deviator stresses smaller than the usual undrained compressive strength.

Undrained strength at liquefaction and stresses during testing can be shown on a $\bar{\rho}$ - q diagram (where $\bar{\rho} = \frac{\bar{\sigma}_v + \bar{\sigma}_H}{2}$, and $q = \frac{\sigma_v - \sigma_H}{2}$). Figures 10 through 13 are summary plots of this type for the four major test series. Each isotropic test originates at q = 0, and $\bar{\rho} = \bar{\sigma}_{co}$, the initial effective confining stress. During initial compressive stress-controled loading (first cycle) the sample behaves as if undergoing undrained shear. When cycling begins each sample has a "stable" stress state in both extension and compression which can be graphically shown. A locus of points would trace horizontal lines, both above (compression) and below (extension) the $\bar{\rho}$-axis, progressing toward the q-axis. Although friction angle during liquefaction has yet to be defined, large strains could be expected somewhere in the vicinity of the drained shear envelope. Undrained strength is, of course, the applied deviator stress (providing liquefaction occurs).

It is apparent that in each of the four series plotted Mohr-Coulomb failure criteria ($q = \bar{\rho} \tan \alpha$) may be applied for developing a failure envelope. (This envelope can only apply over the range in which liquefaction is possible.) It is significant that failure envelopes in each test appear nearly identical to respective criteria for undrained shear. Cyclic stress application, while radically reducing undrained strength, does little to alter mode of sample failure.

Small differences in failure envelope are noted between looser and denser sands. Looser sand envelopes (Figures 10 and 12) in extension appear to be slightly above that from drained shear. Quantitative use of this data is limited, however, by scatter in individual plots and by scarcity of test information. It was impossible to present all tests because axial stress data was not always recorded at the instant of

liquefaction. (Deviator stress changes slightly due to changes in binding friction along the triaxial piston.)

B. Strain During Liquefaction

In comparison of magnitudes, strain during pore pressure buildup is nearly insignificant in comparison to large post-liquefaction straining. Sample deformation in response to cyclic stress changes before and after liquefaction is shown in Figure 2. Axial strain, excluding non-sample movements, between an extension and compression cycle varied from 0.4 to 0.6 percent, depending on applied loads. Little change, if any, was noted during cycling until a state near initial liquefaction was reached. A very slight "drift" toward sample elongation was noted during most tests. Strain increased gradually, to merge at initial liquefaction with large strains. ("Drift" meaning a net elongation, without increasing strains - a decrease in compressive strain being equal to increase in extension strain from cycle to cycle.) Liquefaction was clearly defined by a sudden strain increase in all cases.

Summaries of axial strain vs. number of cycles are plotted for each test series and the preliminary test program in Figures 16 through 20. Strain at initial liquefaction, and at 5 and 10 percent double amplitude strain for three test series are shown in Figures 21 through 23. In Figures 14 and 15 contours of strain have been traced from stress path information regarding the two looser sand test series.

Necking occured in nearly every sample tested. In the denser sands necking took place at or before 15 percent strain, while looser samples consistantly reached 25 to 30 percent strain before necking. Necking is largely caused by reduction in area due to local stress differences

during extension. A larger number of cycles is quite often required to reach 15% strain in looser samples than 30% strain in denser samples.

The number of cycles, after initial liquefaction, to reach any cycle of double amplitude strain increased with increasing N_i, the cycle number at initial liquefaction. For denser samples of Wing-Beach sand which required 7, 47, and 506 cycles to initiate liquefaction, 7, 10, and 20 additional cycles respectively were required to reach 5% double amplitude strain. In looser Wing-Beach sand with 27, 82, and 683 cycles to initial liquefaction, 1, 2, and 5 additional cycles respectively were required to reach 5% double amplitude strain. Modified A3 sand samples displayed the same trend, but took more cycles to reach 5% strain in both cases.

Large strains at initial liquefaction first occured during the extension phase of cycling in all tests. Large compressive strains did not occur until after several more cycles. Figures 14 and 15 show that the stress conditions at initial liquefaction fall somewhat inside the effective stress Mohr envelope from shear tests. Larger stresses and "earlier" liquefaction correspond to data points furthest away from this envelope. In compression, as strain increases following initial liquefaction, data points representing effective stress move closer to the Mohr envelope.

For both sands in compression, the maximum friction angle corresponded to the largest strains recorded, before necking developed. The extension envelopes sketched at various stages of double amplitude strain are not as consistant. For the same extension strain the liquefaction envelope is slightly above the drained value with Modified A3 sand, and slightly below that of Wing-Beach sand. Such scatter is reason to believe break-

down of computational assumptions occurs before actual necking takes place.

Qualitatively, interest in number of cycles to cause varying percentages of strain is limited to tests where initial liquefaction occurs at a low cycle number. It is important if large strains take 1, 3, or 10 cycles to develop when initial liquefaction begins after only several cycles. (Major earthquake induced forces do not generally continue for many cycles.) Large strains are occuring within 20 additional cycles even at tests with initial liquefaction beginning at 800 to 1000 cycles. This amounts to only 2 or 3% more cycling to reach large strains, compared with 100 or 200% more cycling required at a low N_i.

C. Pore Pressure Behavior

Pore pressure changes are controlled by amount of rearangement or collapse of soil structure. Changes in interparticle force occur twice during every cycle, causing small relative movements between particles. In cohesionless soils particle to particle contact is made over many highly stressed small contact areas. Repetitive stressing of these contact points causes particle rearangement from sliding and from abrasive wear. Both actions tend to move particle centers closer together - cyclic loading causes little translational straining with resulting possible dilation. As particles become more closely packed they move away from the sample boundary (rubber membrane). More total confining pressure is then shifted onto the pore water. Through this mechanism pore pressure buildup will occur in all sands - even dense sand which exhibit large dilation during undrained compressive shear.

Increase in pore pressure before liquefaction follows a definite pattern which may be separated into three phases: 1) large initial

increase during the first few cycles 2) more gradual but steady increase in pressure per cycle, and then 3) rapid increase in buildup of pore pressure per cycle until initial liquefaction occurs. Peak pressure during the compression phase of each cycle is plotted in Figure 24 for 9 tests on Wing-Beach sand of RD $\simeq$ 76%. Test SCS-RU35 on Wing-Beach sand at RD = 52% failed at N = 26,000, the longest test, and is also shown. Figures 25 through 27 present pore pressure data for comparison of compression vs. extension buildup, and for comparison of Wing-Beach vs. Modified A3 sand. Pore pressure during extension and compression for many tests are also plotted in Appendix D.

Phases of pore pressure buildup are clearly shown by Figure 24. Large initial buildup during phase 1 is partially shown by lines connected to values of initial pore pressure. It might be expected that dense dilatant sands would decrease in pore pressure during the first application of stress (by stress controled loading), but this is not the case. Even in sands showing a strong dilatant tendency during compressive shear, volume decreases slightly until 0.3 or 0.4 percent axial strain. Applied deviator stress causes about 0.15 percent strain in most repeated loading tests on Wing-Beach sand, showing a tendency for pore pressure to increase.

Pore pressure buildup during Phase 2 is remarkably linear on a pressure vs. log cycle plot. The two curves that deviate slightly from this behavior, SCS-RU12 and RU41, have the lowest pore pressure response. RU41 is partially saturated while RU12 has a response of 90 percent and is considered near fully saturated. The beginning phase 3 is indicated by a point of inflection at about 40 to 60% of the number of cycles at initial liquefaction. Appendix D plots of pore pressure are to an arithemetic cycle scale. (The inflection point is less well defined on these

figures.)

An increasing rate of pressure rise characterises phase 3. Pore pressure buildup over the last few cycles before liquefaction is larger than in any other test period. Reduction of effective confining stress during phase 2 significantly increases the deviator stress ratio $\frac{\Delta(\sigma_1 - \sigma_3)}{\bar{\sigma}_3}$. Shearing force is now large in comparison to effective confining stress and causes more particle slipping per cycle. As state of stress approaches the failure criteria, large strains associated with liquefaction begin, in turn causing more particle reorientation. Following liquefaction, pore pressure in compression and extension level off, respectively increasing and decreasing slightly.

Figures 24 and 27 are dimensionless graphs of pore pressure vs. number of cycle. Excess pore pressure divided by initial effective confining stress is plotted vs. number of cycles divided by the cycle at initial liquefaction. Figure 24 indicates that with longer tests pore pressure shows significant increase proportionately later in the test. Figure 27 plots pore pressure increase for samples from all four series in the range of 300 to 700 cycles to cause initial liquefaction. Figure 25 plots three tests, from the range of 2000 to 6000 cycles to cause initial liquefaction, on a conventional scale of log number of cycles. These two figures (and others plotted but not included in the thesis) show that there is no consistent pattern in pore pressure increase as a function of density and nature of sand.

D. Liquefaction Potential of Tested Sands

Summary curves for Wing-Beach and Modified A3 sands are shown on

Figures 8 and 9. All saturated tests from the four principal series are shown. Each test is represented by two points, the average deviator stress, and the deviator stress during the extension part of the loading cycle. Contours were drawn with respect to extension deviator stress if a test involved a significant difference between those two values. Contours of 60 and 80 percent relative density for each sand are shown in Figure 28. Figure 29 presents a comparison of the same density sands using Wing-Beach curves of Figure 28 and Modified A3 sand curves at the same dry density.

Wing-Beach sand is considerably less succeptable to liquefaction than is Modified A3 sand. This is true over both density ranges shown, and according to both relative density and dry unit weight comparisons. The dry unit weight comparison indicates a smaller degree of difference, especially at higher stress applications. Relative density is considered by the author as a more meaningful method for comparison. On this basis 30 and 40 percent more deviator stress is required to liquefy Wing-Beach sand in 100 cycles at densities of 80 and 60 percent. At 10 cycles the same ratio drops to 22 and 33 percent.

Considerably more resistance to liquefaciton is shown by the rounded uniform sand than by a more angular and well graded sand of the same density. Some aspects of stress-strain behavior, strength, dilatency and grain characteristics will be discussed as contributing factors in influencing this result.

"Reason" might first suggest that a soil with a higher friction angle is likely to be less susseptible to liquefaciton. There are a number of reasons why this may not be the case in the two sands tested. If liquefaction is approached from the mechanism of pore pressure buildup as

presented in section C, effects on this buildup are of overiding importance. This mechanism views pressure increase as being solely dependent on how much particle slippage and wear occurs during cycling.

Drained shear tests (Figures 5 and 6) on Modified A3 sands indicate an initial elasticity modulus only 25 percent that of Wing-Beach sand. For the same amount of stress, strain in the "MA3" samples will be four times greater. (This arguement is tempered by the fact that stress-strain behavior is not the same in undrained and drained loading.) From these same figures a lower tendancy for dilation is noted in MA3. A lower such tendancy means particle interference plays even less of a role in strain than does sliding. It is apparent that more particle slippage is occuring in the MA3 samples. Consequently, more rearangement is likely to take place. Sharp angular grains of MA3 sand may be slightly more susceptible to wear or fracture than are the rounded water worked beach sand grains.

It is suspected that these results and subsequent reasoning cannot be extrapolated to all uniform or all angular sands. At this time sufficient data on susceptibility of various sands to liquefaction does not exist to act as a basis for generalization. Each sand in question will have to be analyzed for liquefaction potential.

E. Effect of Saturation, Pre-cycling and Confining Stress

It was possible during this testing program to obtain considerable data on the effects of saturation, and to a lesser degree on the effects of pre-cycling and confining stress differences.

Partial saturation was found to have an extremely large effect on resistance to liquefaction. The deviator stress required to initiate

liquefaction at a given number of cycles is increased with decreasing saturation for otherwise identical samples. The ratio of number of cycles when S < 100% to number at S ≈ 100% for initial liquefaction increases logarithmicly with decreasing pore pressure response. Figure 31 is a summary of these effects for tested samples at low pore pressure response.

Pore pressure response between 60 and 80 percent continuously back-calculates to a saturation of only slightly less than 100 percent. Data shows that these tests require 2 to 10 times the number of cycles for liquefaction than do samples with a higher response. SCS-RU41 with a response of 38%, has a computed S > 99 percent, but took 5297 cycles to fail. RU13, a comparable test at 95% response, failed after 47 cyclic applications of the same deviator stress. When the deviator stress of RU41 is plotted on the summary curve (Figure 8), it is 40 percent higher than that required to fail an "equivalent" saturated sample at 5297 cycles.

Test SCS-RU20 failed in 605 cycles and has S ≈ 84 percent with a pore pressure response of 5 percent. When compared to the summary curves on Figure 7, deviator stress is about 2.9 times that for failure at the same number of cycles of a saturated sample. For the same stress applied to a saturated sample, failure should occur during the first few cycles. The summary data on Figure 31 was compiled with no reference to relative density or type of sand. Not enough data is available to form a basis of comparison in either case.

Figure 32 compares, on a dimensionless basis, pore pressure buildup for partially saturated tests SCS-RU41 and RU20 with tests upon saturated specimens of the same relative densities. Large pore pressure increase

occurs later in the partially saturated tests when compared to saturated samples which liquified at the same number of cycles. (Section B found that difference in pore pressure buildup was consistantly dependent only on cycle range.) In partially saturated samples a buildup of pore pressure causes air to go into solution. An increase in saturation as well as in sample density results. Test RU41 had a pore pressure response before testing of 36 percent and after testing of 88 percent. Considerably more rearangement of soil grains is required to build up pore pressure in the unsaturated state.

Pore pressure in compression and extension for test RU20 is plotted in Figure 33. When pressure increase per cycle begins to rise shortly before liquefaction, difference in the extension and compression pore pressure value also increases. This is not noticeable in saturated tests, and is a good indicator of increasing saturation in RU20. Pore pressure responds more to stress changes when at a higher state of saturation.

If a sample is pre-cycled at a lower deviator stress and not liquefied, it will be more resistant to liquefaction than a non pre-cycled sample. Two tests run after pre-cycling and reconsolidation provided the basis for this conclusion. Test SCS-RU17 was cycled 16,800 times at a deviator stress of 9.0 psi with no liquefaction (this test called RU16). (Reconsolidation changed the relative density by only 2%). Test RU17 is plotted in Figure 34 and pore pressure data for RU16 is shown in Figure 24. Test RU12 is comparable to RU17 and failed at 46 cycles, as shown in Figure 35. The pre-cycled test RU17 failed after 2446 cycles, or over 5 times as many.

Test RU40 was pre-cycled in several stages for 500 cycles per stage.

Finally deviator stress was increasedduring cycling and the sample liquefied at an extension stress of 24.5 psi. This is 40 to 50 percent higher than that stress required to fail a similar sample on the first cycle. Initial pore pressure response of this test was only 38 percent, somewhat complicating any use of its data, and the test is not shown plotted in this thesis.

It is clear from these two tests that to some degree resistance to liquefaction is increased by pre-cycling. Similar strength increase from pre-cycling was noted in cyclic (non-reversing) drained tests run on Ottawa sand for the Inter-American Program during 1967. (Reported in Progress Report No.1)

Volume change measurements were made after liquefaction, when drainage was allowed as samples were returned to the pre-test isotropic state. A summary of these volume decreases is shown in Figure 35. Although considerable data scatter is evident, curves could be sketched for each test series but the looser Wing-Beach sand. Scatter can well be expected because of many influencial factors not considered, such as number of cycles after liquefaction, amount of necking, and slight density variations. Even so, two definite patterns of behavior emerge from this plot:

1. Induced volume decrease is larger with increasing number of cycles to initial liquefaction in every tested series.
2. Looser sands undergo more volume change than do denser sands after failure at the same number of cycles. It is noted that strains reached before necking in loose sands are about twice as large as dense sample strains.
3. Modified A3 sands tend to decrease in volume more than Wing-Beach sands.

CHAPTER VI

COMPARISON OF RESULTS WITH PREVIOUS STUDIES

Comparison of soil liquefaction behavior will be made to similar testing of Sacremento River sands at the University of California. This data has been published primarily by Dr. Kenneth L. Lee and Dr. H. Bolton Seed in several A.S.C.E. Soil Mechanic Journals from November, 1966 (see reference list). Similarities in behavior, test results, and possible differences in these and in test conditions will be noted.

Triaxial isotropic cyclic tests were reported by Dr.'s Lee and Seed primarily in Journals SM6, November 1966, and in SM1, January 1967. Fractionated samples of Sacremento River sand were tested under a number of confining stress values at cyclic loadings of 2 cycles per second and 6 seconds per cycle. Sacremento River sand is quite similar in gradation and void ratio range to Wing-Beach and Modified A3 sands. Figure 39 presents the gradation curve of all three tested sands and respective maximum and minimum void ratios. Grain size at D_{50} is virtually the same with uniformity of Sacremento grains about midway between Wing-Beach and Modified A3. Microphotographs of untested Sacremento River sand indicate a composistion of sub-rounded or subangular grains.

Performance of the three sands during liquefaction is quite similar. Both testing programs conclude the following general behavior:

1. Cyclic stress applications will induce liquefaction over the range of density tested in this thesis.
2. Number of cycles required to induce liquefaction increases as deviator stress is reduced.

3. Increasing test confining pressure causes a similar increase in cyclic deviator stress necessary to fail a sample in the same number of cycles.
4. Deformations after liquefaction in looser sands become large at fewer cycles than do deformations in denser sands.
5. Cyclic deviator stresses required to fail a sample are considerably lower than the static stress required under similar sample conditions.

It is evident that deviator stress magnitude, number of cycles of stress application, confining pressure, and void ratio at time of test are major factors governing liquefaction behavior. Comparison of recorder traces for pore pressure and strain are quite similar. (In fact both pore pressure traces record a curious impulse of pressure following load changes after liquefaction.)

Comparison of initial liquefaction potential of the three sands mentioned is shown in Figure 37. Curves for a relative density of 78 percent in Wing-Beach sand and Modified A3 sand are compared to a reported curve for Sacremento River Sand (as referenced in Figure 37). The California tests were run at 1 and 5 kilograms per square centimeter but not at 2 kg. per sq. cm., the confining pressure of most tests in this thesis. Both Sacremento curves are shown and indicate considerable difference in required deviator stress for liquefaction even after "normalization". It is evident from these curves that both sands at M.I.T. appear more susceptable to liquefaction than does the Sacremento River sand. That is, they will fail after fewer cycles under the same deviator stress. Three possible reasons for this difference are now suggested:

1. Wing-Beach sand and Modified A3 sand are more susceptable to

liquefaction than is the Sacremento River sand.

2. The sands tested are not being compared correctly on a basis of relative density, due to differences in definition.
3. Test conditions are not similar enough to keep test-associated differences at an insignificant level.

Figure 38 compares Wing-Beach sand at RD = 78% and 60% to Sacremento River sand at RD = 78%, 60% and 38%. Tests at both 1 and 5 kg. per sq. cm. are shown for Sacremento sands of RD = 78% and 38%, but were not available at 5 kg. per sq. cm. for RD = 60%. (It is interesting to note that at RD = 38% both confining stress levels yield similar normalized curves, but not at RD = 78%.) Figure 38 indicates that the second proposed reason for difference is unlikely to be of great significance. For this to explain differences, a relative density of 38 percent for Sacremento River sand would have to be equivilant to RD = 60 percent in Wing-Beach sand.

The author considers reasons 1 and 3 to be plausable influences on reported behavior. Both "true" and testing-related differences are likely to be of influence in comparison of results. Although the three sands are very similar on an indirect and outward comparison they may not behave similarly when subjected to cyclic loadings.

Differences in test conditions have been known to cause varying test results in even the most standardized of tests. It may well be that enough difference exists in equipment to accentuate or even reverse true potential for liquefaction. The author is not familiar enough with testing equipment and precedures used at the University of California to offer an explanation on this basis. Several considerations which may play a significant role in test-oriented factors are now suggested:

1. Sample size effects (2 inch ϕ by 3.5 inch high at M.I.T. and (?) 1.4 inch ϕ by 3.5 $\pm$ inch at California)
2. Sample uniformity, stress history or disturbance differences
3. Stress application effect (slight play in top cap connection at M.I.T. may cause different mode of application than a locked connection)
4. Stress measurement difference (load cell located inside the triaxial cell at M.I.T. and outside at California)
5. Saturation difference
6. Rate of cycling and shape of stress wave

In conclusion, no direct comparison of liquefaction potential for two sands can be made at this time if testing was on different equipment. This is a "temporary" conclusion which could be clarified by comparative tests.

Such tests may be available in the future on Wing-Beach sand. Dr. Lee, at the University of California at Los Angeles, has been sent a quantity of Wing-Beach sand and plans to run several cyclic tests on similar density samples as those reported in this thesis.

CHAPTER VII

CONCLUSIONS AND RECOMMENDATIONS

Conclusions are outlined for the two main areas under study in this thisis: 1) behavior of isotropically consolidated triaxial samples under reversing cyclic load changes, and 2) comparison of liquefaction potential of Wing-Beach sand and Modified A3 sand.

This study into behavior of triaxial samples during a liquefaction test results in the following conclusions:

1. Although strength of sand samples is much lower under cyclic loading than under static testing, failure criteria appears to follow the effective stress Mohr-Coulomb failure envelope from drained static shear tests.
2. Stress application by reversing cyclic loads of equal magnitude will result in failure occuring initially during the extension phase of cycling.
3. Pore pressure buildup before liquefaction follows a definite pattern with three distinct stages:
   a. large initial increase on first few cycles,
   b. smaller but steady increase in pressure over intermediate cycles
   c. rapid increase in new pore pressure generated per cycle near liquefaction.
4. Ultimate pore pressure buildup during liquefaction is a function of effective stress principles, Mohr-Coulomb failure envelope, and applied deviator stress.

5. Deviator stress magnitude, number of cycles of stress application, confining pressure, and void ratio at time of testing are major factors governing liquefaction behavior.

6. Partial saturation will have a very large effect on liquefaction, even at levels of saturation near 99 percent. The effect will be to increase the number of cycles required for failure at a given cyclic deviator stress.

7. Triaxial samples undergoing pre-cycling of deviator stress (with no liquefaction) will require more cycles for failure to occur than will non-precycled samples.

Conclusions from the study into liquefaction potential of Wing-Beach sand compared to Modified A3 sand can be summarized as outlined below:

1. Modified A3 sand is more susceptable to liquefaction than is Wing-Beach sand - at all comparable values of relative density tested.

2. It is not unreasonable for a rounded uniform sand (Wing-Beach) with a lower friction angle to be more resistant to liquefaction than an angular, better graded sand (Modified A3).

3. Volume changes, when liquefied samples drain to initial conditions, increase with increasing void ratio of samples. ΔV also appears to increase with decreasing applied deviator stresses.

Conclusions from comparison of test run at M.I.T. with test by Dr.'s Lee and Seed at the University of California are as follows:

1. Basic liquefaction behavior is the same in both test series reported.

2. Both Wing-Beach sand and Modified A3 sands appear considerably more susceptable to liquefaction than does Sacremento River sand.

3. A large possibility exists that potential for liquefaction is much influenced by test and sample conditions which may vary from one laboratory to another.
4. No direct comparison of liquefaciton potential for sands tested in different equipment can be made until a comparison of equipment is made.

Recommendations for future research in cyclic loading effects are virtually unlimited. Several suggestions for areas particularly of interest to the author are:

1. Isolate and investigate the effect of gradation on liquefaction potential of sands.
2. Isolate and investigate the effect of grain shape on liquefaction potential of sands.
3. Investigate the effects of partial saturation, especially near the threshold of complete saturation.
4. Investigate the effects of pre-cycling loads on samples in a systematic program.
5. Investigate and define effects of testing equipment and of proceedure on liquefaction. Compare results from several testing apparatus in use.

REFERENCES

Healy, Kent A., (1963). "The Dependence of Dilation in Sand on Rate of Shear Strain", Ph.D. Thesis, Massachusetts Institute of Technology.

Lambe, T. W. and Whitman, R. V., (1964). "An Introduction to Soil Mechanics", notes from a forthcoming book, published by Massachusetts Institute of Technology.

Lee, K. L., and Seed, H. B., (1967). "Drained Strength Characteristics of Sand", Proceedings, ASCE Journal of the Soils Mechanics and Foundations Division, Vol. 93, No. SM6, pp 117-142.

Lee, K. L., and Seed, H. B. (1967). "Cyclic Stress Conditions Causing Liquefaction of Sand", Proceedings, ASCE, Journal of the Soil Mechanics and Foundations Divison, Vol. 93, No. SM1, pp 47-70.

Lee, K. L., and Seed, H. B., (1967). "Dynamic Strength of Anisotropically Consolidated Sand", Proceedings, ASCE, Journal of the Soil Mechanics and Foundations Divison, Vol. 93, No. SM5, pp 169-190.

Luscher, U., Ortigosa, P., Rocker, K., and Whitmen, R. V., (1967). "Repeated Load and Vibration Tests upon Sand, Progress Report No. 1", Research Report R67-29, Soils Publication No. 203, Massachusetts Institute of Technology.

Ortigosa De Pablo, P. (1968). "Densification of Sand by Vertical Vibrations with Almost Constant Stresses", Masters Thesis, Massachusetts Institute of Technology.

Seed, H. B., and Idriss, I. M., (1967). "Analysis of Soil Liquefaction: Niigata Earthquake", Proceedings, ASCE Journal of the Soil Mechanics and Foundations Division, Vol. 93, No. SM3, pp 83-108.

Seed, H. B., and Lee, K. L., (1966). "Liquefaction of Saturated Sand During Cyclic Loadings", Proceedings, ASCE, Journal of the Soil Mechanics and Foundations Engineering, Vol. 92, No. SM6, pp 105-134.

Seed, H. G., and Lee, K. L., (1967). "Undrained Strength Characteristics of Cohesionless Soils", Proceedings, ASCE, Journal of the Soil Mechanics and Foundations Engineering, Vol. 93, SM6, pp 333-362.

TABLE I SUMMARY OF CYCLIC LOADING TESTS

TEST SCS-	SAND	N_i	γ_d - PCF	e_o	RD%	σ_e - psi	u_o - psi	$\Delta(\sigma_1 - \sigma_3)$ - psi COMP.	EXT.	f	PORE PRESSURE RESPONSE %	ΔH_2O AFTER TEST CC
RU1	WBS	238	—	—		54.2	40.0	3.8	4.8	8 CPM	92	—
RU2	WBS	657	—	—		54.2	40.0	11.2	6.4	8 CPM	100	—
RU3	WBS	1	100.6†	.657	85	54.2	40.0	15.1	13.4	8 CPM	—	—
RU4	WBS	1	100.1∝	.676	77	54.2	40.0	9.8	10.8	8 CPS	100	—
RU5	WBS	21	100.8	.653	86	54.2	40.0	6.7	6.9	1 CPS	99	—
RU6	WBS	330	100.4	.660	84	54.2	40.0	4.6	5.6	1 CPS	95	—
RU7	WBS	1,341	99.6	.673	80	54.2	40.0	6.1	5.9	1 CPS	100	—
RU8	WBS	1,067	100.5	.658	84	54.2	40.0	6.6	5.6	1 CPS	100	—
RU9	WBS	1	100.0	.667	82	54.2	40.0	8.1	7.7	1 CPS	95	—
RU10	WBS	5	100.4†	.660	84	54.2	40.0	4.1	4.8	1 CPS	98	—
RU11	WBS	1	100.8∝	.663	86	54.2	40.0	4.1	4.8	1 CPS	100	0.70
RU12	WBS	46	99.8	.658	81	58.4	30.0	11.4	10.2	1 CPS	90	3.55
RU13	WBS	47	99.0†	.672	78	58.4	30.0	10.3	10.7	1 CPS	95	≈ 2.30†
RU14	WBS	6	98.4	.682	75	58.4	30.0	9.7	14.5	1 CPS	98	1.92
RU15	WBS	510	97.9∝	.690	73	57.4	29.0	8.8	9.1	1 CPS	95	—
RU16	WBS	16,800N/L	98.6	.679	75	56.4	28.0	7.3	7.5	1 CPS	90	—
*RU17	WBS	2,446	99.0	.671	80	56.4	28.0	11.8	10.0	1 CPS	75	5.04
RU18	WBS	5,350N/L	97.7∝	.693	72	56.4	28.0	8.6	7.4	1 CPS	6	1.48
RU19	WBS	7,247	98.6	.678	76	56.4	28.0	8.9	7.7	1 CPS	68	5.48
RU20	MOD A3	605	92.9∝†	.781	62	56.4	28.0	14.5	14.4	1 CPS	5	5.32
RU21	MOD A3	8	97.5†	.696	79	56.4	28.0	16.9	15.0	1 CPS	63	4.99
RU22	MOD A3	30	99.1	.669	85	55.4	27.0	11.9	9.7	1 CPS	87	≈ 2.82
RU23	MOD A3	81	98.8	.673	84	55.4	27.0	11.0	10.8	1 CPS	65	4.38
RU24	MOD A3	23	98.4	.681	83	55.4	27.0	11.8	10.1	1 CPS	96	4.06
RU25	MOD A3	167	99.3	.666	86	55.4	27.0	8.1	8.7	1 CPS	80	4.35
RU26	MOD A3	24	95.3	.736	71	55.4	27.0	8.1	8.6	1 CPS	87	5.87

RU27	MOD A3	24	93.8	.765	65	55.4	27.0	9.5	9.5	1 CPS	77	8.27
RU28	MOD A3	51	93.3	.774	64	54.4	26.0	6.9	7.0	1 CPS	93	4.83
RU29	MOD A3	297	94.8	.745	69	54.4	26.0	5.4	5.7	1 CPS	95	5.82
RU30	MOD A3	3	92.4	.791	60	54.4	26.0	11.4	10.3	1 CPS	88	4.20
RU31	MOD A3	934	91.1	.816	55	54.4	26.0	4.6	3.8	1 CPS	95	8.37
RU32	MOD A3	324	98.1	.686	82	54.4	26.0	6.5	7.9	1 CPS	92	4.72
RU33	WBS	683	95.1	.740	60	54.4	26.0	5.6	7.3	1 CPS	94	4.79
RU34	MOD A3	1	90.6	.827	37	54.4	26.0	8.0	8.5	1 CPS	83	4.69
RU35	WBS	26,500	93.5	.770	52	54.4	26.0	5.2	5.4	1 CPS	80	9.00
RU36	MOD A3	3,724	94.8	.744	59	53.4	25.0	6.7	6.7	1 CPS	88	5.62
RU37	WBS	82	94.1	.758	55	53.4	25.0	8.0	8.9	1 CPS	88	7.25
RU38	MOD A3	27	95.2†	.739	60	53.4	25.0	11.1	11.1	1 CPS	90	1.05
RU39	WBS	1	94.9	.761	54	53.4	25.0	11.5	11.9	1 CPS	95	2.65
*RU40	MOD A3	500 N/L	97.9∝	.689	73	53.4	25.0	10.9	12.9	1 CPS	38	4.10
RU41	WBS	5,297	98.4∝	.682	75	53.4	25.0	12.1	10.7	1 CPS	36	5.70

∝ Values shown for γ_d, e_o, RD are computed from physical sample measurements, all other values are from water contents.

† A small void was visible near the top cap after sample preparation.

* Stage test, where more than one level of deviator stress was applied all data shown is for stage reported under N_i.

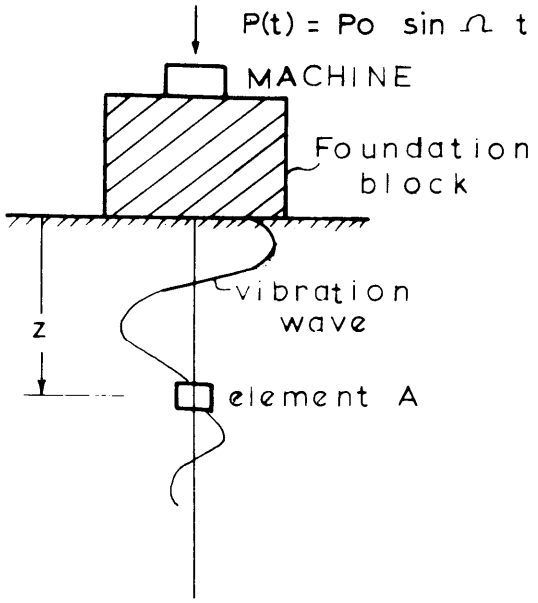

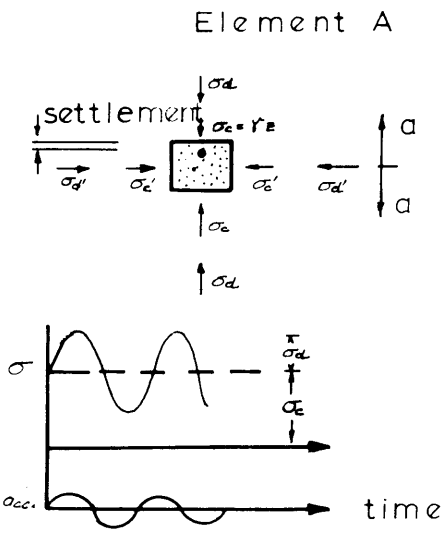

(a) Element of soil under vertical dynamic loads

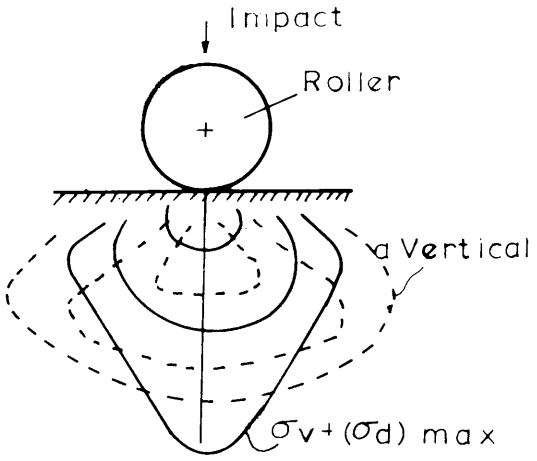

(b) Soil under vibratory compaction

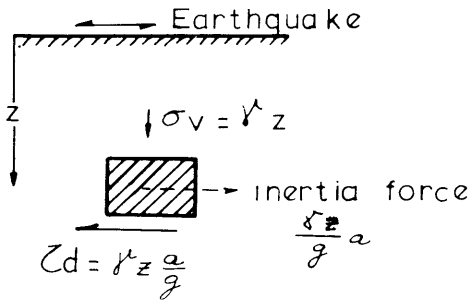

(c) Element of soil under horizontal accelerations

FIG. 1 Sources of dynamic loading in soils

FIGURE 2

STRESS - STRAIN CONDITIONS DURING LIQUEFACTION TEST

STRESS APPLIED TO SAMPLE

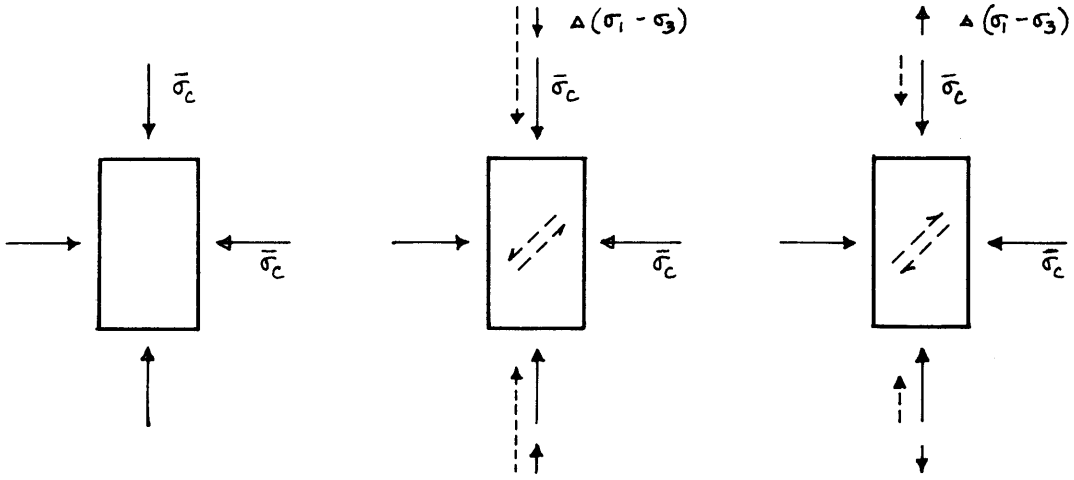

(a) After Consolidation (b) In Compression (c) In Extension

SAMPLE DEFORMATION

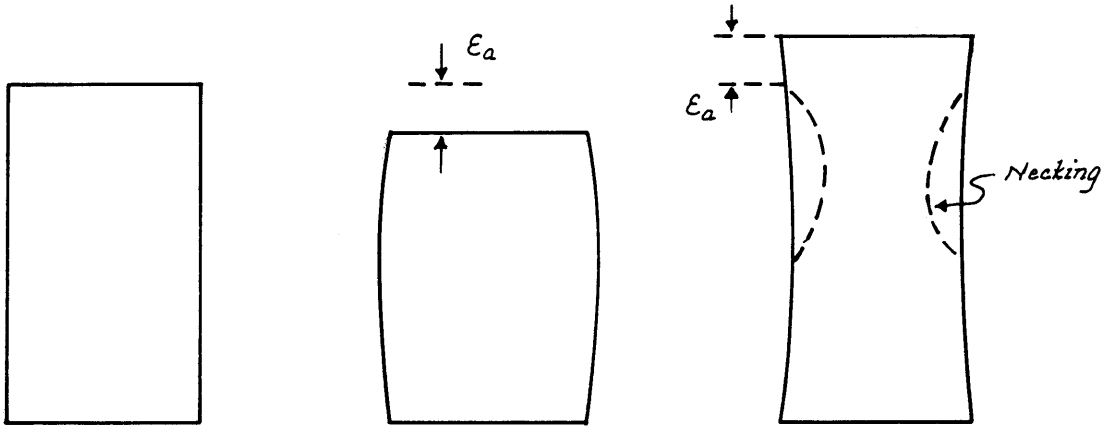

(a) Before Liquefaction (b) In Compression (c) In Extension

After Liquefaction

FIGURE 8

TYPICAL RECORDED TRACES OF MEASURED PARAMETERS

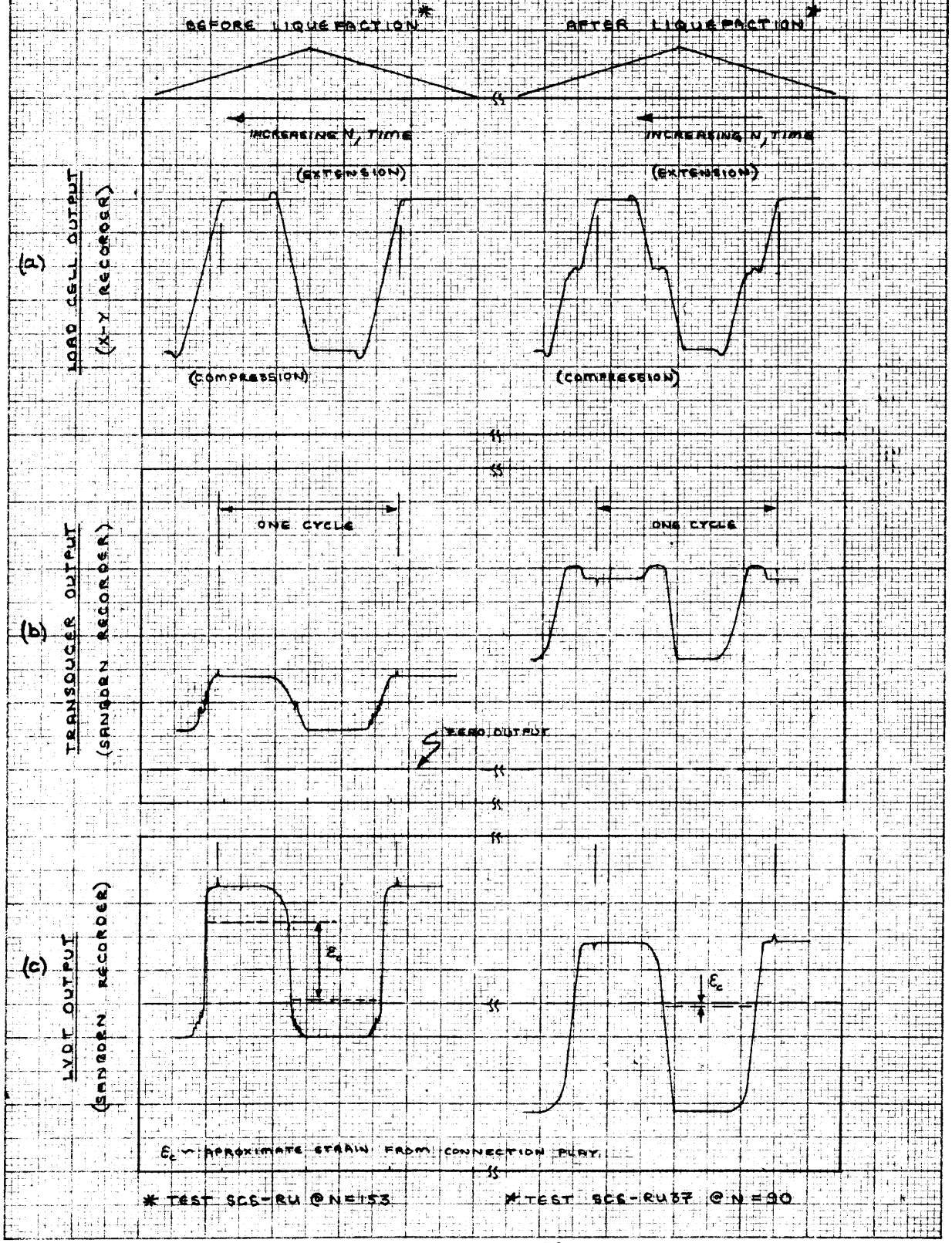

* TEST SC6-RU @ N=153

* TEST SC6-RU37 @ N=90

FIGURE 4
GRAIN SIZE DISTRIBUTION

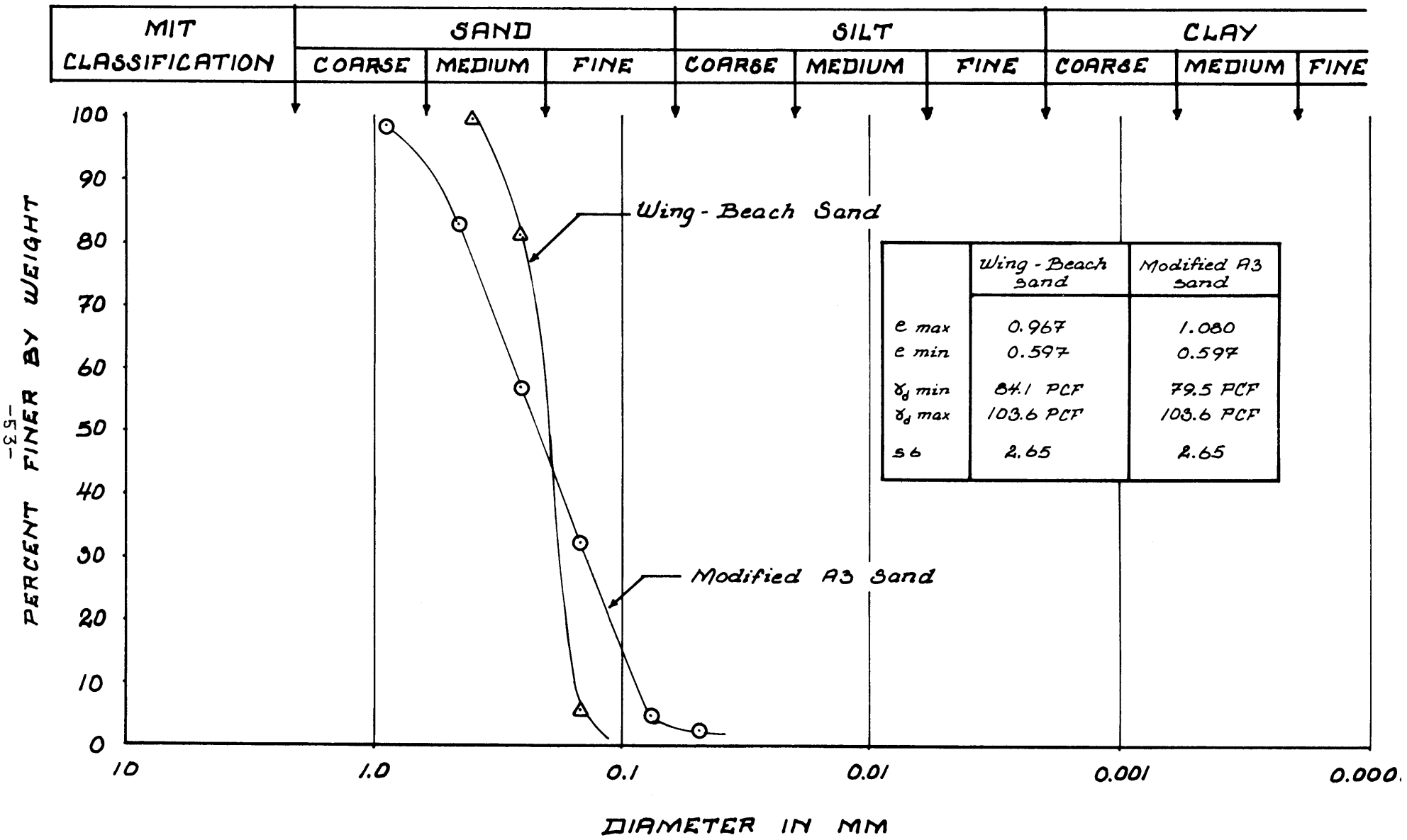

	Wing - Beach Sand	Modified A3 Sand
e_{max}	0.967	1.080
e_{min}	0.597	0.597
γ_d min	84.1 PCF	79.5 PCF
γ_d max	103.6 PCF	103.6 PCF
s_6	2.65	2.65

FIGURE 5

PHOTOGRAPH OF SAND GRAINS

(50x MAGNIFICATION)

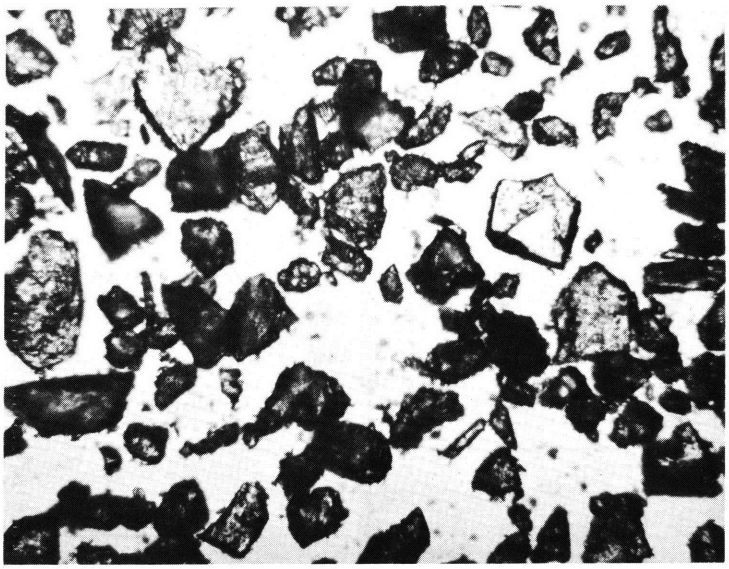

(a) Modfied A3 Sand (from SCS-RU 39)

(b) Wing Beach Sand (from SCS-RU 41)

FIGURE 6

SUMMARY OF DRAINED TRIAXIAL SHEAR TESTS

WINA-BEACH SAND

FIGURE 7

SUMMARY OF DRAINED TRIAXIAL SHEAR TESTS

MODIFIED AS SAND

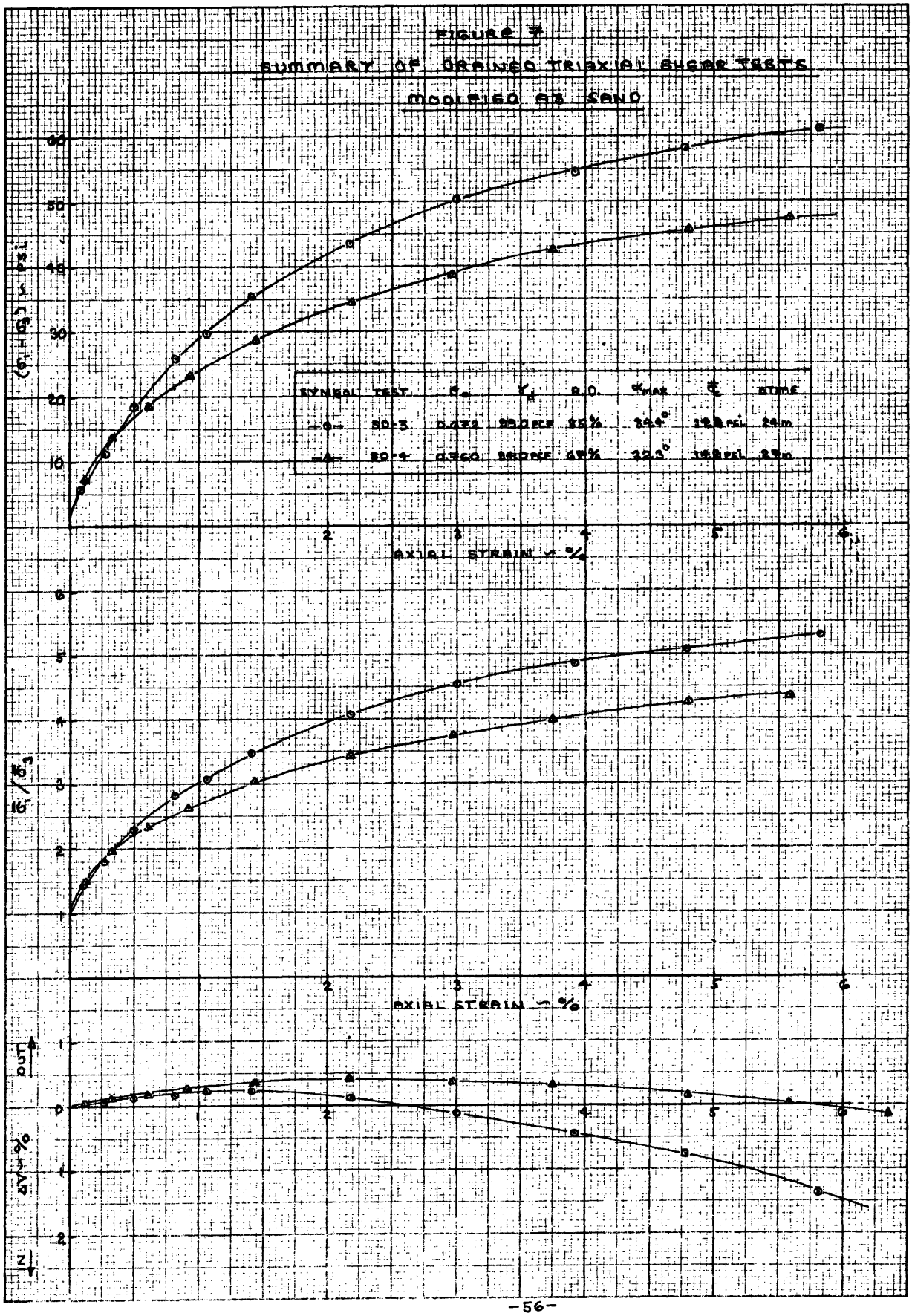

FIGURE 8

EFFECT OF RELATIVE DENSITY ON LIQUEFACTION

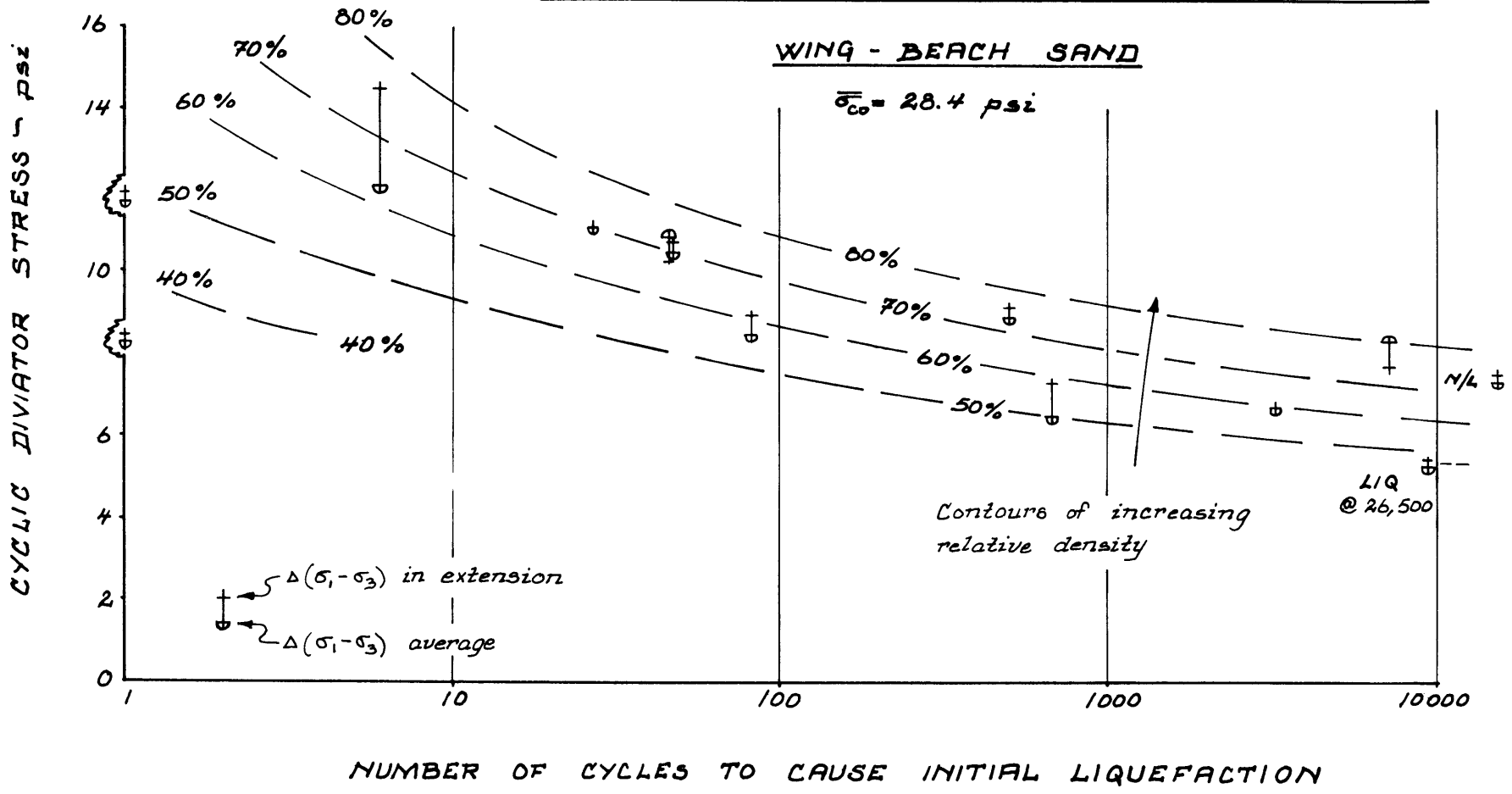

FIGURE 9

EFFECT OF RELATIVE DENSITY ON LIQUEFACTION

MODIFIED A3 SAND

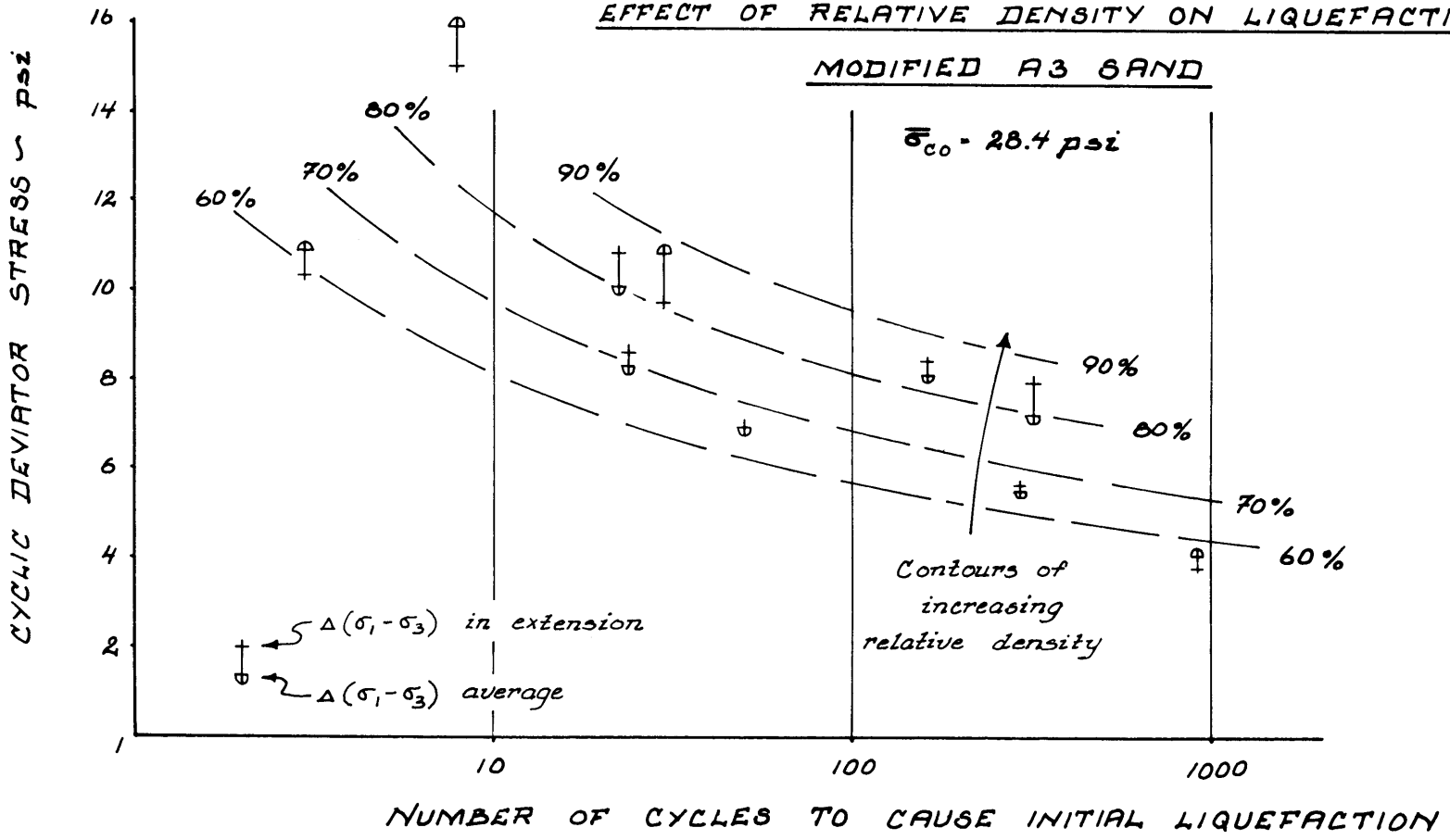

FIGURE 10

STRESS PATH DURING LIQUEFACTION

WING-BEACH SAND RD≅57%

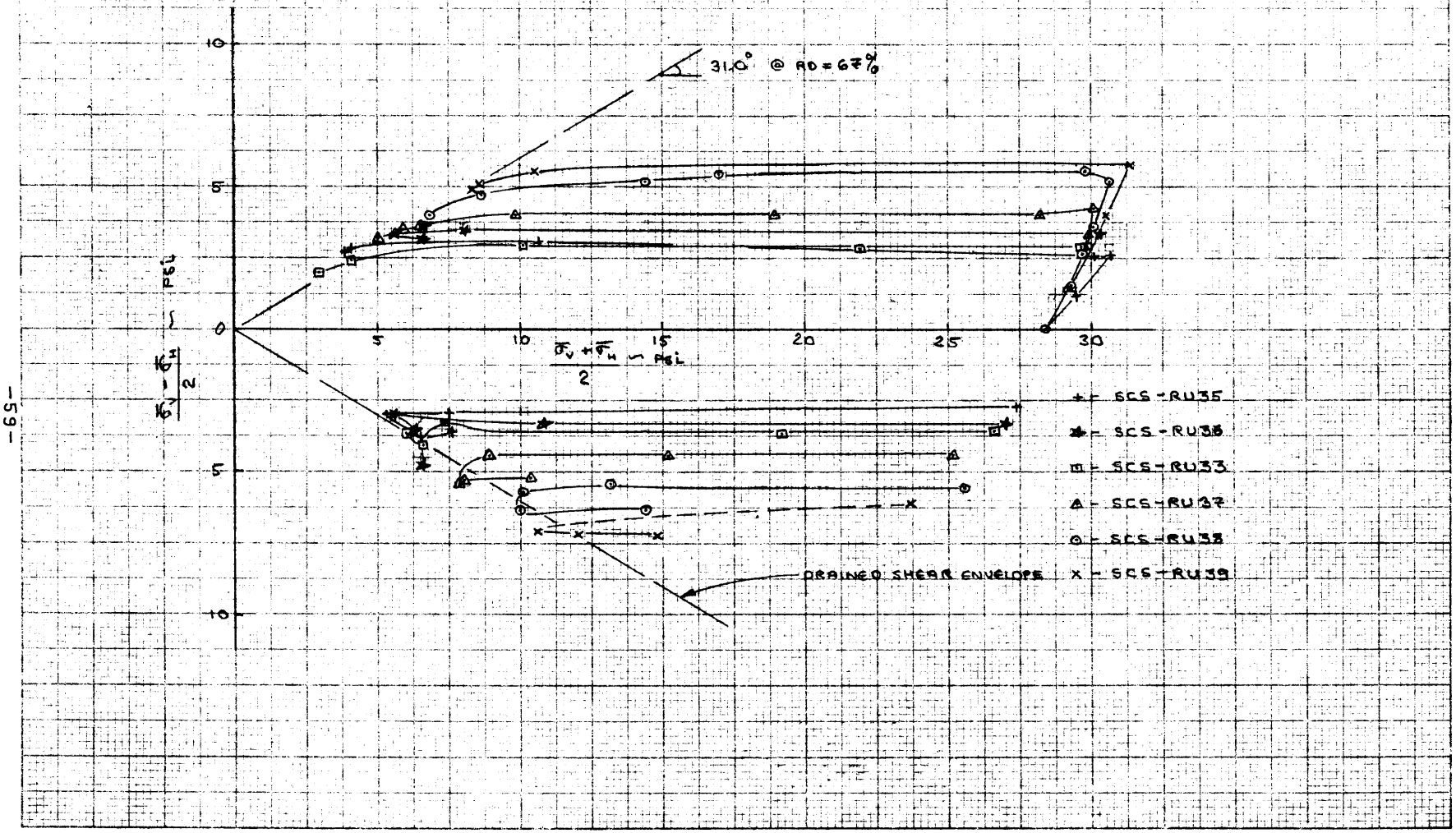

FIGURE 11

STRESS PATH DURING LIQUEFACTION

WING-BEACH SAND RD=76%

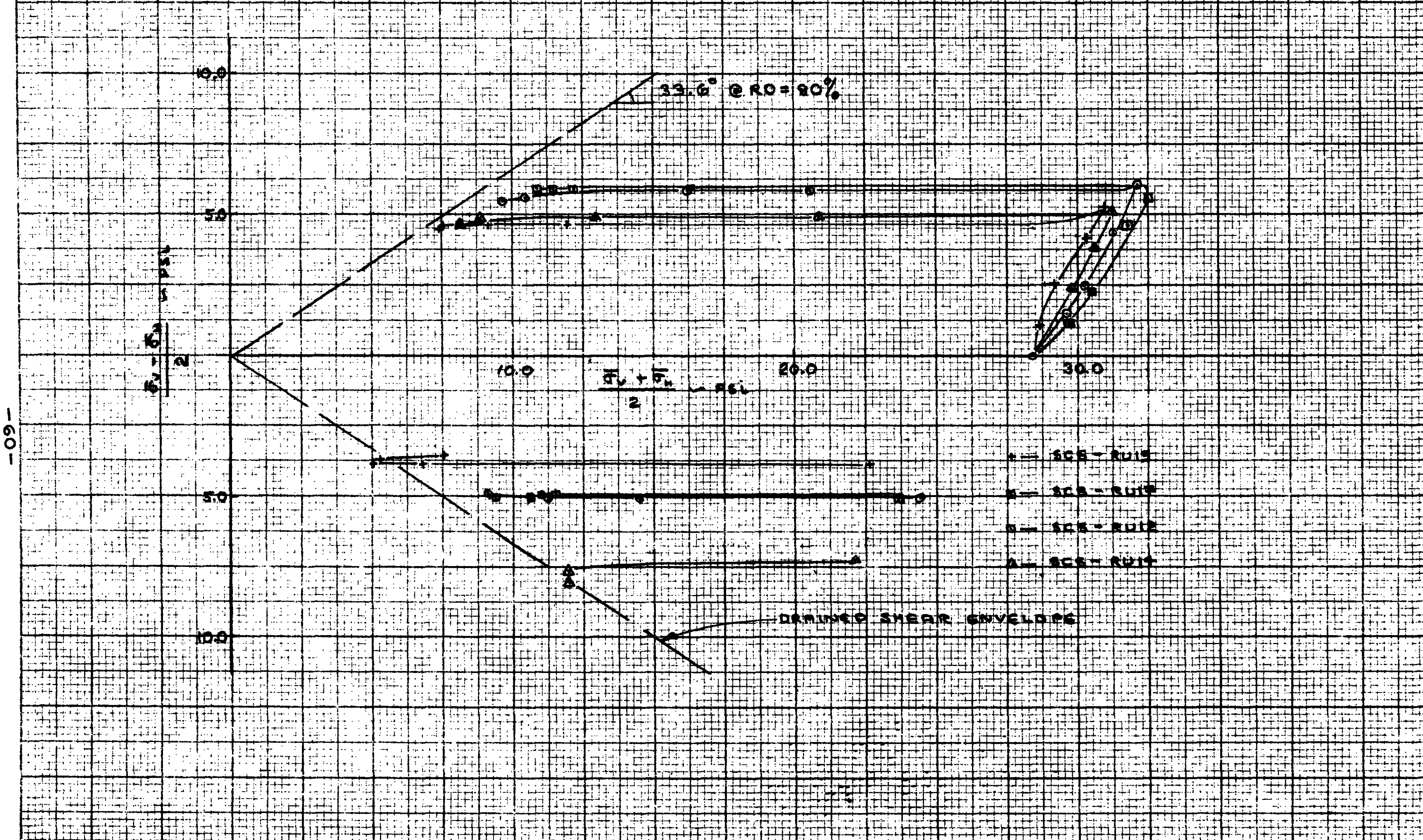

FIGURE 12

STRESS PATH DURING LIQUEFACTION

MODIFIED AS SAND ROW 62%

FIGURE 13

STRESS PATH DURING LIQUEFACTION

MODIFIED AS SAND RD = 83%

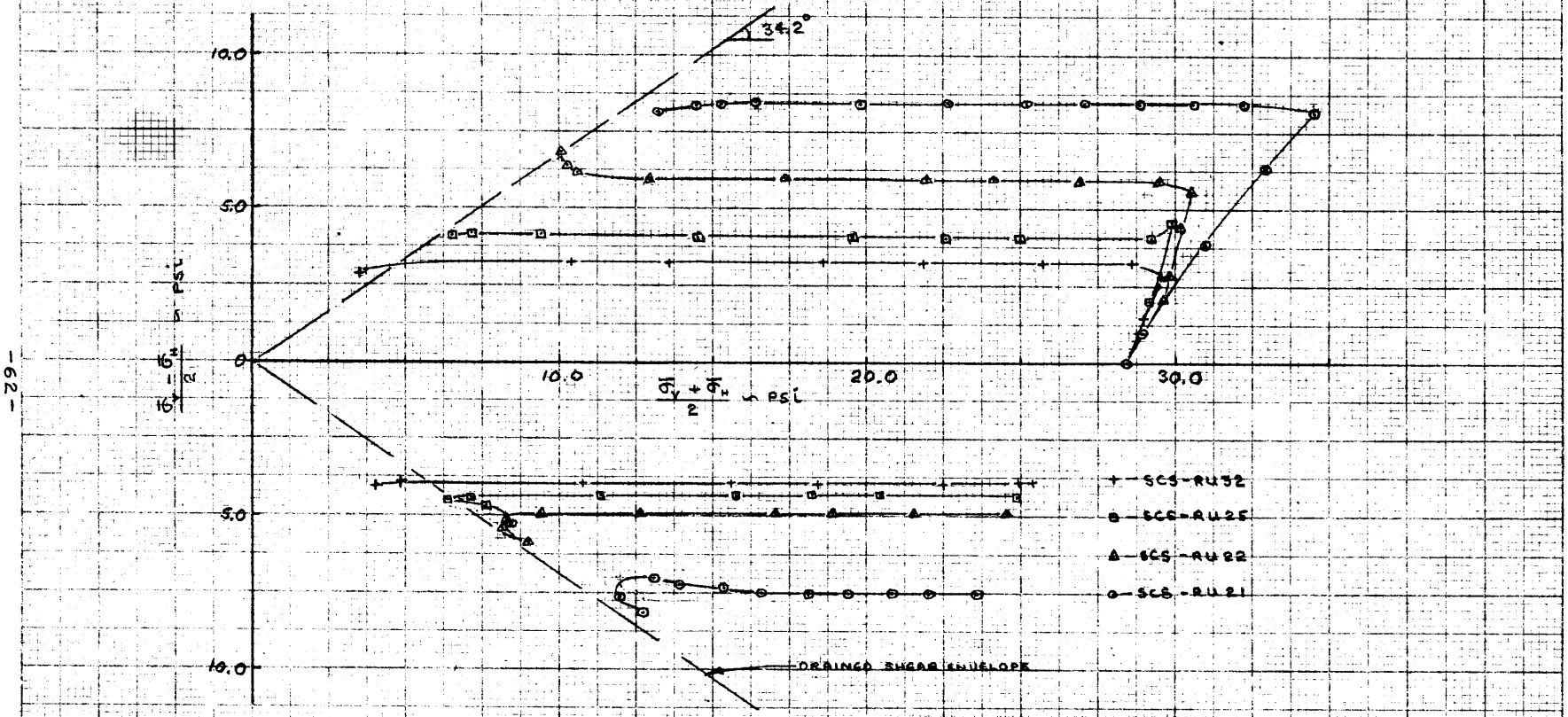

FIGURE 14

STRAINS DURING STAGES OF LIQUEFACTION

WING-BEACH SAND RD = 57%

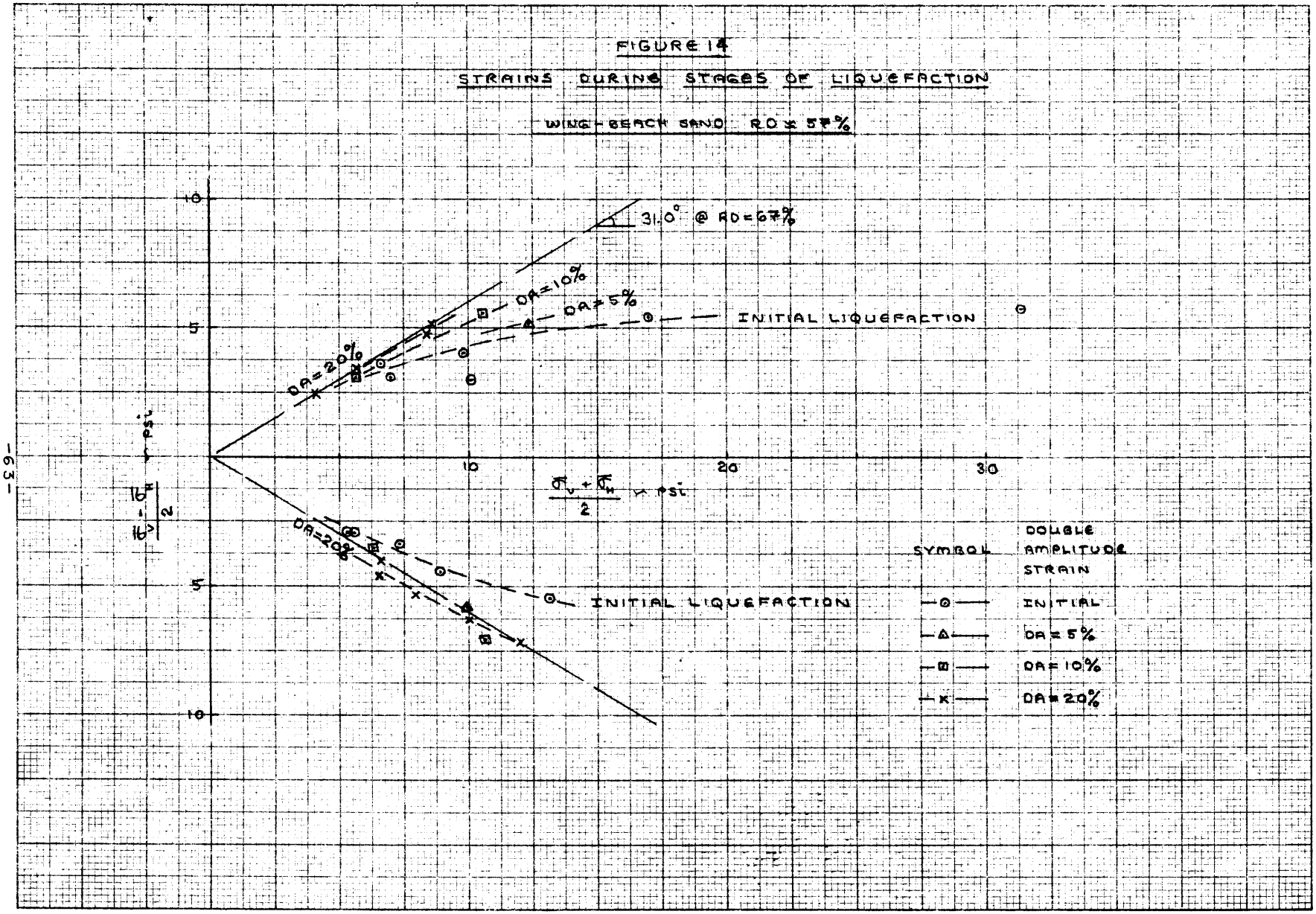

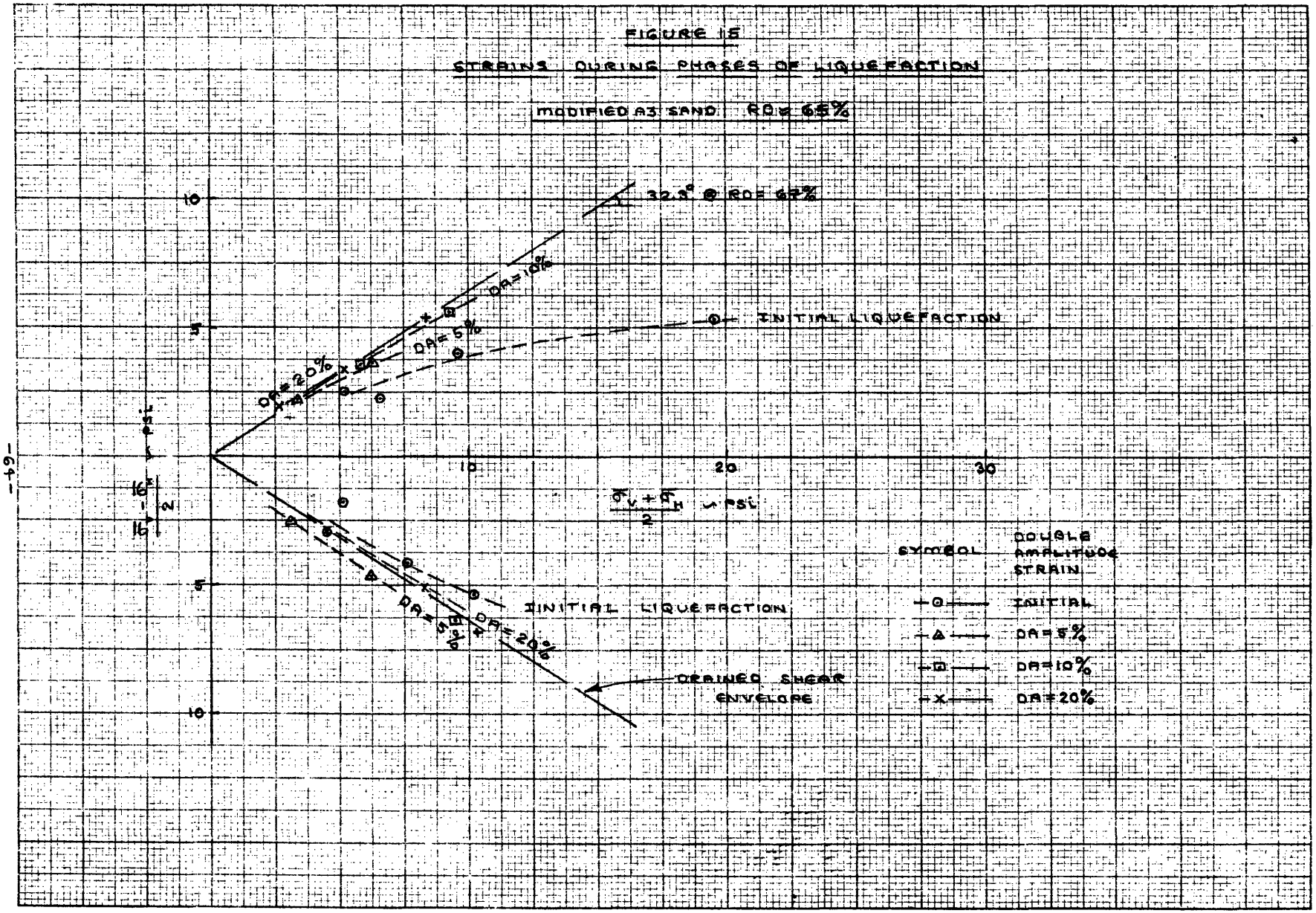
FIGURE 15
STRAINS DURING PHASES OF LIQUEFACTION
MODIFIED A3 SAND RD = 65%
32.3° @ RD= 65%
INITIAL LIQUEFACTION
DA=10%
DA=5%
DA=20%
INITIAL LIQUEFACTION
DRAINED SHEAR ENVELOPE
SYMBOL
DOUBLE AMPLITUDE STRAIN
INITIAL
DA=5%
DA=10%
DA=20%
10
5
10
20
30
5
10
1 PSI
1 PSI

FIGURE 16: SUMMARY OF LOOSER WING - BEACH SAND STRAIN DATA

RD = 57%

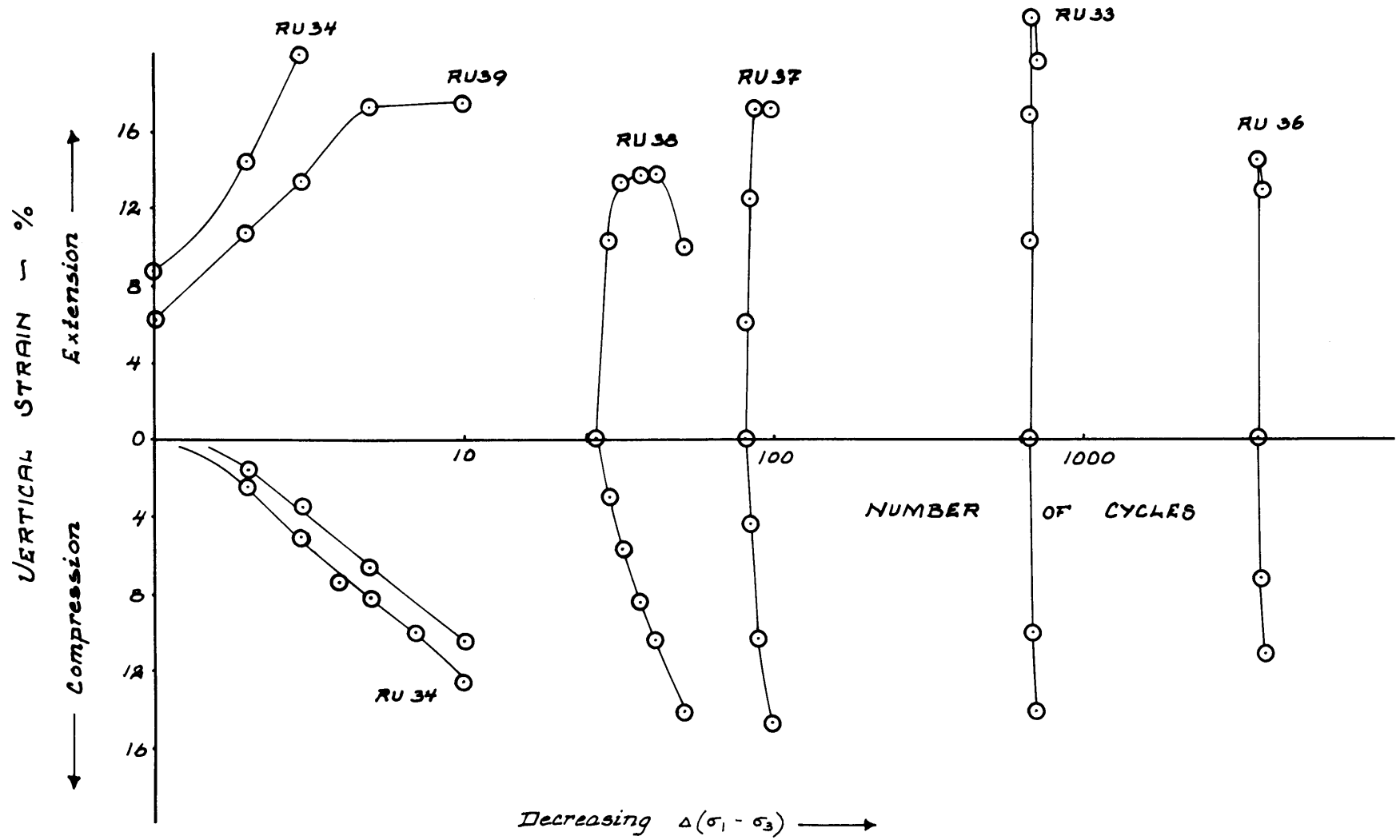

FIGURE 17: SUMMARY OF DENSER WING - BEACH SAND STRAIN DATA

RD ≈ 76%

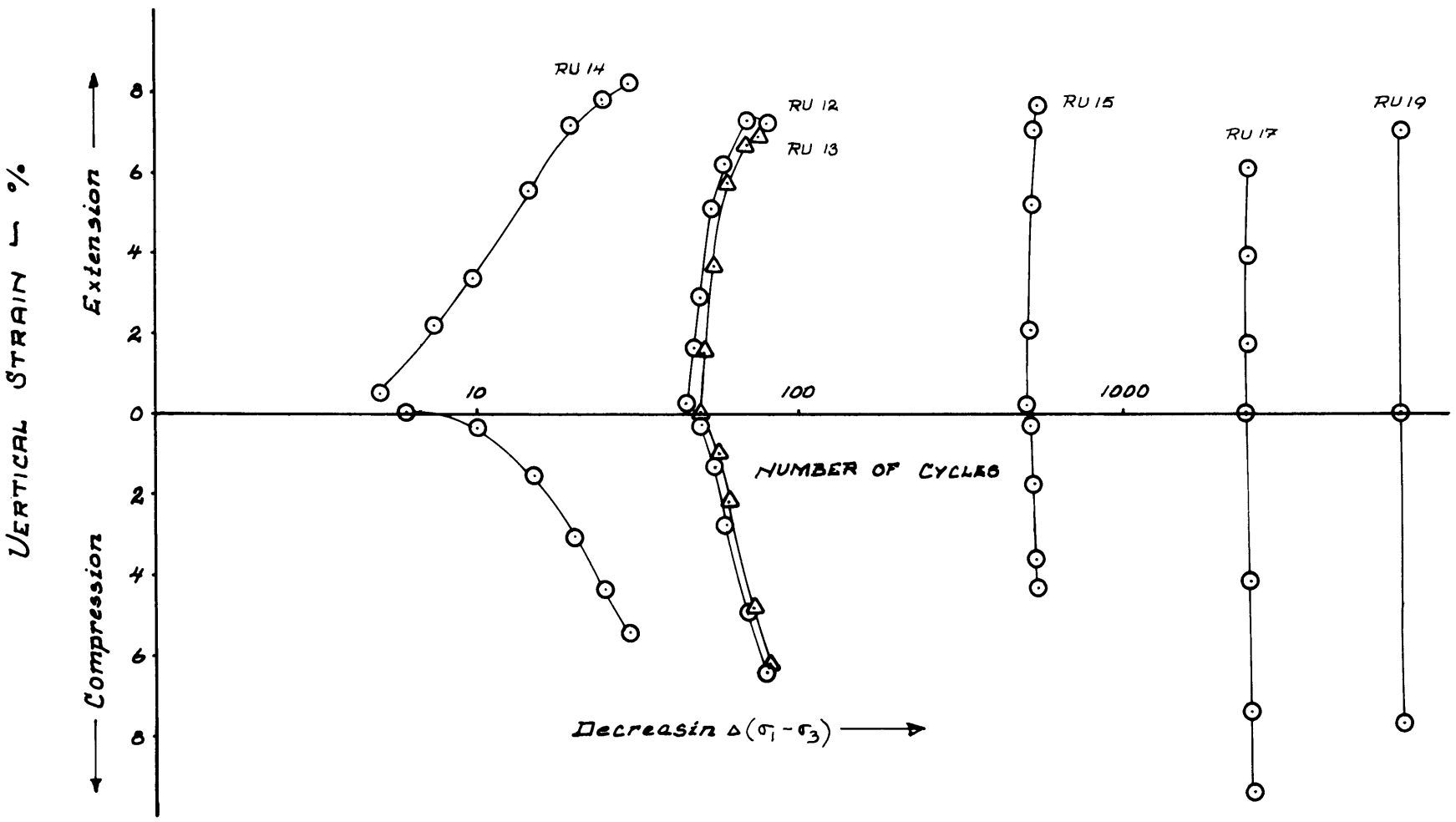

FIGURE 18: SUMMARY OF LOOSER MODEFIED - A3 SAND STRAIN DATA

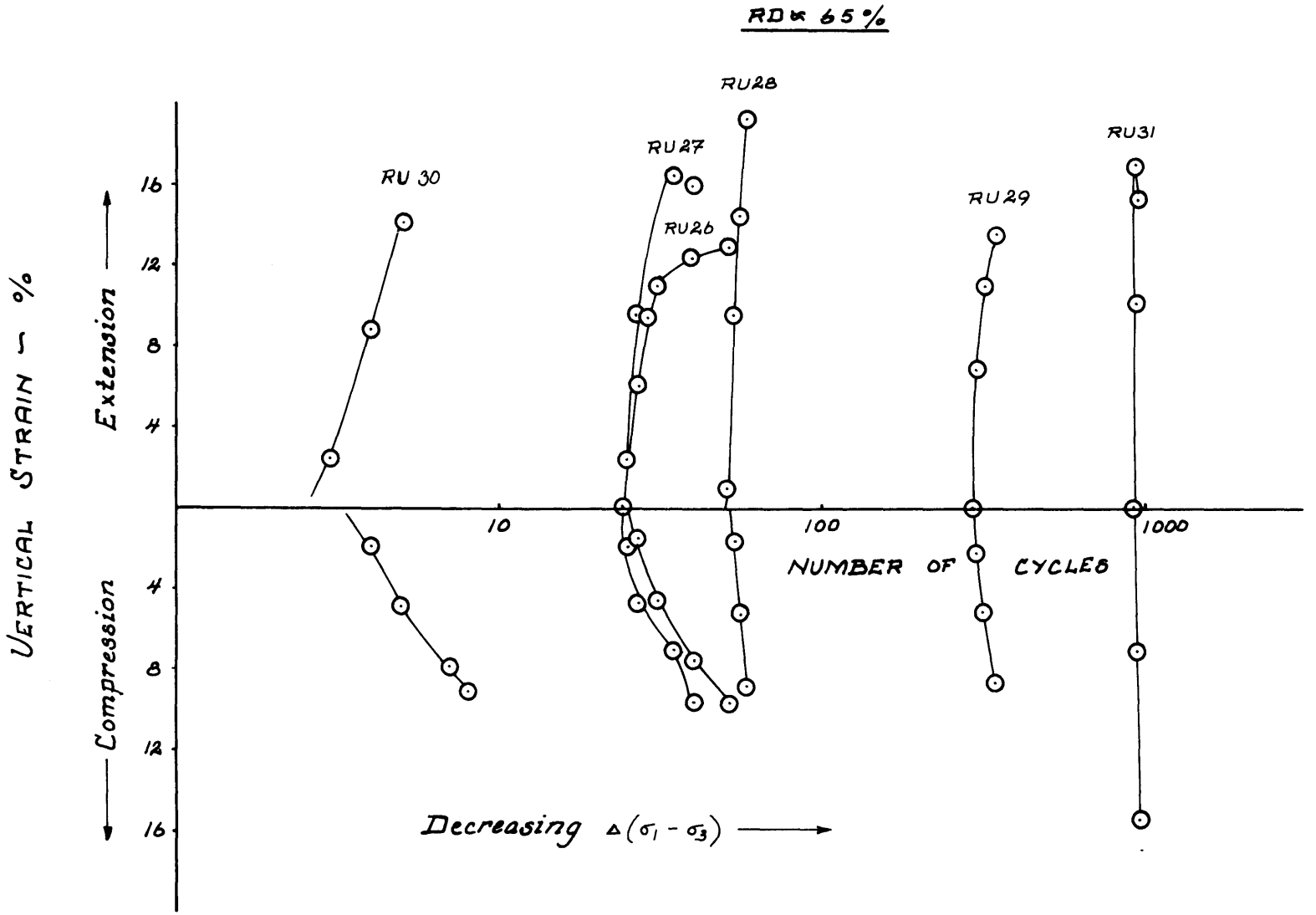

FIGURE 19: SUMMARY OF DENSER MODIFIED - A3 SAND STRAIN DATA

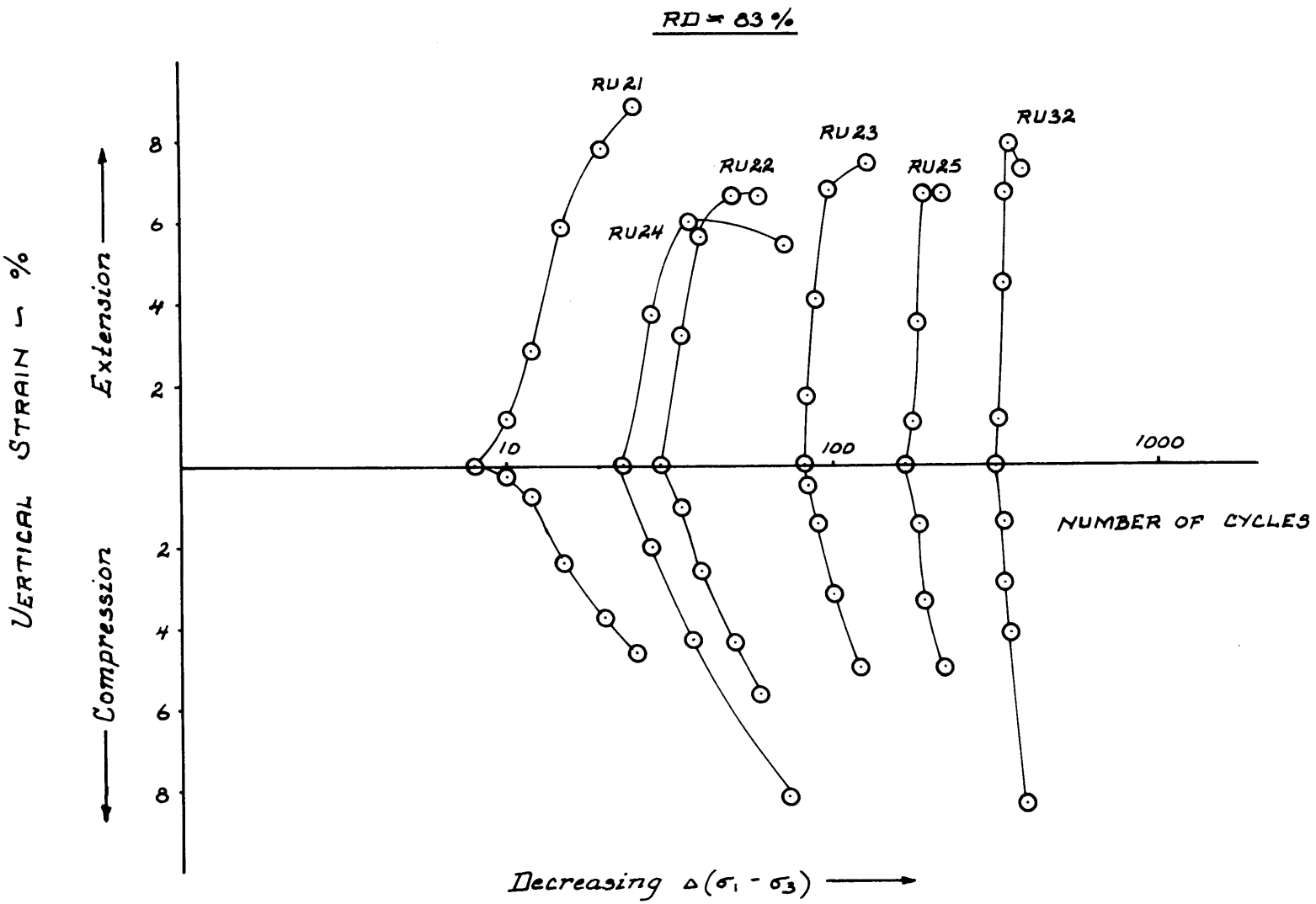

FIGURE 20: SUMMARY OF INITIAL TEST STRAIN DATA FROM DENSE WING-BEACH SAND TEST

RD = 84 %

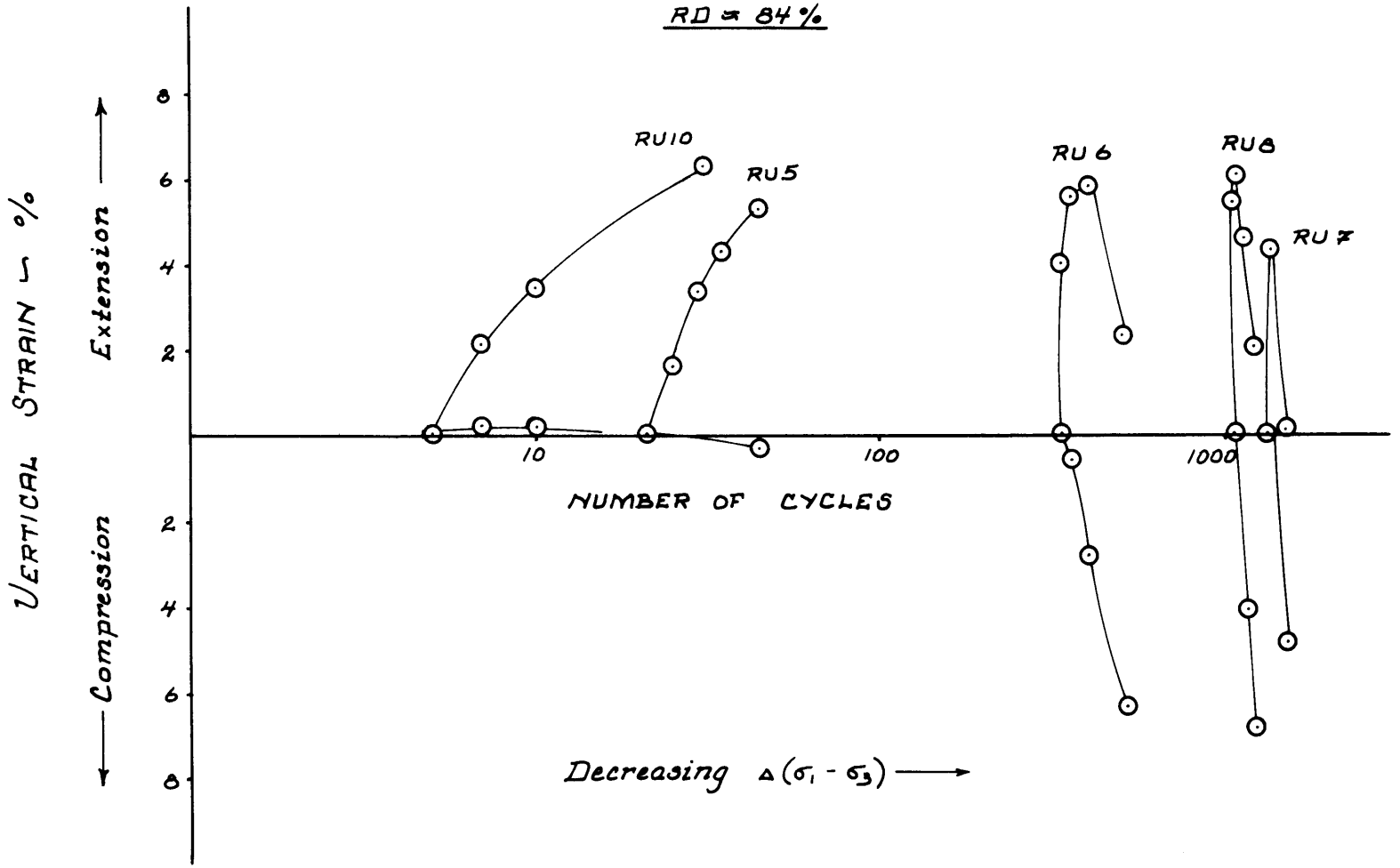

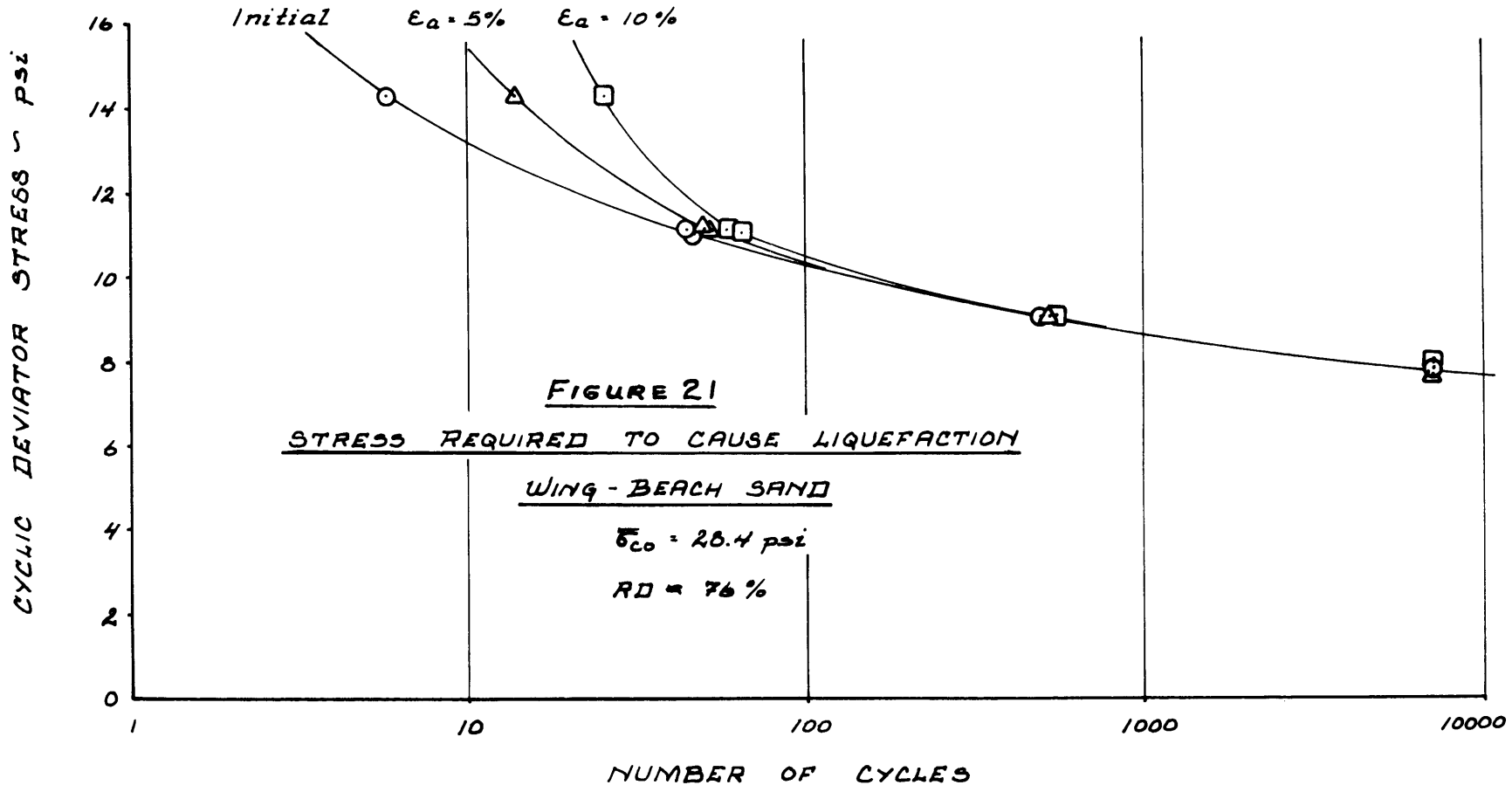

FIGURE 21

STRESS REQUIRED TO CAUSE LIQUEFACTION

WING - BEACH SAND

$\bar{\sigma}_{co}$ = 28.4 psi

RD = 76 %

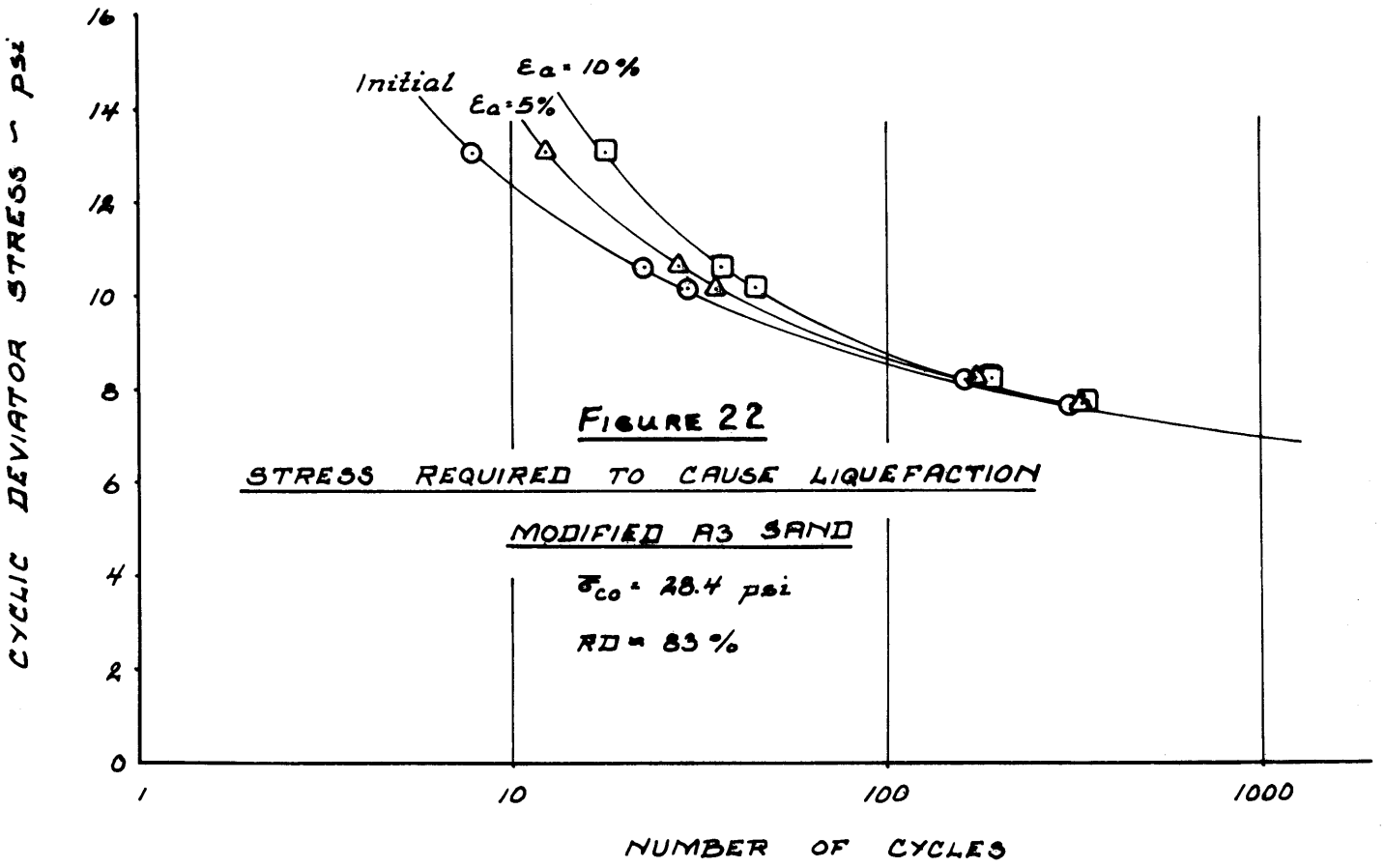

FIGURE 22

STRESS REQUIRED TO CAUSE LIQUEFACTION

MODIFIED A3 SAND

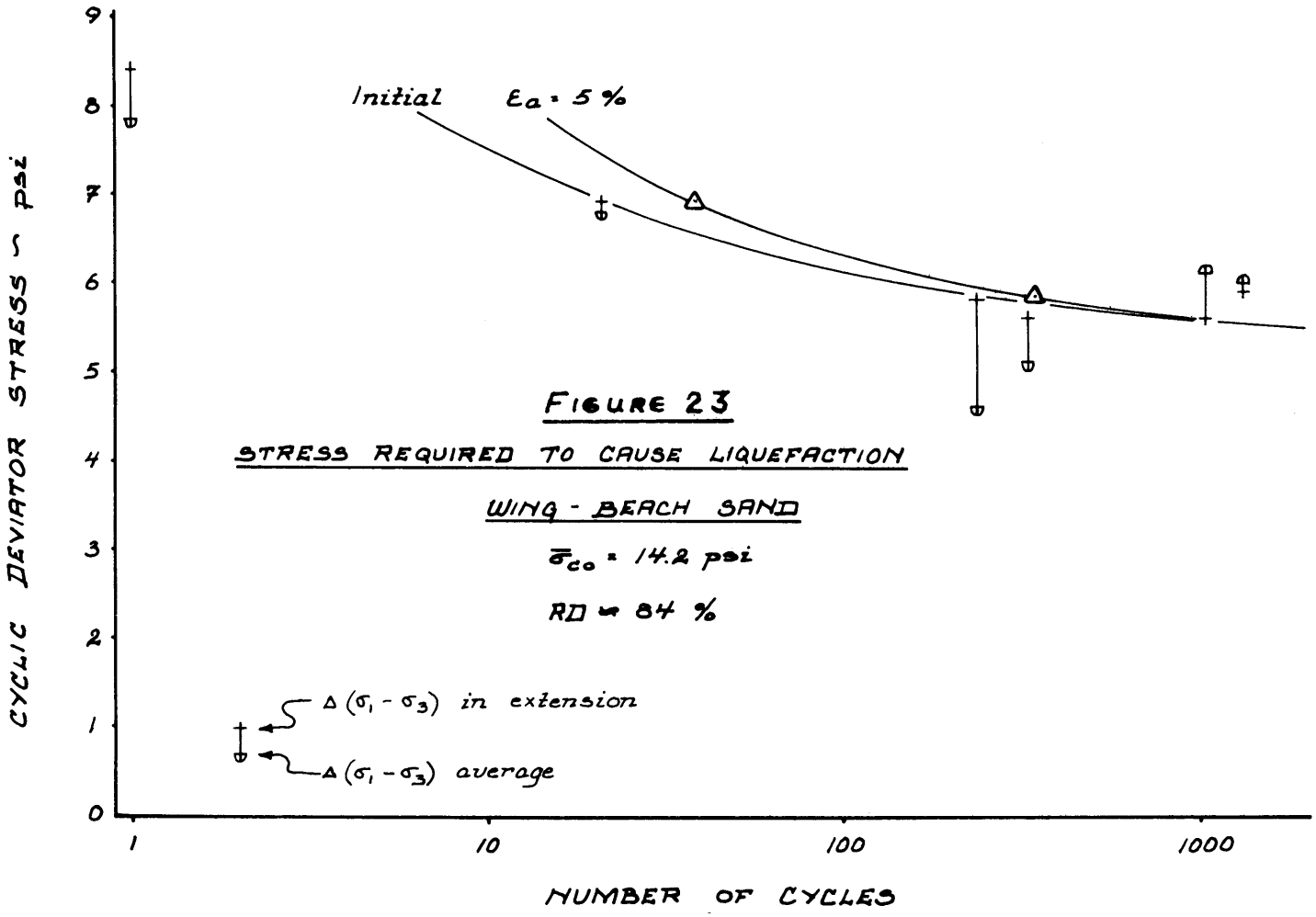

FIGURE 23

STRESS REQUIRED TO CAUSE LIQUEFACTION

WING - BEACH SAND

$\bar{\sigma}_{co}$ = 14.2 psi

RD = 84 %

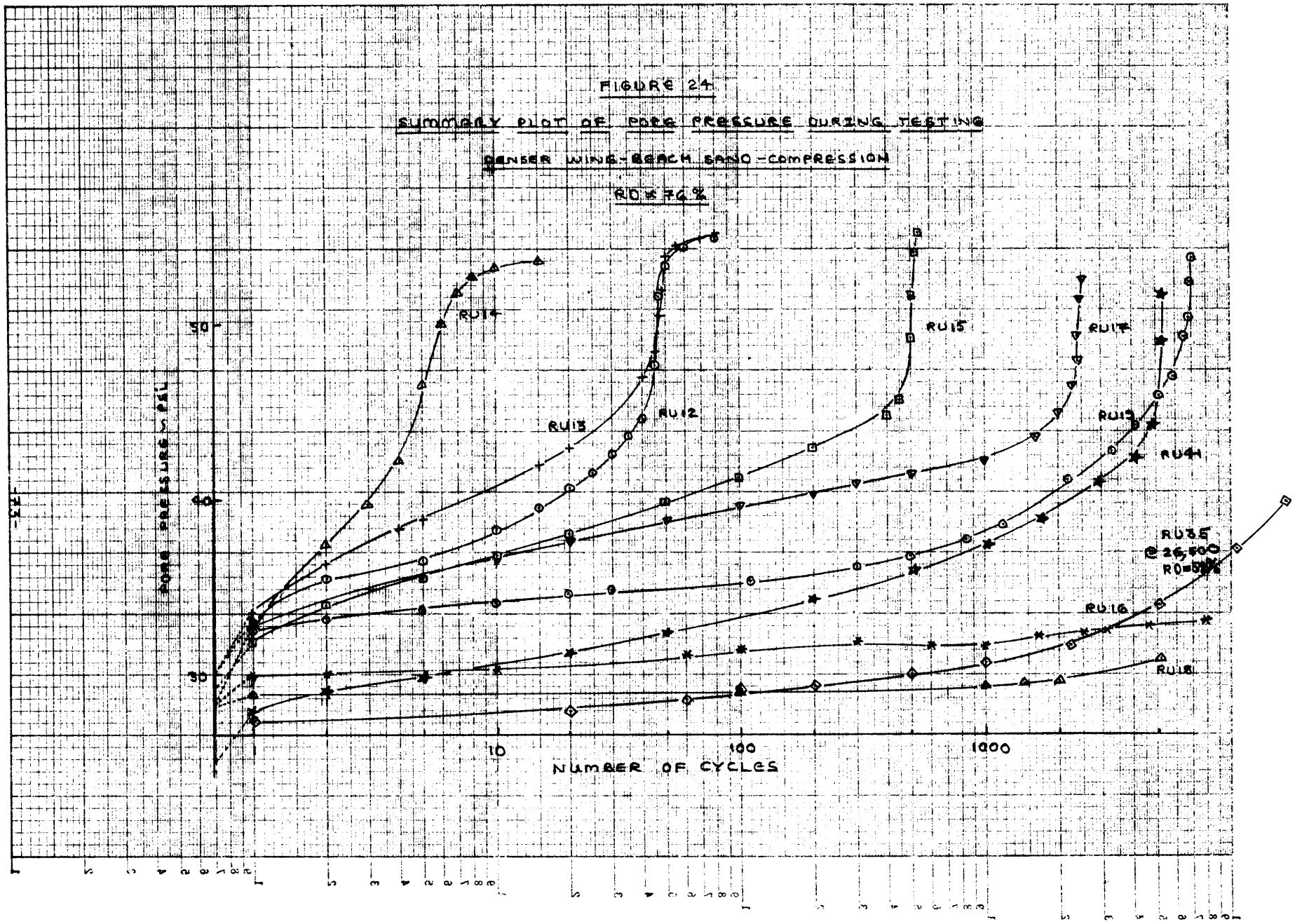
FIGURE 24
SUMMARY PLOT OF PORE PRESSURE DURING TESTING
DENSER WING - BEACH SAND - COMPRESSION
RD ≈ 76%
PORE PRESSURE - PSI
NUMBER OF CYCLES
RU14
RU15
RU17
RU12
RU13
RU11
RU4
RU16
RU18
RU35
@ 26,500
RD=
50
40
30
10
100
1000

FIGURE 25

INFLUENCE OF NUMBER OF CYCLES TO LIQUEFACTION (N_L) ON PORE PRESSURE BUILDUP

—▲— SCS-RU35 N_L = 3224

—□— SCS-RU36 N_L = 693

—△— SCS-RU38 N_L = 23

$\frac{\Delta u}{\sigma_c - \sigma_d}$

N/N_L

COMPRESSION

EXTENSION

FIGURE 26

BEHAVIOR OF PORE PRESSURE DURING CYCLING

2000 ≤ N_L ≤ 60000

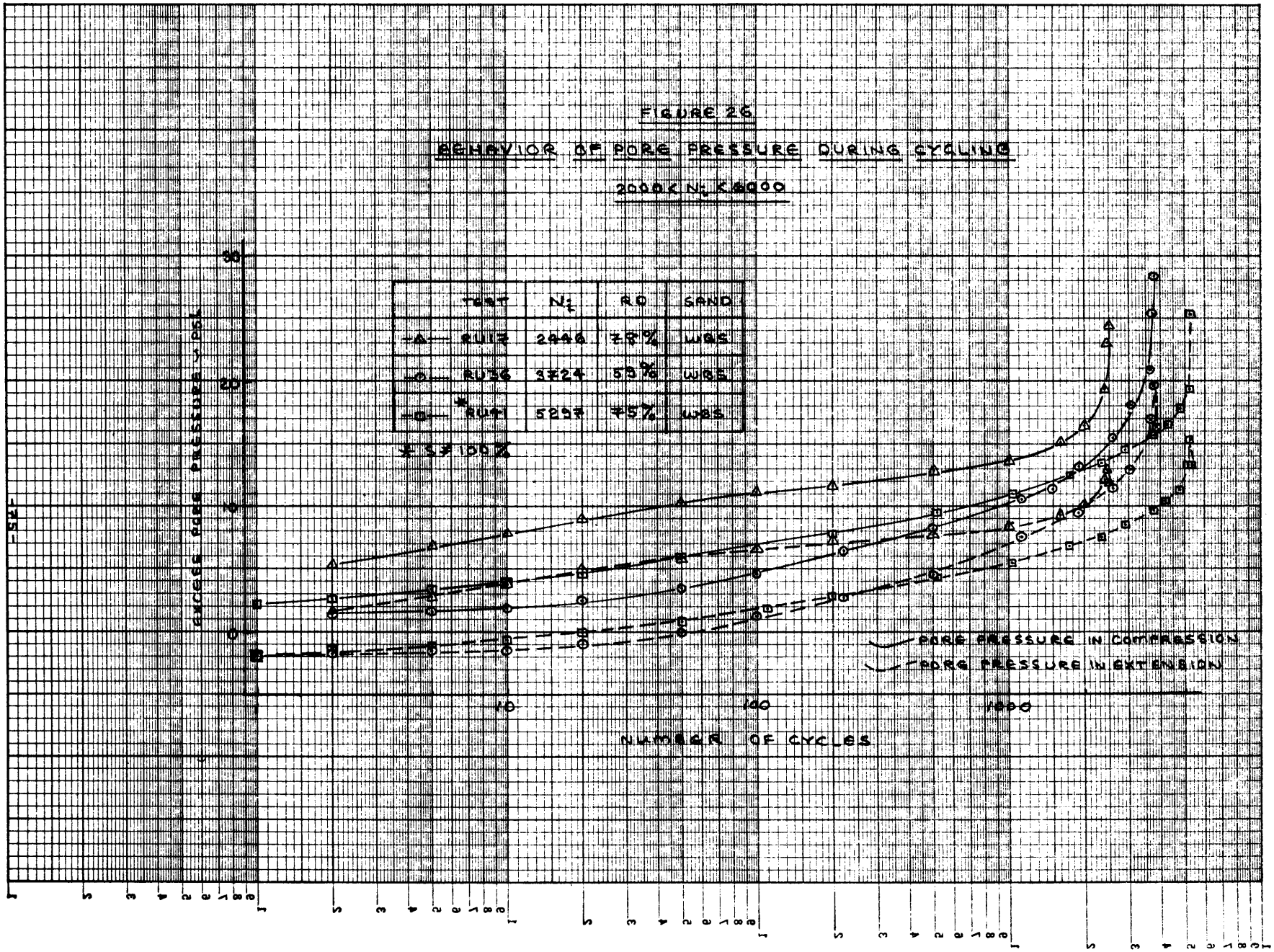

FIGURE 27

BEHAVIOR OF PORE PRESSURE DURING CYCLING

$300 < N_L < 700$

PORE PRESSURE IN EXTENSION

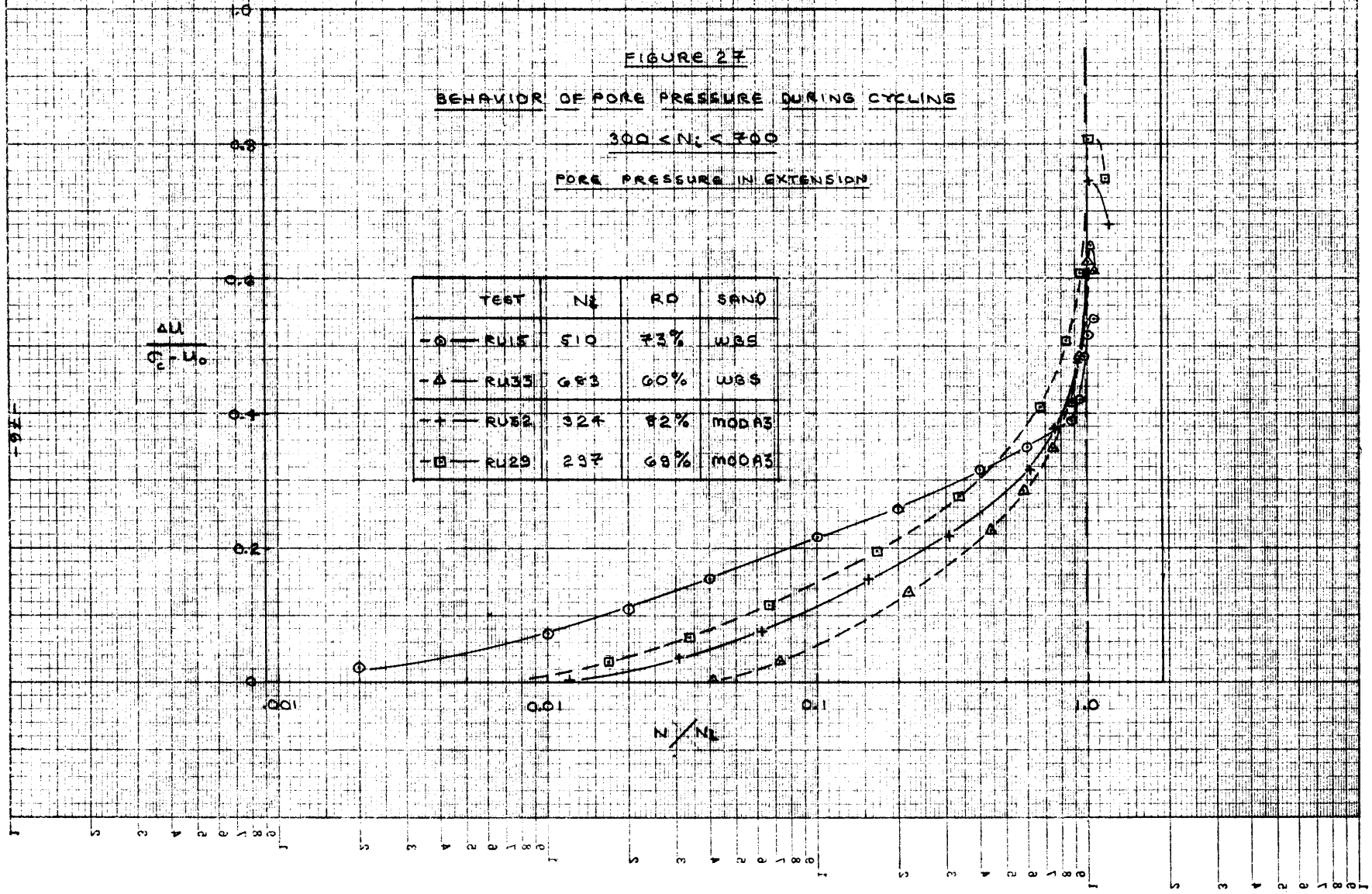

TEST	N_L	RD	SAND
-⊙— RU15	510	73%	WBS
-△— RU33	683	60%	WBS
-+— RU52	324	82%	MODA3
-⊡— RU29	237	68%	MODA3

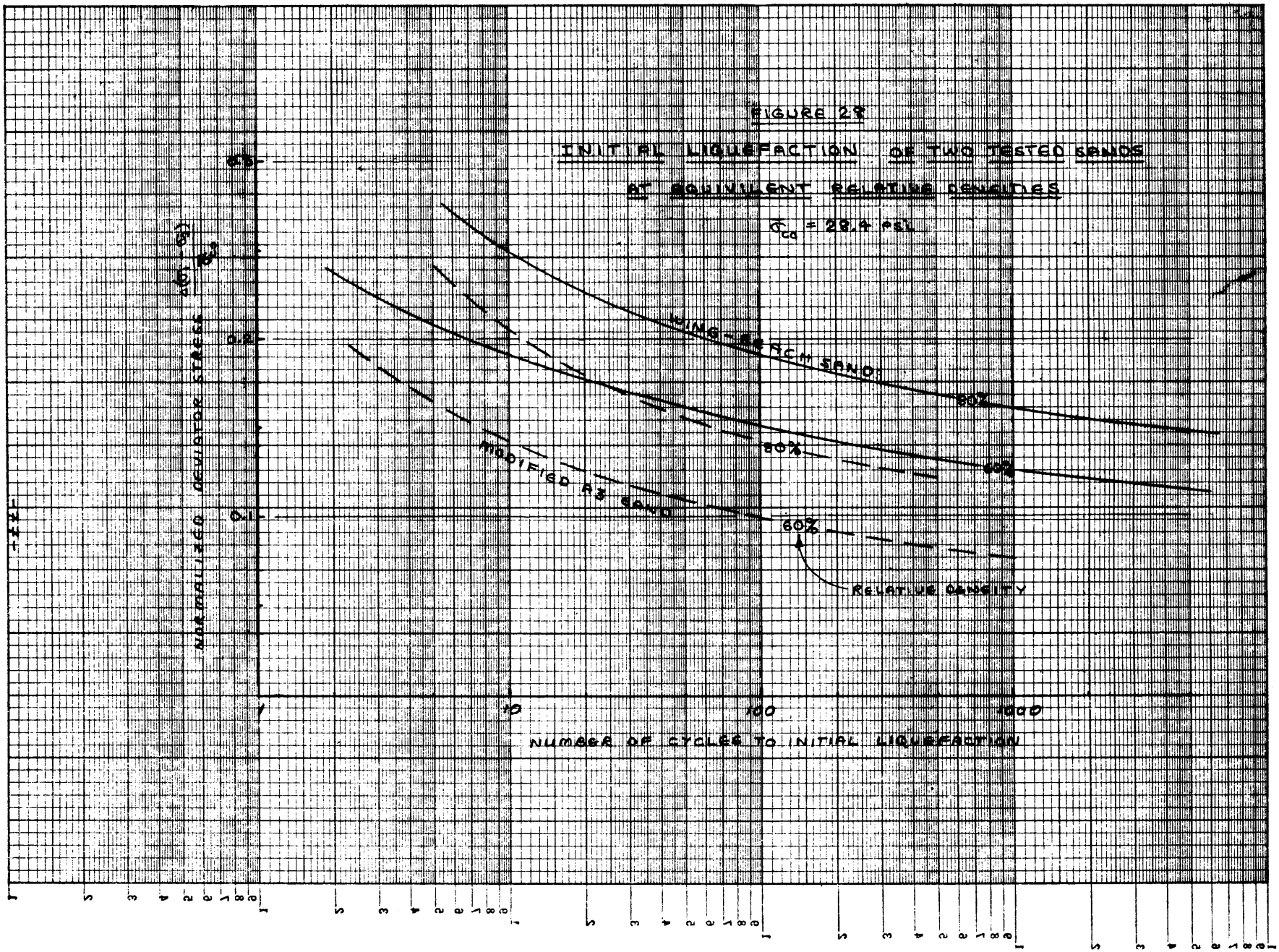
FIGURE 23
INITIAL LIQUEFACTION OF TWO TESTED SANDS
AT EQUIVALENT RELATIVE DENSITIES
σ_{cc} = 28.4 PSI
FINE - TO MEDIUM SAND
80%
60%
MODIFIED AF SAND
60%
RELATIVE DENSITY
NORMALIZED DEVIATOR STRESS, $\frac{\sigma_d}{2\sigma_{cc}}$
0.5
0.2
0.1
1
10
100
1000
NUMBER OF CYCLES TO INITIAL LIQUEFACTION

FIGURE 29

INITIAL LIQUEFACTION OF TWO TESTED SANDS AT EQUIVALENT DRY UNIT WEIGHTS

$\sigma_{3c} = 28.4$ psi

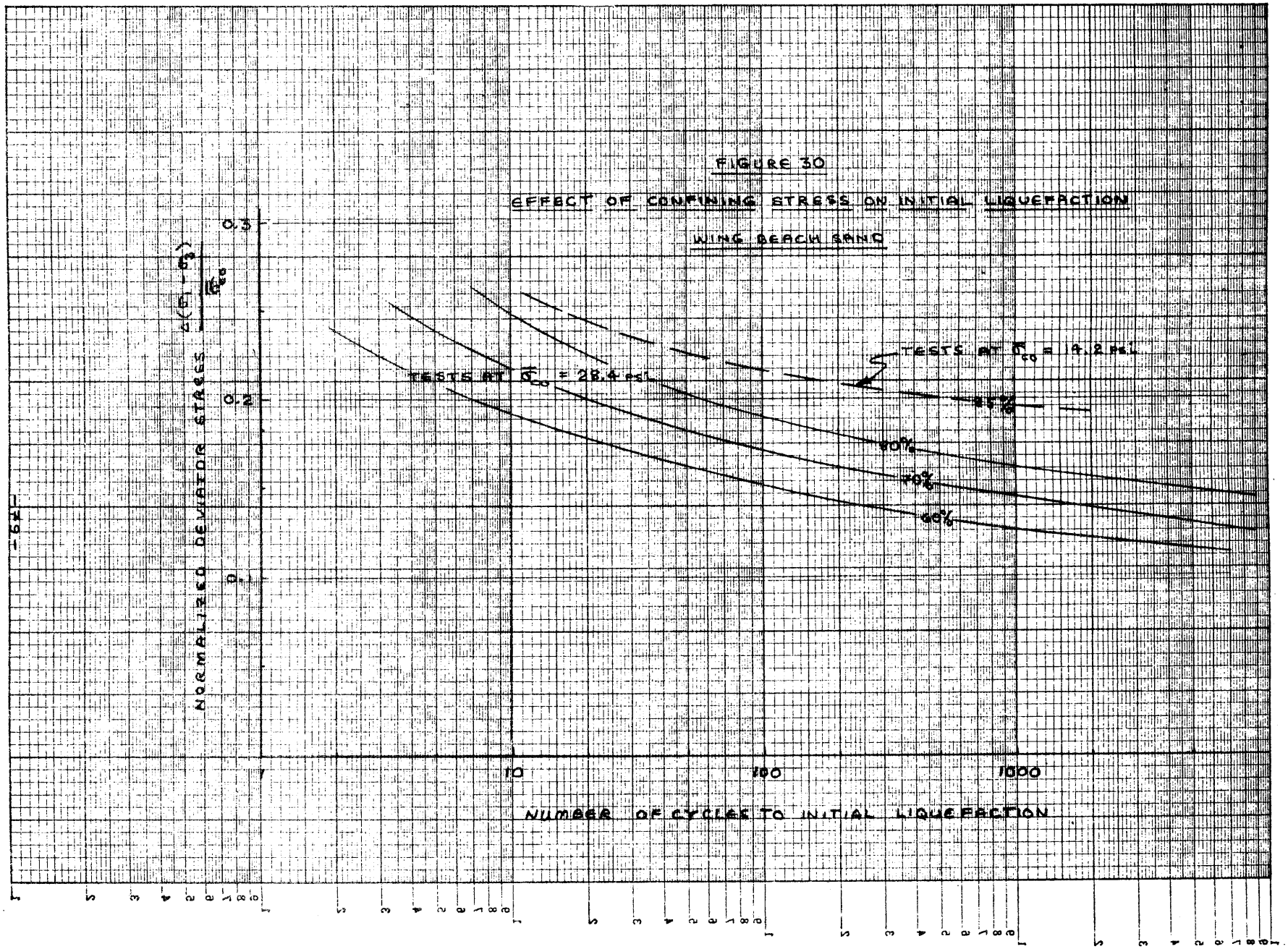
FIGURE 30
EFFECT OF CONFINING STRESS ON INITIAL LIQUEFACTION
WING BEACH SAND
NORMALIZED DEVIATOR STRESS $\frac{\Delta(\sigma_1 - \sigma_3)}{2\bar{\sigma}_{c_0}}$
0.3
0.2
TESTS AT $\bar{\sigma}_{c_0}$ = 28.4 psi
TESTS AT $\bar{\sigma}_{c_0}$ = 14.2 psi
80%
70%
60%
10
100
1000
NUMBER OF CYCLES TO INITIAL LIQUEFACTION

FIGURE 31

EFFECT OF INCOMPLETE SATURATION ON LIQUEFACTION

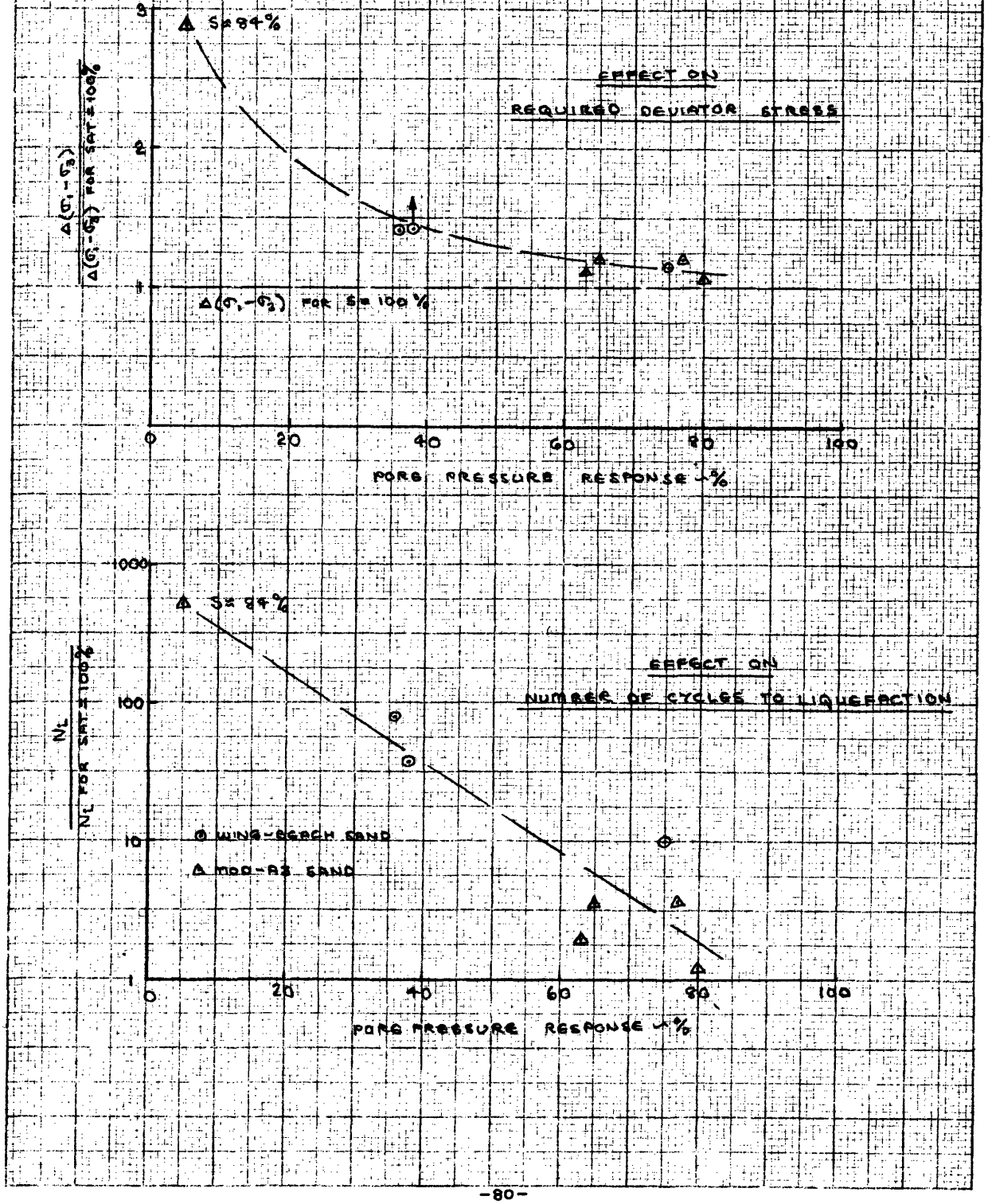

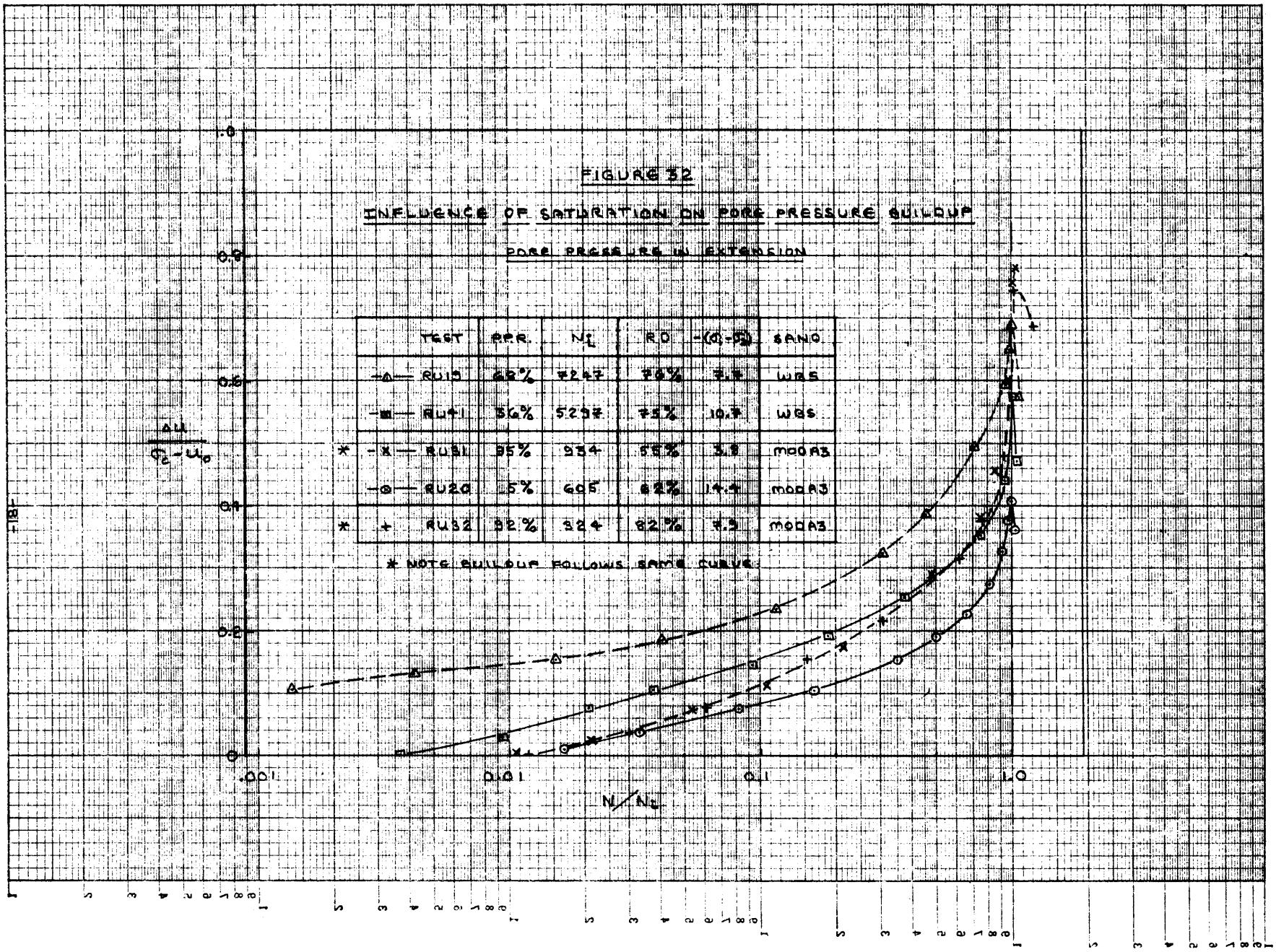
FIGURE 32
INFLUENCE OF SATURATION ON PORE PRESSURE BUILDUP
PORE PRESSURE IN EXTRUSION
TEST | APP. | N_L | RD | $-(\sigma_3-u_0)$ | SAND
RU13 | 62% | 2247 | 76% | 7.7 | WBS
RU11 | 56% | 5237 | 75% | 10.7 | WBS
RU31 | 35% | 934 | 56% | 3.8 | MODAB
RU20 | 5% | 605 | 82% | 14.4 | MODAB
RU32 | 32% | 324 | 82% | 4.3 | MODAB
* NOTE BUILDUP FOLLOWS SAME CURVE
$\frac{\Delta u}{\sigma_3 - u_0}$
N/N_L
1.0
0.8
0.6
0.4
0.2
0
.001
0.01
0.1
1.0

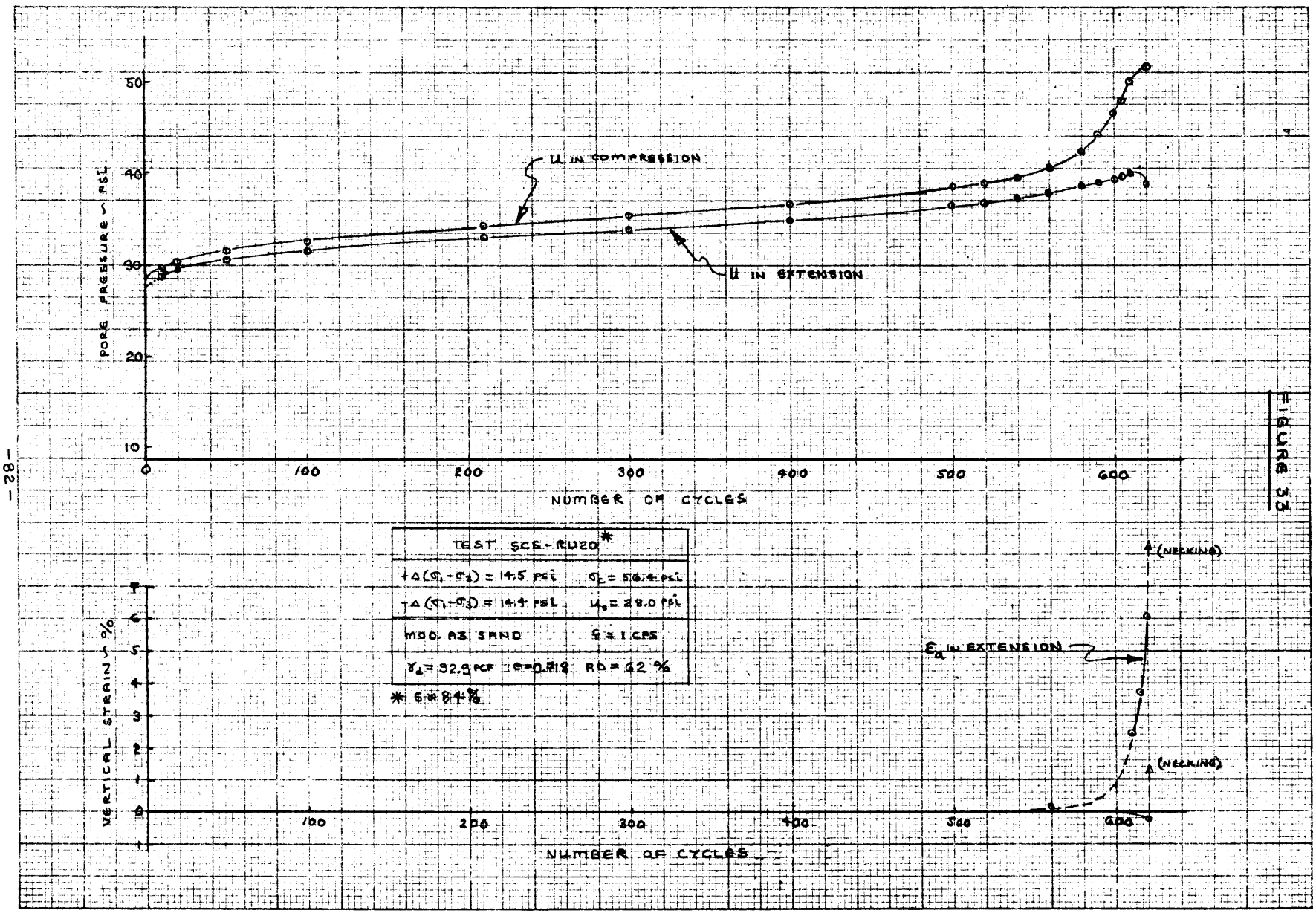
PORE PRESSURE, PSI
50
40
30
20
10
0
100
200
300
400
500
600
NUMBER OF CYCLES
U IN COMPRESSION
U IN EXTENSION
TEST SCS-RU20*
+Δ(σ1-σ3) = 14.5 PSI
σc = 51.4 PSI
-Δ(σ1-σ3) = 14.4 PSI
Uo = 28.0 PSI
MOD. A3 SAND
f = 1 CPS
γd = 92.9 PCF
e = 0.718
RD = 42 %
* S = 84 %
VERTICAL STRAIN, %
6
5
4
3
2
1
0
-1
100
200
300
400
500
600
NUMBER OF CYCLES
εa IN EXTENSION
(NECKING)
(NECKING)

FIGURE 33

FIGURE 34

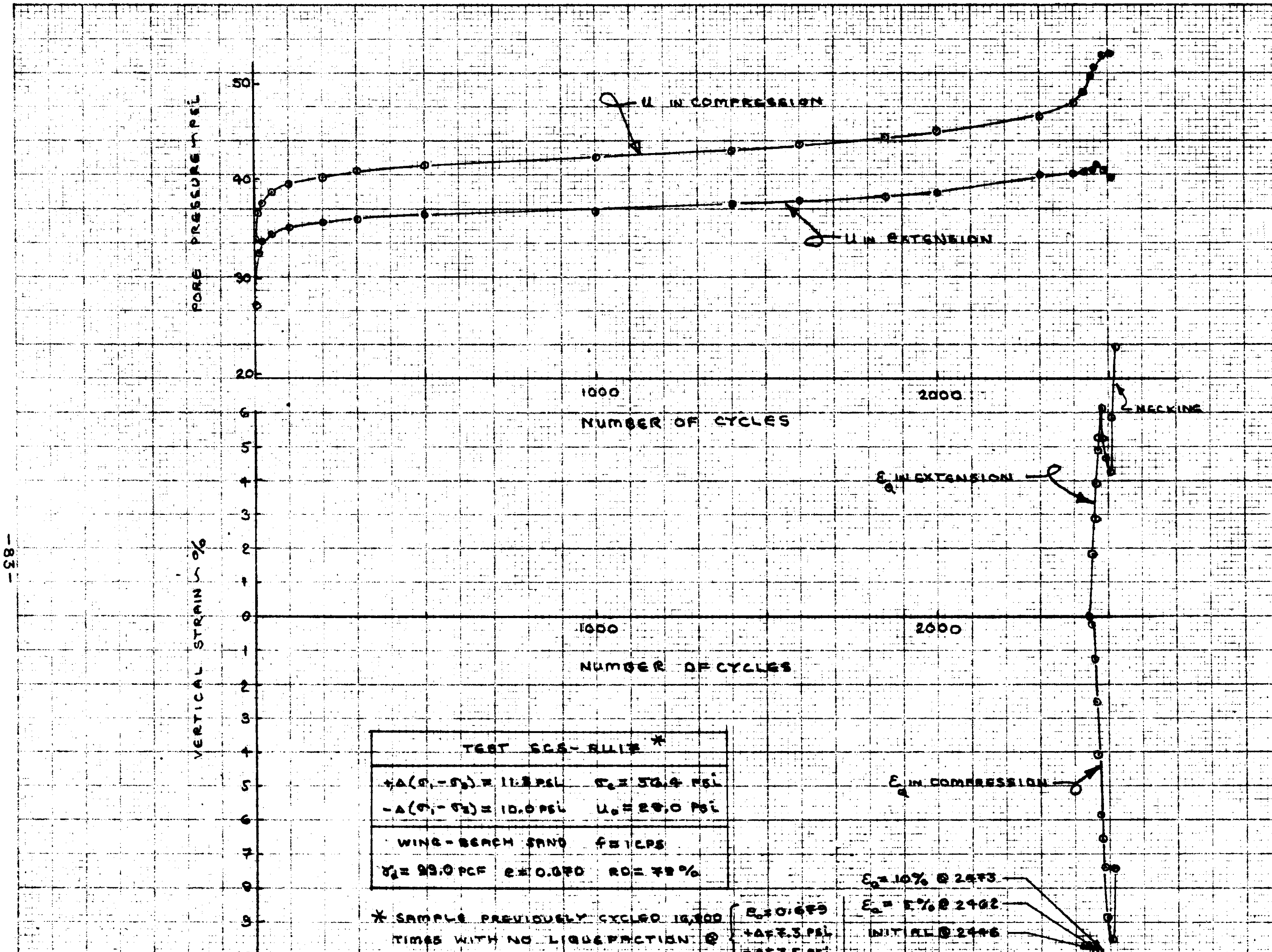
PORE PRESSURE ~ PSI
50
40
30
20
U IN COMPRESSION
U IN EXTENSION
1000
2000
NUMBER OF CYCLES
NECKING
VERTICAL STRAIN ~ %
6
5
4
3
2
1
0
1
2
3
4
5
6
7
8
9
10
ε_a IN EXTENSION
ε_a IN COMPRESSION
1000
2000
NUMBER OF CYCLES
TEST SCS-RUIZ *
$+\Delta(\sigma_1-\sigma_3)$ = 11.8 PSI σ_c = 50.4 PSI
$-\Delta(\sigma_1-\sigma_3)$ = 10.0 PSI u_o = 29.0 PSI
WING-BEACH SAND   f = 1 CPS
γ_d = 99.0 PCF   e = 0.670   RD = 78 %
* SAMPLE PREVIOUSLY CYCLED 16,800 TIMES WITH NO LIQUEFACTION @
e_o = 0.679
$+\Delta$ = 7.3 PSI
$-\Delta$ = 7.5 PSI
ε_a = 10% @ 2473
ε_a = 5% @ 2462
INITIAL @ 2446

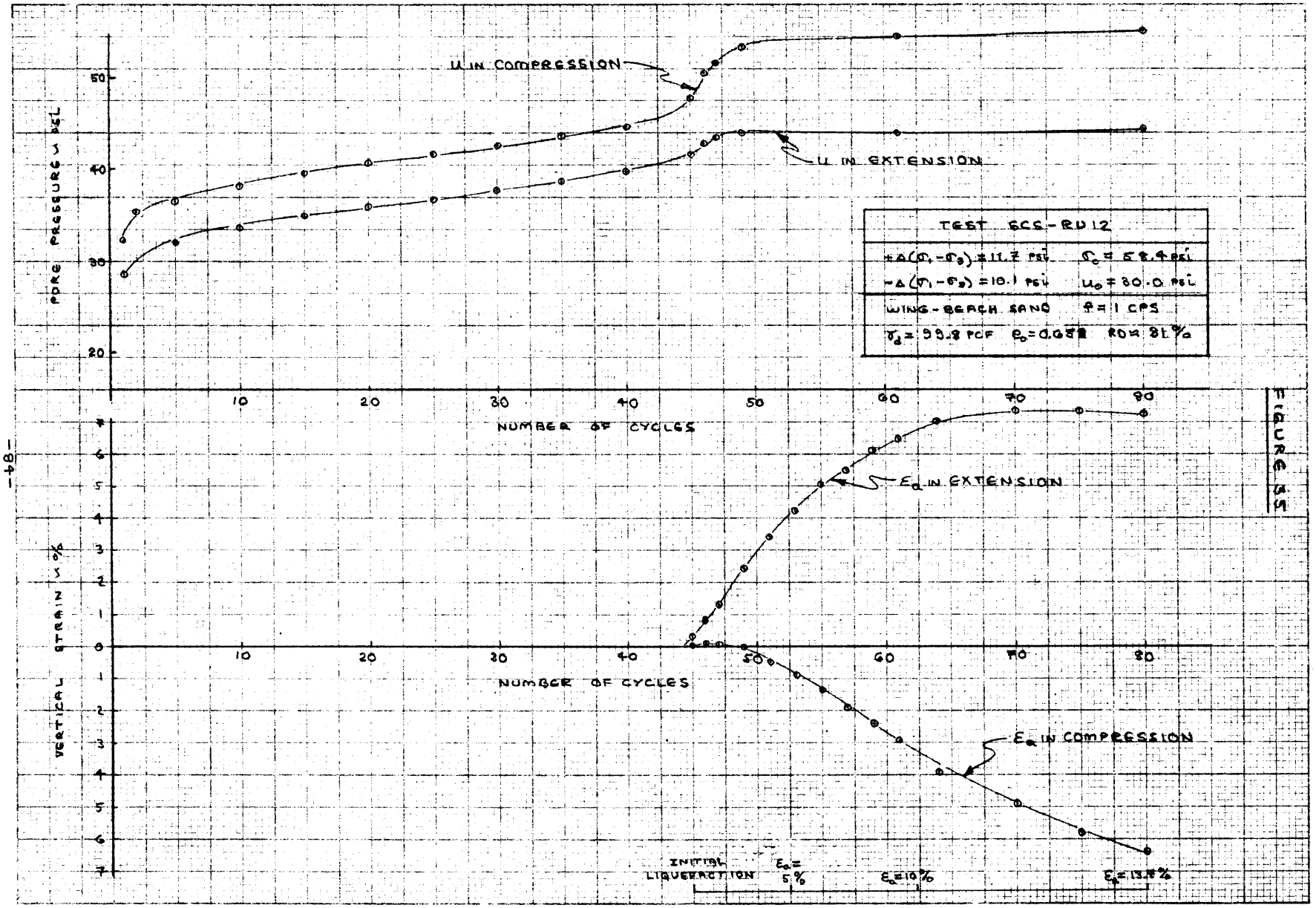
u IN COMPRESSION
u IN EXTENSION
PORE PRESSURE, psi
NUMBER OF CYCLES
TEST SCS-RD 12
+Δ(σ1-σ3) = 11.7 psi
σc = 58.4 psi
-Δ(σ1-σ3) = 10.1 psi
uo = 30.0 psi
WING-BEACH SAND
f = 1 CPS
γd = 99.8 PCF
eo = 0.658
RD = 81%
VERTICAL STRAIN, %
εd IN EXTENSION
εd IN COMPRESSION
INITIAL LIQUEFACTION
εd = 5%
εd = 10%
εd = 13.8%

FIGURE 55

FIGURE 36

CHANGE IN VOLUME AFTER LIQUEFACTION

FIGURE 37

COMPARISON OF SACRAMENTO RIVER SAND LIQUEFACTION* WITH TESTED SANDS (ALL TESTS AT RD=78%)

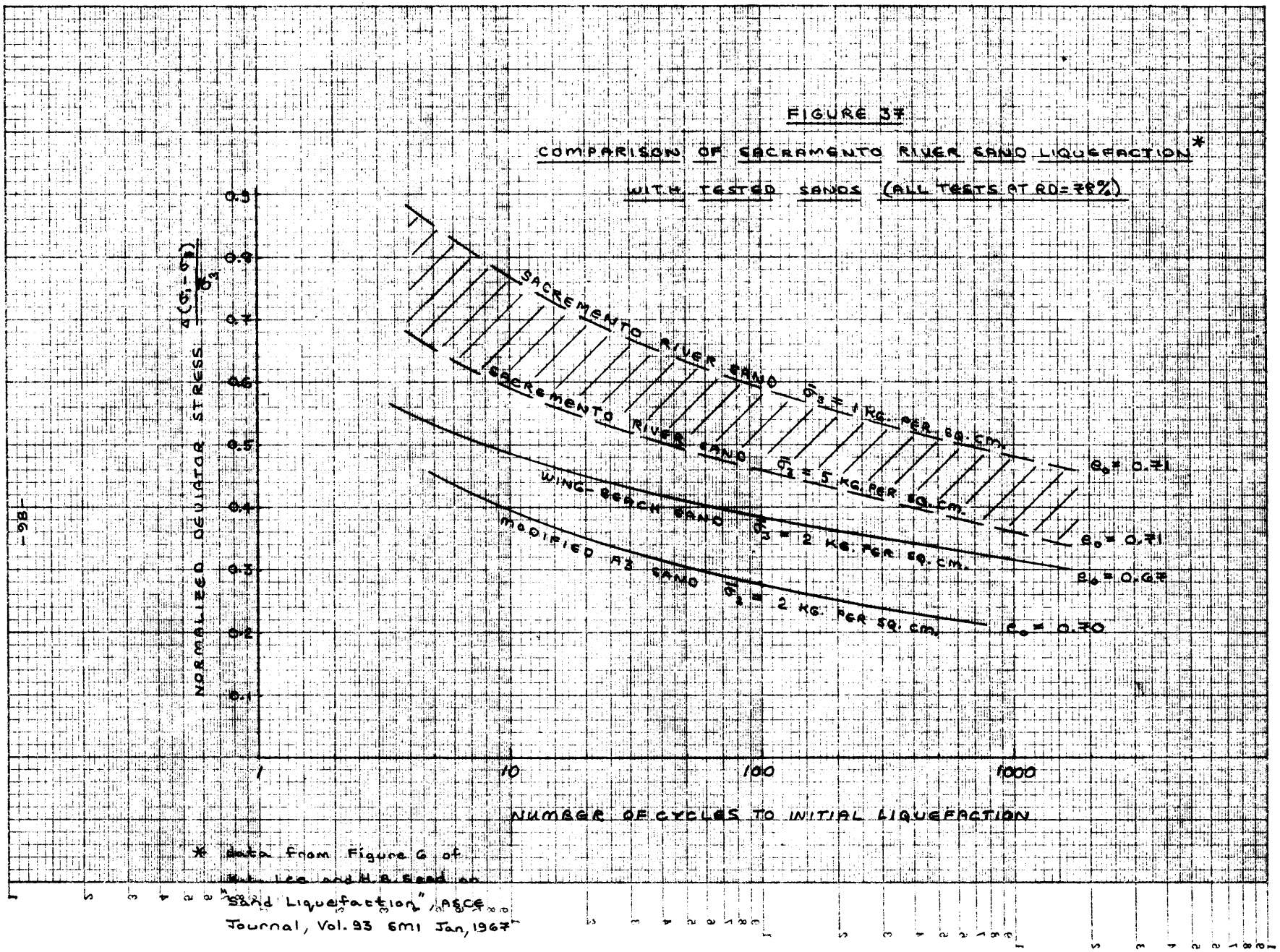

* Data from Figure 6 of H.B. Seed and I.M. Lee, "Sand Liquefaction", ASCE Journal, Vol. 93 SM1 Jan, 1967

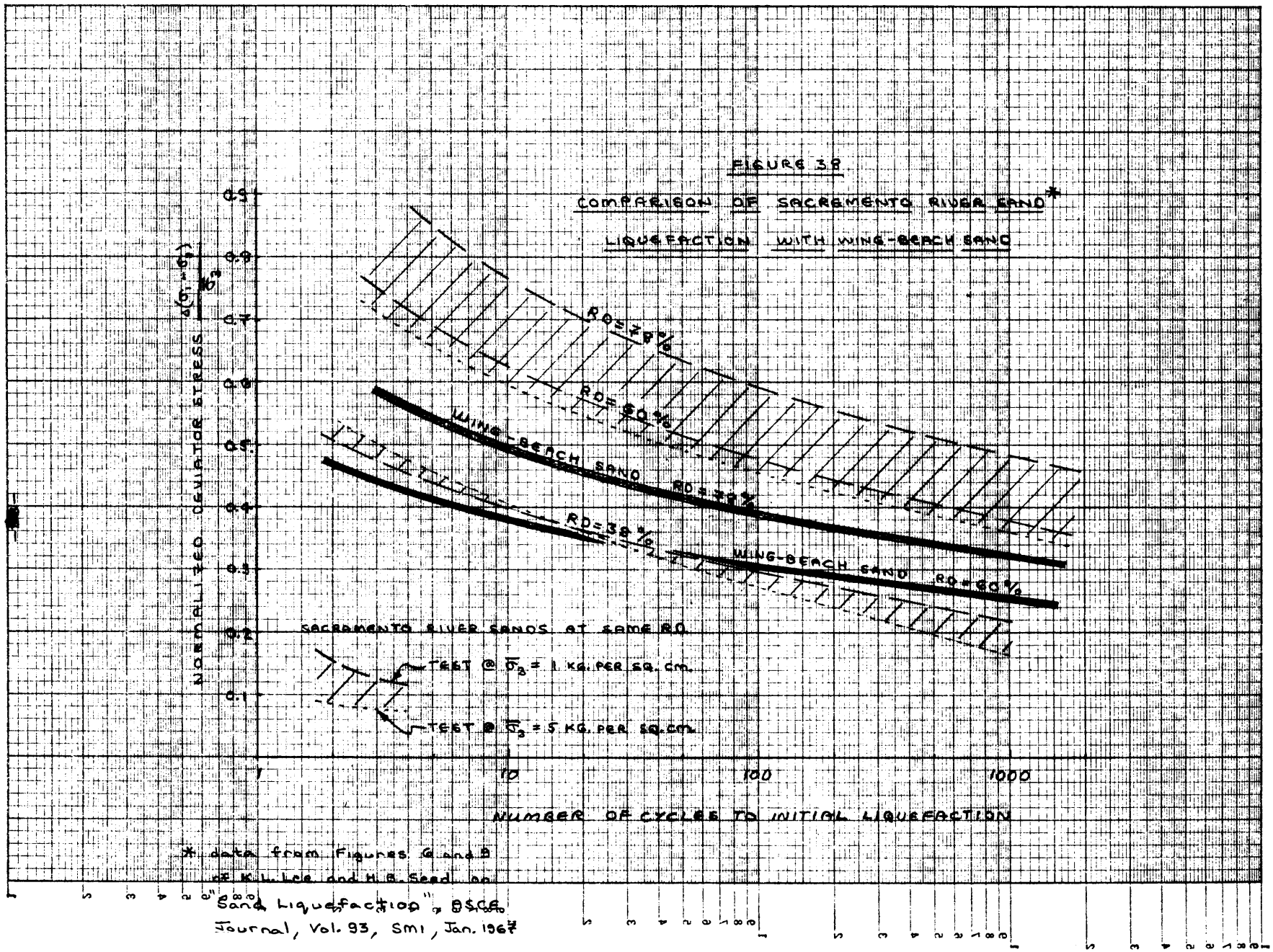
FIGURE 38
COMPARISON OF SACRAMENTO RIVER SAND* LIQUEFACTION WITH WING-BEACH SAND
NORMALIZED OSCILLATOR STRESS $\frac{\Delta(\sigma_1-\sigma_3)}{2\sigma_3}$
RD = 90%
RD = 80%
WING-BEACH SAND RD = 70%
RD = 38%
WING-BEACH SAND RD = 60%
SACRAMENTO RIVER SANDS AT SAME RD
TEST @ σ_3 = 1 KG. PER SQ. CM.
TEST @ σ_3 = 5 KG. PER SQ. CM.
0.9
0.8
0.7
0.6
0.5
0.4
0.3
0.2
0.1
1
10
100
1000
NUMBER OF CYCLES TO INITIAL LIQUEFACTION
* data from Figures 6 and 8 of H. B. Seed and K. L. Lee "Liquefaction of Saturated Sands", ASCE Journal, Vol. 93, SM1, Jan. 1967

FIGURE 39

GRAIN SIZE DISTRIBUTION

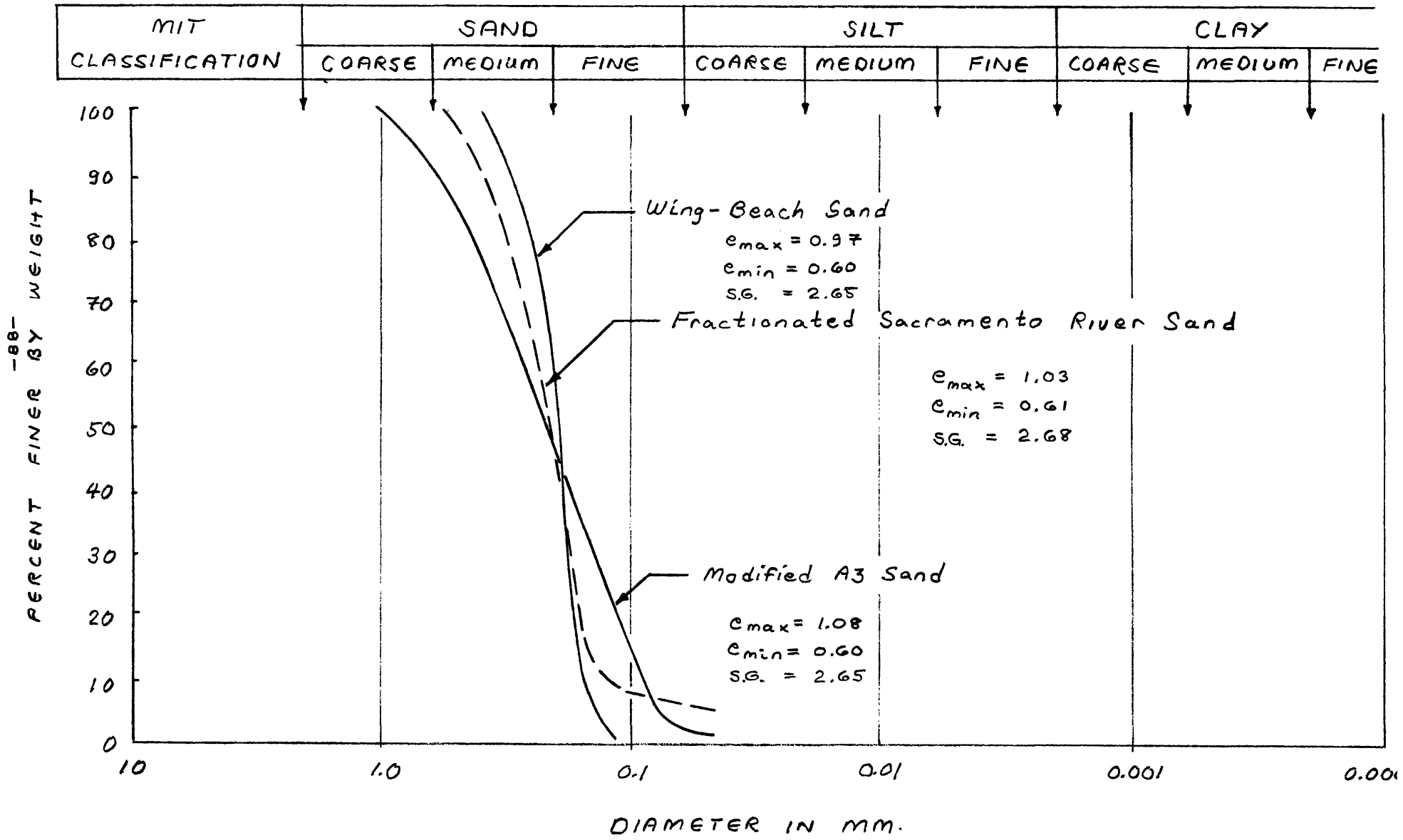

APPENDIX A

EQUIPMENT

The equipment used in the cyclic loading tests is shown in Figure A-1 with a test in progress. Appendix A will describe individual characteristics under sub-headings of loading, testing and measurement equipment.

A.1 Loading Equipment

The stress application device is shown in Figures A-2 and B-2.c. This apparatus consists of two pressure chambers or "pots" with rubber diaphram seals at both ends of each pot. A movable piston passes through the center of each pot and is guided by bushings at either end of the device. Air pressure in the top or bottom pot forces the piston upward or downward over a total distance of travel equal to 2 inches. The stress applicator is positioned over a triaxial cell and is rigidly connected by three legs, adjustable for allignment. Attachment to the piston of the terminal cell is made through a threaded connector into which both pistons are clamped. The lower half of this connection appears in Figure B-2.b with the slotted piston grove and split washer covered by the connection nut. Each pot can withstand inside pressures greater then 100 psi, although not over 40 psi was used during testing. An axial piston force of approximately 40 pounds is created by a change in pot pressure of 10 psi.

The dynamic stress control device used for cycling air pressure to the stress applicator is shown schematically in Figure A-3 and is the wooden box in the center of Figure A-1. This device consists basically

of two large capacity pressure tanks, a solenoid valve, an electric counter, and tubing with required pressure regulators. Cyclic loads are applied by maintaining a constant pressure in the bottom pot of the stress applicator while cycling pressure between 0 psi and the pressure required to produce an equal but opposite stress. The "bottom pot pressure tank" is connected to the bottom stress pot and a compressive deviator stress is built up to the first cycle slowly with air pressure. The top stress applicator pot is connected to the "top pot pressure tank" through a solenoid initially open to atmospheric pressure. Activation of the solenoid opens the flow path between the pot and tank, thus applying tank pressure to the top stress pot.

When the maximum pressure in the top pot produces twice the axial force as does the constant pressure in the bottom pot, equal but opposite deviator stresses are applied to the triaxial cell piston. Actual pressures are not simply X psi and 2X psi because of cell pressure acting over the triaxial piston area, adding an extra force in the extension direction. The pressures must be adjusted for this force dependent on cell pressures, and for piston friction. Cell pressure is maintained by another connection to a regulated high pressure source.

Pore pressure and volume flow measurements are controled by a system of mercury pots, burettes, and valves shown in Figure A-1. The control board is set up in such a way as to permit easy measurement of volume changes and control of top and bottom pore pressure lines.

Two timer systems were used for this testing program. All tests run after SCS-RU5 were cycled at 1.0 cycles per second. Tests SCS-RU1 to RU5 were run at 8.0 cycles per minute, and are part of the equipment testing series. In the later tests, two Intermatic industrial control

timers (solid state SS-10222-B1) were connected so to provide continuous ON-OFF timing controls, and theoretically has a timing range of .05 to 0.5 seconds for each half cycle. Calibration of the device shows that cycling periods between 1.0 and 6.0 cycles per second are possible. The other timer system (described in IAP Progress Report I, 1967) has a range of 5 cycles per hour to 5 cycles per minute.

A.2 Testing Equipment

This section contains a description of the modified Norwegian (Geonor) triaxial cell shown in Figures A-2 and B-1.a. This cell was previously used for test series reported in two previous M.I.T. Inter-American publications. The latest tests were run in the saturated state and under reversing cyclic loads, requiring considerable change.

An additional lift or shim was added to the base plate to allow room for large strains in extension. A pore pressure transducer connection was machined to provide for measurement of pressure at the base of tested samples (Figure A-4.a). High rigidity is required to prevent expansion during pore pressure increases in this and all other connections open to the sample pores. A new top cap was designed to allow for addition of a top drainage line and for positive connection to the piston during the extension phase of cycling.

Several methods of top cap to piston connection were studied. Consideration was given to limited space available, sequence of assembly, degree of freedom, and degree of "positive" grip. The design chosen is shown connected in Figure A-4.b and unconnected in Figure B-1.c. This is the most simple method considered, but because of its pin connection allows some relative movement between the top cap and piston. The

connection, visible in the two figures mentioned, is actually made between the sample top cap and the load cell attached to the piston.

Constant volume valves were installed in pore pressure line connections. Due to allignment problems it was necessary to provide constant lubrication of piston area in contact with the triaxial cell bushing. Standard methods could not be used because the cell stays only two thirds full of water, and bushing-piston clearance was great enough to cause some oil flow toward the atmospheric end. A continuous oil bath was fed at 0.2 psi above cell pressure to a small ring chamber directly beneath the bushing. This allowed significantly better calibration of the stress applicator and prevented most air leakage from the triaxial cell.

A.3 Measurement Equipment

In rapid cyclic testing it is virtually a necessity to monitor desired quantities electrically. This was done with the three parameters measured during testing. A load cell, pressure transducer and L.D.T. (Linearsyn Differential Transformer) were used for axial force, pore pressure, and strain measurements. Electircal output from each device was then recorded on either a dual channel continuous recorder or on an X-Y recorder.

The load cell used was placed above the sample top cap and measured force transmitted directly on the sample as shown in Figure A-4.b. This cell, manufactured by Strainsert of Bryn Mawr, Pennsylvania, is unaffected by chamber pressure and has its connections sealed against water contact. The seal had to be replaced several times due to cracking. Calibration checks (over a dozen) were run after every few tests and revealed a

drift in zero-load output but no change in slope of the calibration curve. A zero-load reading was taken before each test for accurate force calculation. Specifications on the load cell are as follows:

(Strainsert Flat Load Cell-Universal)

Output signal = 3 mv/volt

Force range = 0 to 1000 pounds

(also linear over - 50 to 0 pounds)

Single bridge

Accuracy = 0.2 pounds (under conditions used)

Excitation voltages used were 6.00, 20.00 and 24.00 volts D.C. depending on magnitude of output desired and on available power sources. Load cell output was traced by an X-Y recorder described later in this section. A sample test record of X-Y trace for SCS-RU12 is shown in Figure A-5. Because of poor recorder response, tracings such as that in Figure A-5 serve only to monitor the magnitude of pulsating deviator stress. Special tests (at short tracing-arm movements) were used to establish the load-time history form as shown in Figure 3.a.

The pore pressure transducer used in testing is shown in Figure A-4.a. It is connected to the base plate at the triaxial cell and has a one sixteenth of an inch channel open to a porous stone at the base of the sand sample. This transducer is built by Dynisco of Cambridge, Massachusetts, and has the following characteristics:

Output signal = 3 mv/volt

Pressure range = 0 to 100 PSIA

Excitation voltage ~ 6 volts

Transducer output was traced continuously on one channel of the dual track recorder described later in this section. Performance of this

transducer was checked with several calibrations. Zero drift from temperature and seating changes did not affect output because of re-zeroing for initial readings before each test.

The L.D.T. used for registering strain is shown in Figure A-4.c. Measurement is made of vertical displacement from the triaxial piston to the cell top. Measured movement includes sample strain, movement in the pin connector between top cap and load cells as well as strain in other "rigid" connections. Movement of the pin connection is considerably larger than all other non-sample strains. This movement is of concern in cyclic measurements before liquefaction, making up approximately 50 percent of recorded strain. This movement, however, allows for better maintainance of isotropic conditions during applition of cell pressure and was considered an advantage. The L.D.T. is manufactured by Hewlett-Packard's Sanbord Division in Waltham, Massachusetts and has the following characteristics:

Output signal = 1.12 volts/inch/volt

Stroke range = ± 0.5 inches

Accuracy > .001 inches at small strains

(Resolution limited by recording apparatus)

Excitation voltage for both the L.D.T. and pressure transducer was 4.5 volts, supplied internally within the Sanborn recorder. Output is traced continuously on the recorder as shown by an actual test record (SCS-RU24) in Figure A-6.a. Magnitude of strains shown can be judged by the indicated traces at 5.7 and 10.3 percent strain after liquefaction.

The Sanborn dual-channel recorder used to trace strain and pore pressure output is shown in Figure A-4.d. Separate controls for each

channel are located on either side of the control panel. The recorder has built in D.C. power at 4.5 volts for both channels, if desired. A test recording is shown full size in Figure A-6. Important specifications and characteristics are as follows:

(Sanborn 321 Dual Channel
Carrier Amplifier - Recorder)
Power Requirements = 120 v, 60 cycle, single phase
Recording speeds = 1, 5, 20, 100 mm/second
Sensitivity = 0.01 mv/paper division
Attenuation factors = 1, 2, 5, 10, 20, 50, 100, 200
Response time = 5 milleseconds (10% to 90% deflection)
Overshoot = 4% maximum
Excitation = 4.5 to 5.0 volts at 2400 cycles per second

Recordings were made on the dual 10 cm. (50 division) track paper shown in Figure A-6. Timer markings are traced on the extreme right of the paper at one second intervals for speed-time correlation. The paper itself is heat sensitive and is marked by heated "points" on galvanometer arms. Positioning and balancing for initial output are accomplished by a relatively simple proceedure of resistance bridge adjustment. Performance of the recorder was excellent for this work although some channel interaction was discovered under specific conditions. This interaction was linear and could be corrected with calibration curves. From the listed specifications above, it can be seen that limitations on these cyclic tests are not imposed by the Sanborn recorder.

The X-Y recorder used for load cell output recordings is shown in the lower right of Figure A-1. The recorded trace (Figure A-5) used as an example shows the time (cycles) versus load cell output (in millivolts)

mode of operation. Tracings are made by mechanical movement in an arm weighing several grams. Controls enable amplification and horizontal travel speed to be varied over any range desired in the tests.

Use of this recorder in dynamic tests is limited by relatively slow following ability of the recording arm and point. Most tests were run at higher attenuation (less arm movement) than is shown in Figure A-5 because of this following difficulty. The trace in Figure A-5 yields stress data, but no information on "form" of load application . With carefully set controls it would be possible to work at a cycling speed of 2 to 3 cps. Calibration checks were made before each test over the scale of output to be used in the test. No data on specifications is presented for this recorder because the device is really not suitable for future use.

FIGURE A.1: CYCLIC STRESS TEST IN PROGRESS

FIGURE A2

CYCLIC TRIAXIAL EQUIPMENT

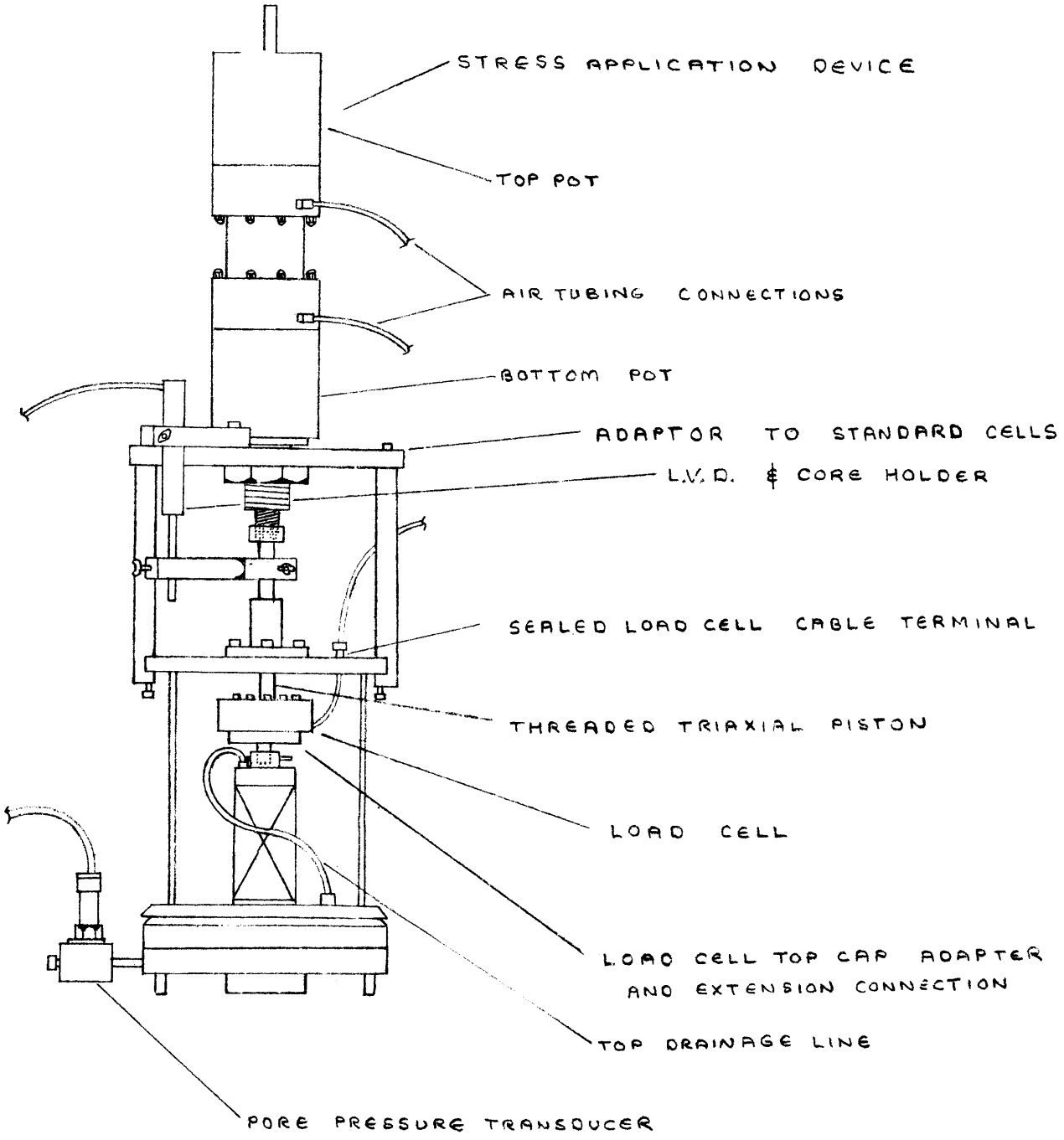

FIGURE A3

DYNAMIC STRESS CONTROL DEVICE

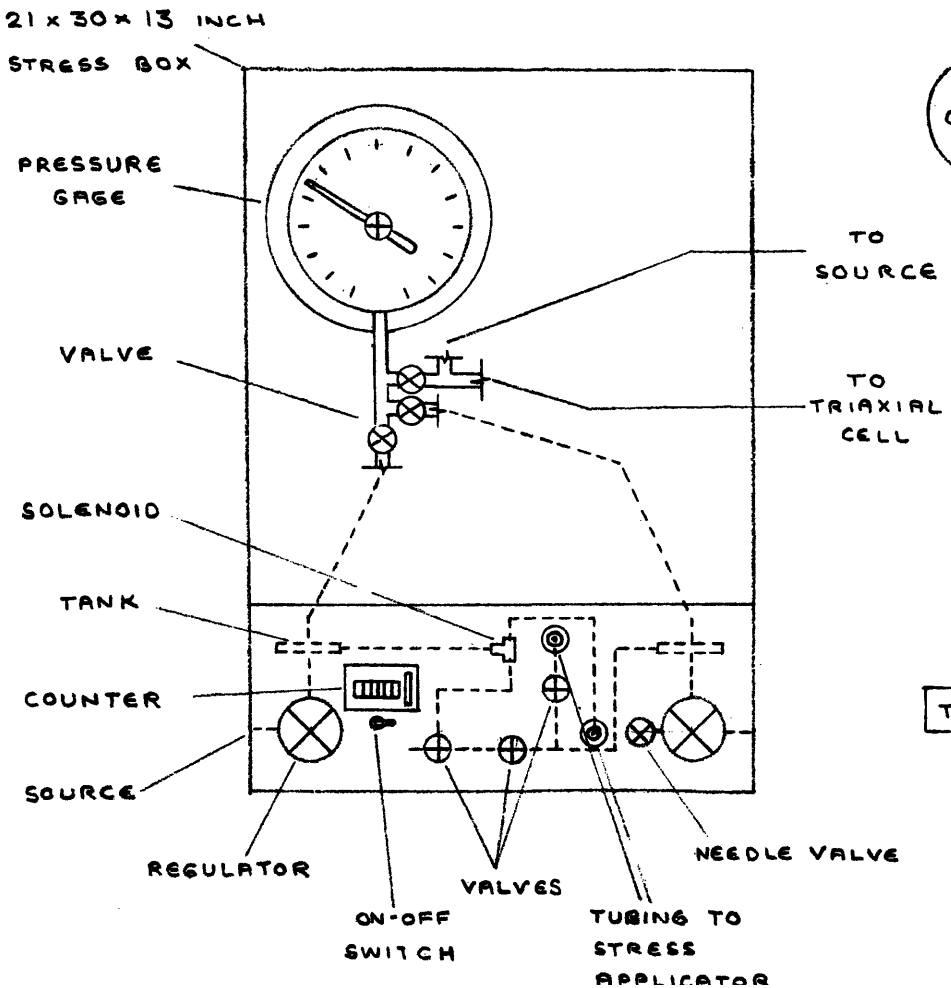

BASIC SCHEMATIC

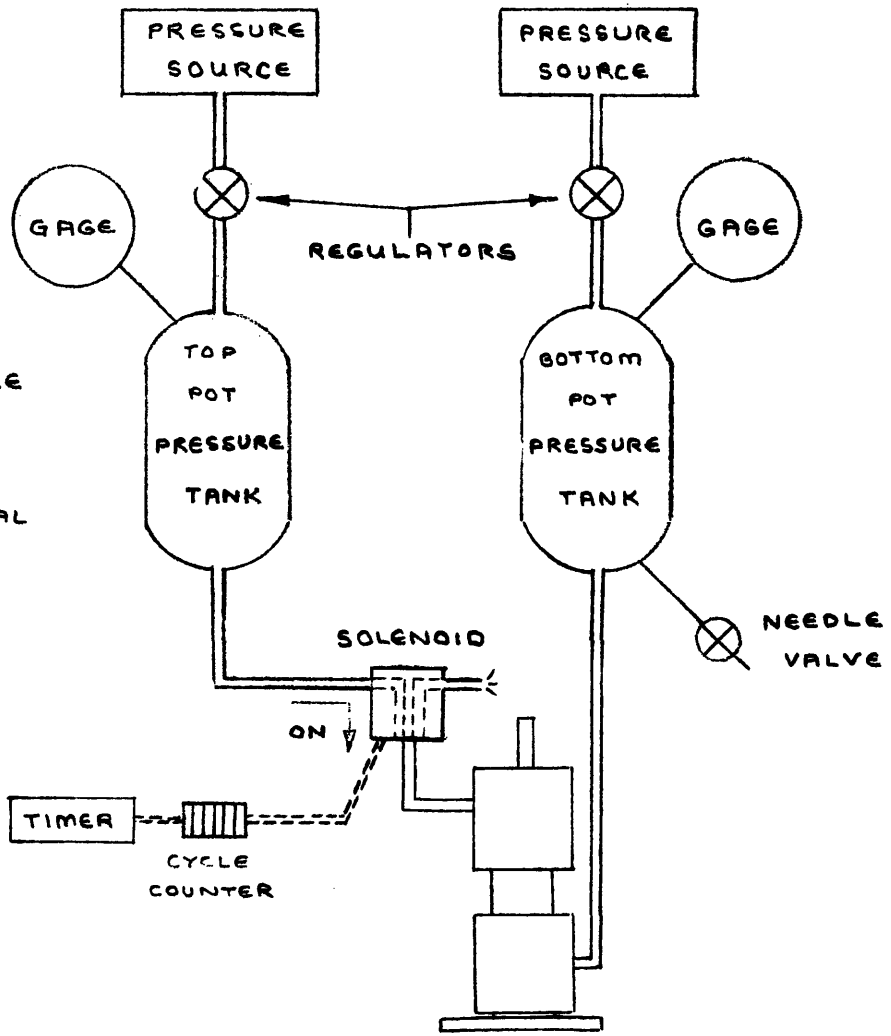

FIGURE A.4: MEASURING EQUIPMENT

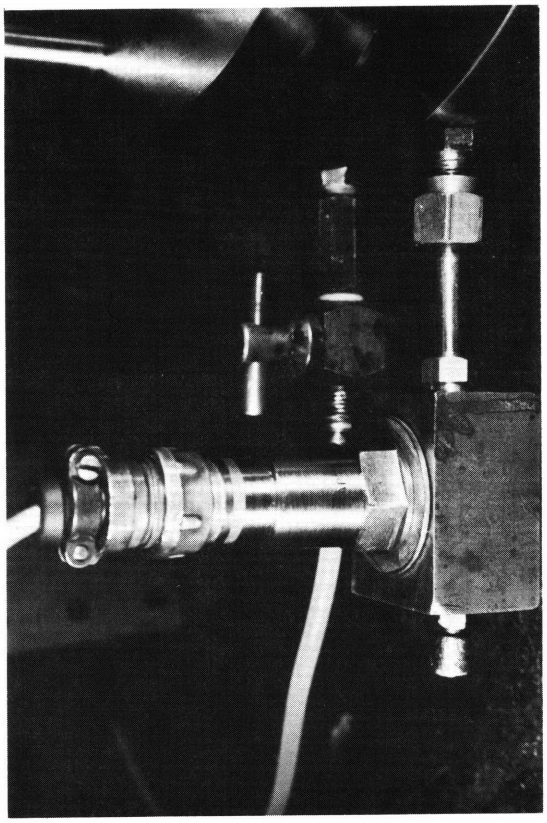

(a) Pore Pressure Transducer

(b) Load Cell on Piston

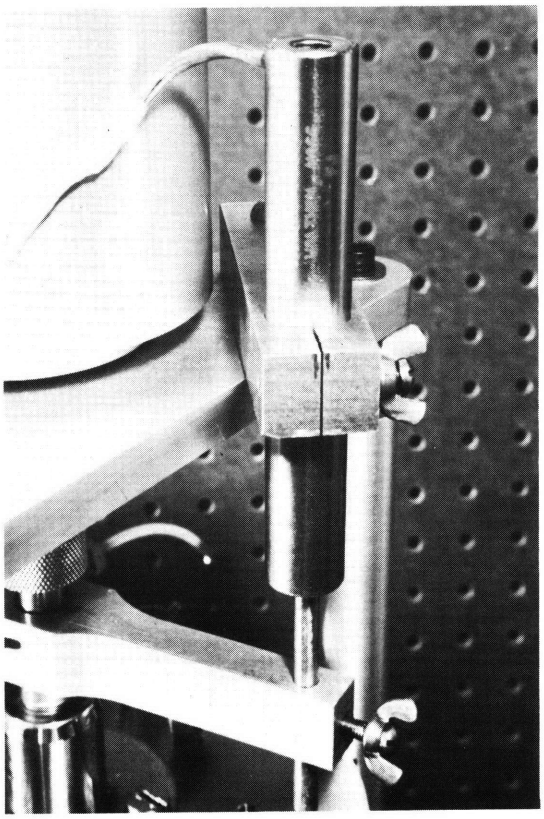

(c) LVDT for Strain Measurement

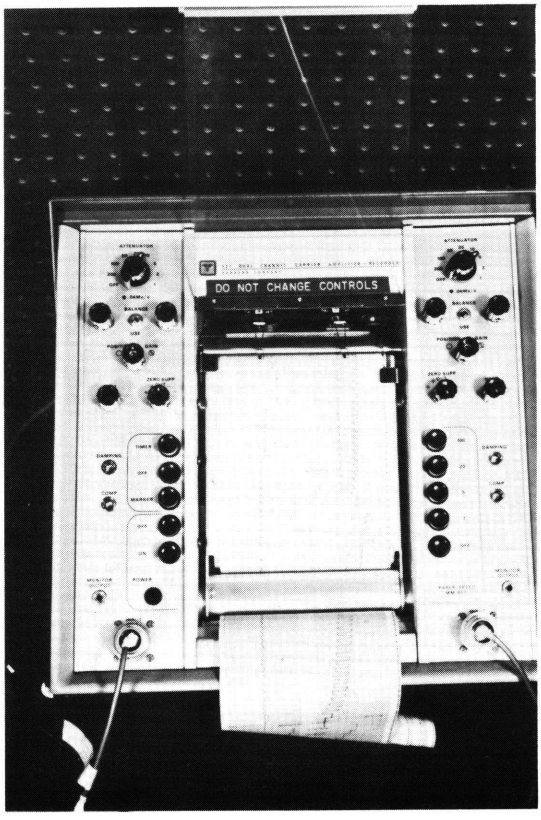

(d) Sanborn Dual Track Recorder

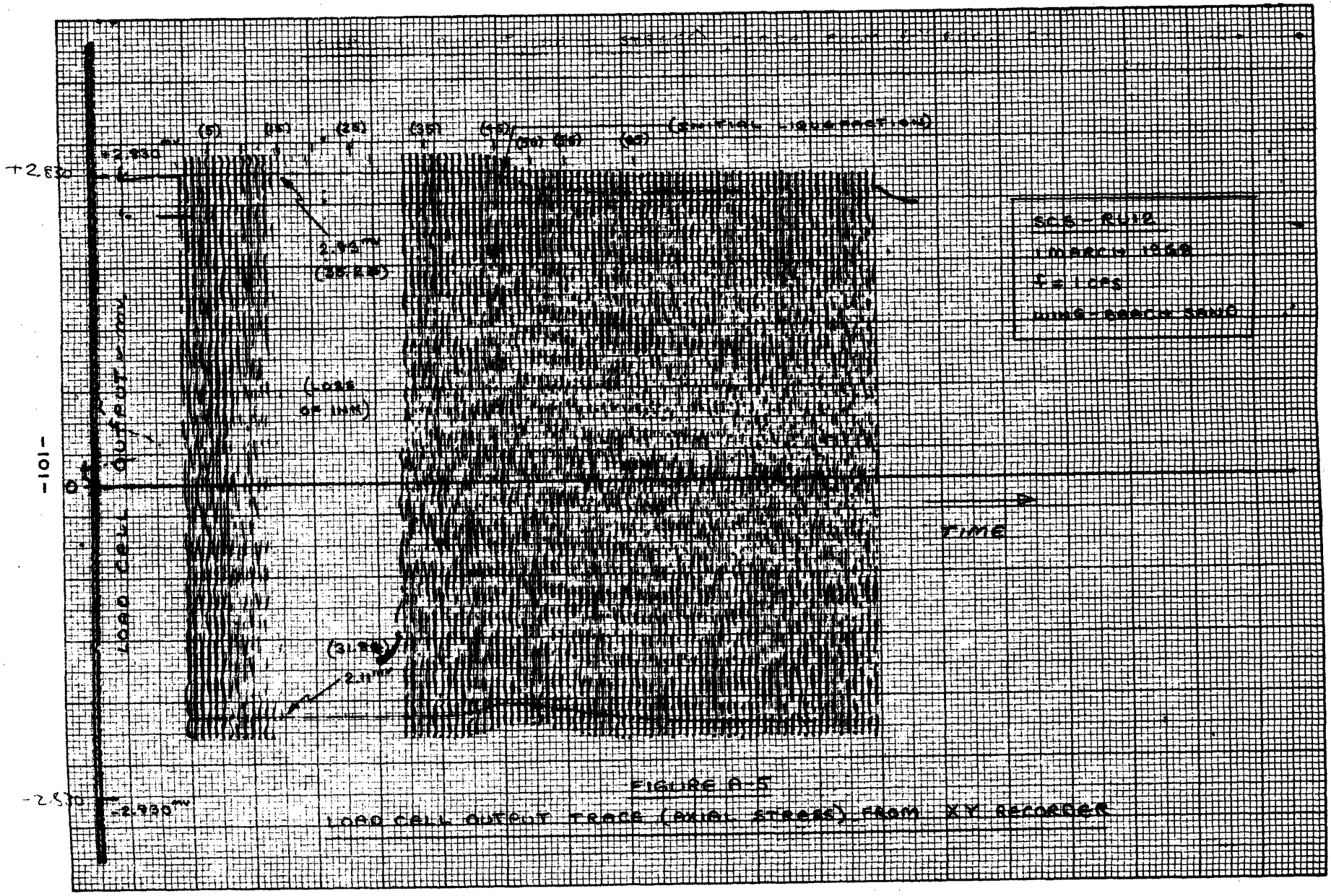

FIGURE A-5

LOAD CELL OUTPUT TRACE (AXIAL STRESS) FROM XY RECORDER

FIGURE A.6

SANBORN RECORDER TRACE

SCS-RU 24

A. LDT Trace

b. Pressure Transducer Trace

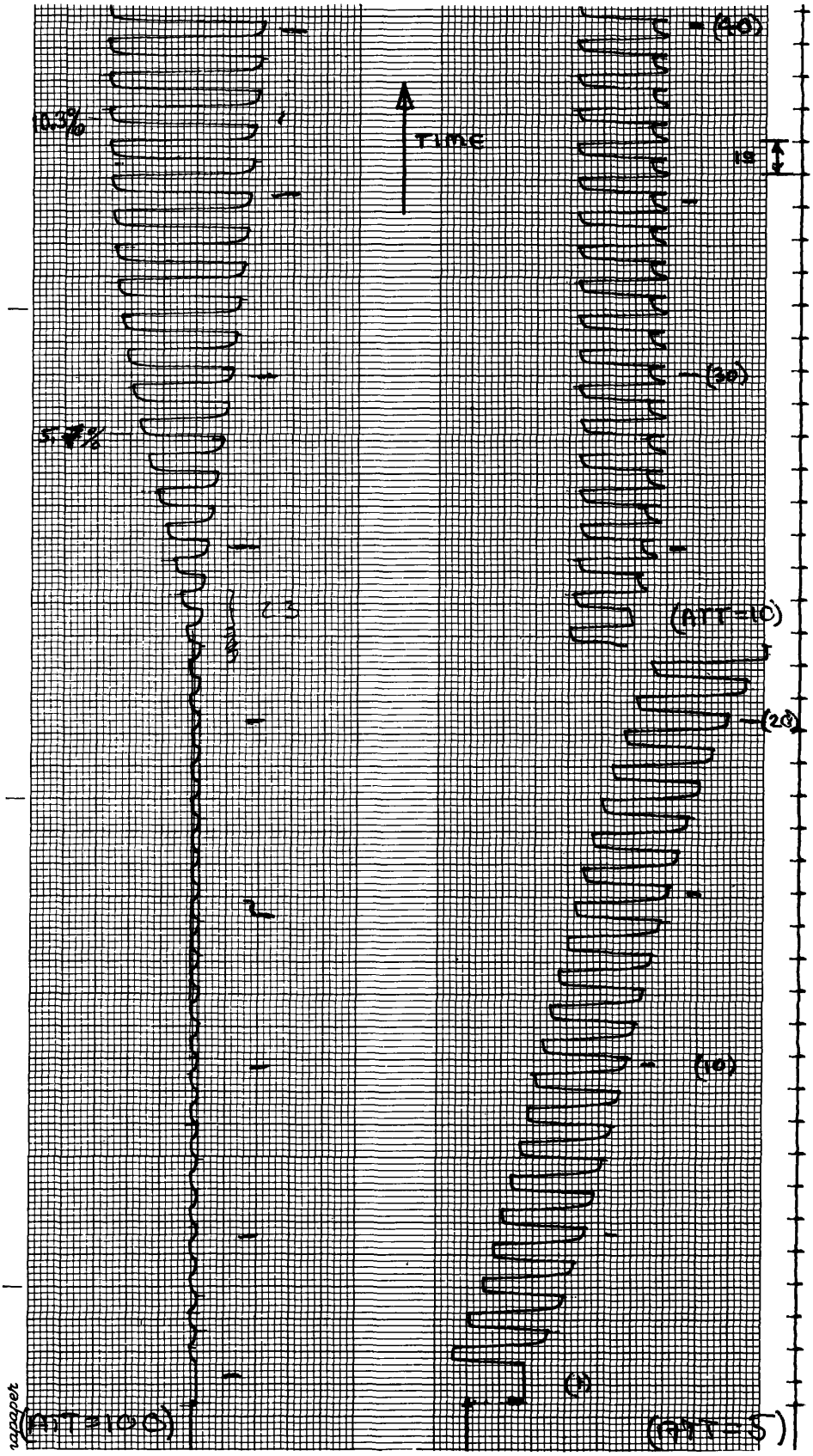

APPENDIX B

TEST PROCEDURES

This appendix will outline testing procedure used for running reversing stress liquefaction tests and drained shear tests. Figure B-1 and B-2 present six sequential photographs of sample preparation.

B.1 Cyclic Loading Tests

B.1.a Sample preparation

All cyclic tests reported were run on unused samples of the two soils described in Chapter III. Tests SCS-RU40 and RU41 on Wing-Beach sand are the only exceptions. (Microphotographs show no increase in partical degredation after these tests.) Different methods of preparation were used on the two sands. Wing-Beach sand was placed in the sample mold in the air dry state while Modified A3 sand was placed into a water filled mold. These two methods were necessary because of different saturation problems at low testing backpressures. Pouring Wing-Beach sand into a water filled mold and placing Modified A3 sand in the dry state both resulted in less than saturated conditions.

For all tests sand was placed in six to eight layers with various degrees of compaction depending on desired density. Figure B-1.a shows a picture of mold, membrane and suction connection at time of sample preparation. The membrane is sealed against the base plate with an O-ring. A saturated porous stone is then placed in the bottom prior to fitting of the three-piece mold. It was necessary to apply a suction pressure be-

tween mold and membrane in order to achieve uniformity of sample shape. Wing-Beach samples were "saturated" by raising the water table up through the sand-filled mold under a slight backpressure. Modified A3 samples were saturating while being prepared and required only matching the water table and sand surface before placement of the top cap. The top cap was put into place at this time and sealed against the membrane by another O-ring.

Sample collapse after removal of the sand mold was avoided by applying a small negative backpressure of 2 to 3 psi. This creates a confining pressure of 2 to 3 psi, preventing the sample from collapsing under its own weight.

B.1.b Sample consolidation and measurement

The triaxial cell top was put into place and the sample consolidated to the effective pressure at which it was to be tested. This stage is shown in Figure B-1.c. Note that consolidation is isotropic and there is no contact between top cap and load cell. Primary consolidation took place within seconds after effective stress application. Drainage was allowed for 5 to 10 minutes under secondary compression with very small volumes of drainage observed.

Pore pressure lines were closed off at this time and the cell pressure was removed. A backpressure of -3 to -6 psi was observed in most nearly-saturated tests. Air comes out of solution when pore pressure drops much below atmospheric pressure, preventing a large negative backpressure. Initial volume was now computed after this sample rebound by making three height and five circumference measurements. Corrections for measured membrane and paper thickness are made. Most samples had

uniform cross-sectional areas with some slight tapering near the top cap. Occasionally a small void would be noticeable against the top cap due to uneveness at time of fitting. Typical sample size is 1.98 inches is diameter by 3.5 inches high. Diameter varied only from 1.97 to 2.00 inches in all tests, while height varied from 3.3 to 3.6 inches. (Several early tests had measured heights of 3.1 or 3.2 inches.)

Sample volume was also measured at the end of testing, after liquefaction. This method depended on determining the total volume of water in a sample. To do this the water content of each sample was taken after the breakdown of equipment. To this was added the volume of water removed with drainage following liquefaction. Volume taken by the soil phase of a sample is computed from known soil weight and specific gravity. If 100 per cent saturation is assumed, γ_d, e, and relative density can be calculated with this data. A sample calculation is shown in Figure B-3 for test SCS-RU21.

B.1.c Reconsolidation and saturation

Steps followed in reassembly of the triaxial cell are attachment of the load cell pin connection, placement of cell top (without bushing), and positioning of bushing and loading equipment. The critical stage in this operation is the triaxial cell lowering over the attached piston and load cell. Weight of the connected piston applies a compressive stress of 0.4 psi on the sample. Care must be taken to prevent binding caused by missallignment that will exert additional stress on the sample. The effective confining stress at this stage is still 3 to 6 psi.

When the triaxial cell is in place, it is bolted together and the bushing screwed to the cell. The cell is then filled with deaired water

to a level somewhat below the load cell electrical connections. After alignment of pistons, the stress application device is firmly attached to the cell and the pistons screwed together. A height adjustment is made to allow piston movement of equal distance in the application device. Reconsolidation takes place when cell pressure is brought up to the level of previous consolidation.

During this and subsequent changes of cell pressure, forces on the piston are being changed. The magnitude is easily computed by multiplying cell pressure changes by the piston area. The problem of preventing anisotropic loading is compounded by movement of the top cap with recompression. The best method of preventing unwanted deviator stress was found to be through use of a wedge (shown in Figure B-2.b) to fix the piston so no force will be applied to the top cap. Sample re-consolidation strains were allowed because of the loosness in the top cap extension pin connection. Monitoring of force transmitted through the load cell reveals proof of the ability to limit deviator stress to less than 1.0 psi. Maximum undesirable stresses occur only after the sample is at an effective confining stress at the testing level (28.4 psi for all cyclic tests after SCS-RU11).

The typical sample will require some time to bring its saturation level up to 100 percent. Saturation was achieved at the effective stress of the test, and at a backpressure 10.0 psi higher than the test condition. Pore pressure response was measured after continued saturation until response was greater than 88 percent. Seven tests (noted) were run at responses lower than 88 percent, when this value could not be reached despite flushing the sample with de-aired water. Several other tests were purposely run in a partially saturated state. Pore pressure response

for saturations of 69 and 84 percent were 6 and 5 percent respectively.

B.1.d Testing

All cyclic tests were loaded to the first compressive cycle in undrained stress controlled loading. The extension half of the first cycle marked the beginning of rapid cycling. All subsequent stress changes took place at the frequency of test (1.0 cps or .12 cps -8 cpm). The apparatus at time of testing is shown assembled in Figure B-2.c. Stress controlled loading for the initial compressive cycle was desirable for two reasons. Stress paths for this loading can be compared to yield data on uniformity of samples and typical behavior. Pore pressure and stress-strain data are plotted in Figures B-5 and B-6 for the four major test series. The second reason is to establish a zero strain position. This is necessary because of ambiguity from movement in the pin connection at zero stress.

During this loading axial force is measured by a voltmeter. The last force reading is approximately the compressive stress during cycling, and is used as a known reference voltage for calibration of the X-Y recorder. Before cycling is begun the attenuation scales on each recording device are set so to record high pore pressures and strains should the sample fail on the first few load applications. These are then adjusted for better resolution if desirable. (Data on one or two early tests were lost when this procedure was not followed.)

Cycling was allowed to continue until necking of the sample. This generally occured after less than 15 percent double amplitude strain in denser sands. Strains up to 30 percent were reached before necking, in the looser sands tested. The point at which "normal" strain increases

with cycling ended and necking-induced strains began was easily identified in most tests. Visual observation and characteristicly large recorded extension strains identify the cycle. Necking usually occured about one third down from the sample top cap.

When cycling was stopped a compressive force remained applied to the sample. In every case observed removal of this force caused an increase in pore pressure. After an isotropic state was again reached, pore pressure was decreased to pre-test conditions. The loss of water in this step was measured and is plotted in Figure 36. In the final step of dis-assembly, water content of each sample was measured and care taken to backfigure the volume of water at the end of each test.

B.1.e Volume changes

Volume changes occur during several phases of the test procedure. Figure B-4 shows these changes, determined by burette measurement, for loose samples of both sands. These samples were the loosest tested for each sand. Measured volume changes before saturation may indicate sample cavitation and not actual volume change.

Most pre-test volume changes occur during consolidation of the sample with negative backpressuring and by pre-consolidation to test stress levels. Disturbance when the piston is attached and the triaxial cell top brought down over it caused significant changes in both tests. They are considered to have been particularly disturbed during this phase. Volume change is then noted when the samples are saturated, and take on up to 0.6 cc of water. Significant volume changes do not occur following this until after liquefaction has taken place.

B.2 Drained Shear Tests

B.2.a Sample conditions

Sample preparation for drained shear tests follows exactly the same procedure as used in cyclic tests, until after physical measurements are made. At this stage the pin-connection to the top cap is not made since only compressive stresses are applied. Standard procedure is still followed but without fear of applying anisotropic forces to the sample.

B.2.b Testing

Drained shear tests were run under stress controled loading. The stress increments were small, requiring several dozen to reach failure. Volume measurements were made through one or more burettes, visible in Figure A-1. As large strains were occuring, volume change was continuous with no definable change for each stress increment. A standard reading pause of 25 seconds after stress application was set up for uniformity of reading times. Each test failed over a total time period of from 24 to 46 minutes. Results of these tests are plotted in Figures 6 and 7.

FIGURE B.1 PREPARATION OF SAMPLE

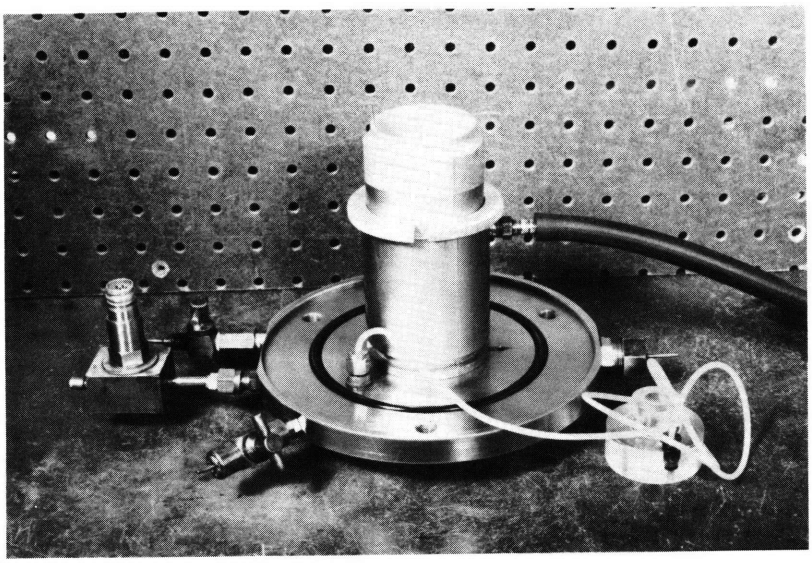

(a) Mold for preparation of sample

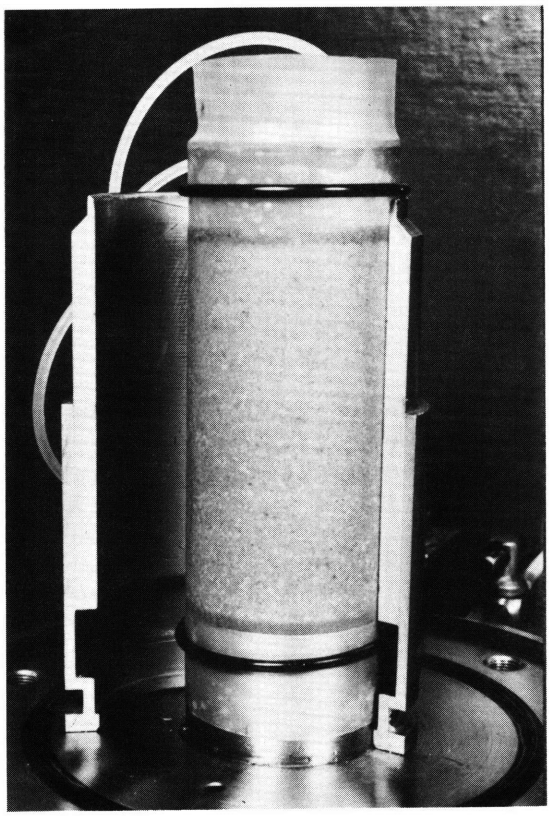

(b) View of prepared sample and mold

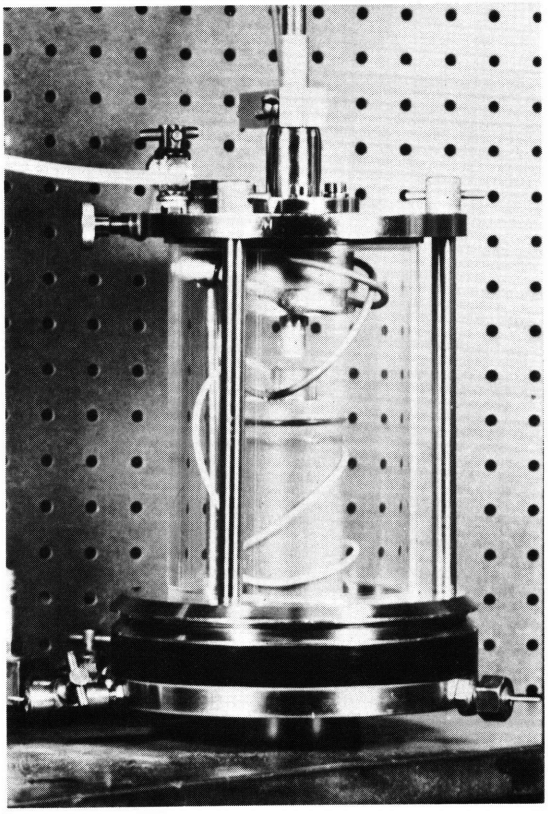

(c) Consolidation of sample (note piston not connected)

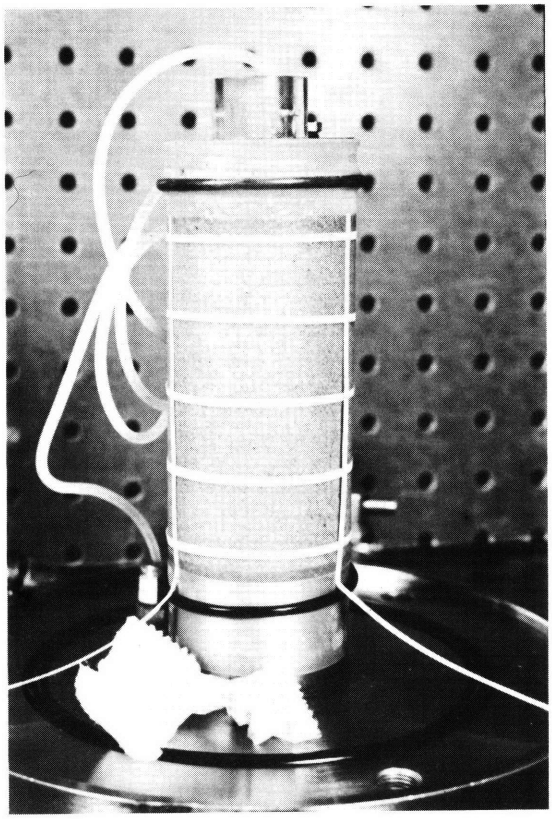

(a)

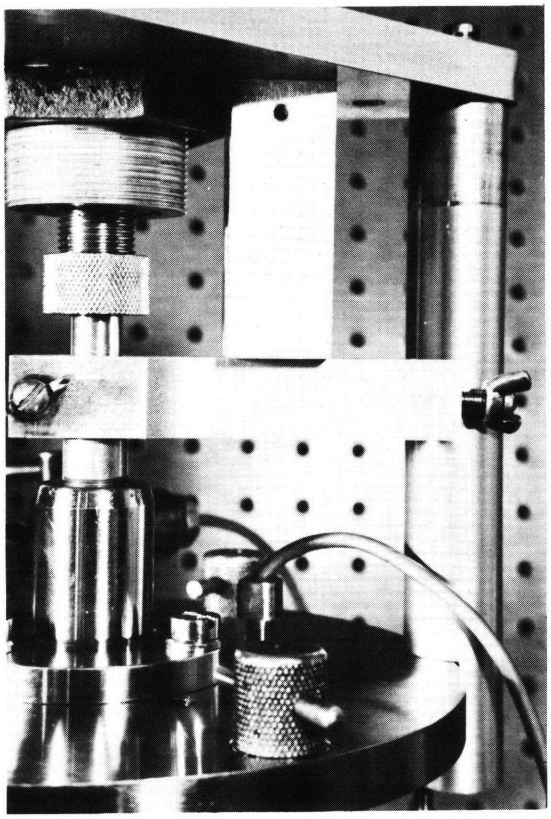

(b)

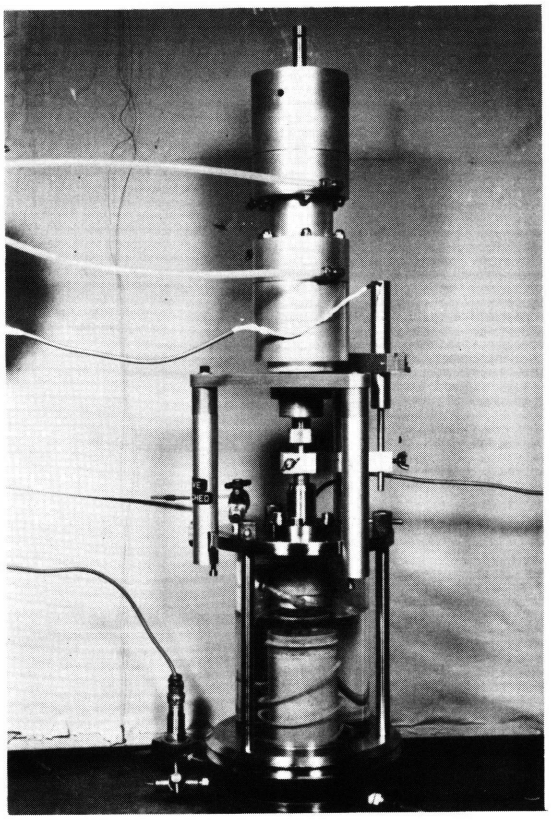

(c)

FIGURE B.2
TEST PROCEDURE PRIOR TO CYCLING

a) Physical measurement of sample
   -3 initial height
   -5 circumference

b) Position of wedge to prevent extension forces from developing during application of confining stress.

c) Triaxial cell and loading equipment at time of testing.

FIGURE B3
TEST SGS-RU21

DATE: 3/27/68
FREQ: 1 CPS
SAND: MODIFIED 95

PREPARATION: Poured into mold in 5 spoon layers; vibrated with rod # 61/layer

SPLIT W/C

	BEFORE	AFTER
CAN NO.	MB-1	MB-1
WT. CAN + SOIL (WET)	391.63	382.42
WT. CAN + SOIL (DRY)		315.75
WT. WATER		66.67
WT. CAN	116.70	43.18
WT. SOIL (DRY)	274.93	272.57
% WATER		24.46

VOLUME CHANGES:

CONDITION / TIME	BURETTE I	BURETTE II
@ σ_c = 28.4 * u = 0		5.68 cc
SET @ σ_c = 56.4, u = 28.0		3.72
(REZERO AFTER FLUSH)		4.20
@ TEST σ_c = 56.4, u = 28.0		4.26
DRAIN AFTER TEST σ_c = 56.4, u = 28.0		9.25

(4.99 — difference between last two readings)

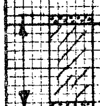

$H_1 = 3\frac{45}{64}$ $\quad C_t = 6\frac{20}{64}$

$H_2 = $ " $\frac{48}{64}$ $\quad C_{mt} = $ " $\frac{20}{64}$

$H_3 = $ " $\frac{46}{64}$ $\quad C_m = $ " $\frac{20}{64}$

3.745 $\quad C_{mb} = $ " $\frac{20}{64}$

− stones = −.259 $\quad C_b = $ " $\frac{22}{64}$

H_{AVG} = 3.486 IN $\quad C_{AVG}$ = 6.316

* NOTE (IFANY): 1 = small void @ top along stone.

DENSITY COMPUTATION

STRESS APPLICATION

σ_{CELL} = 56.4 psi

u_o = 28.0 psi

$(\sigma_1 - \sigma_3)_o = 0$

WANT $\Delta(\sigma_1 - \sigma_3)$ = ± 13.0 (PSI)

= ± 40.8 (LBS)

SET: TOP P = 31.8

BOT P = 20.3

(from measurements)

$D_o = \frac{6.316}{\pi} - .026 = 1.984$ IN

$Vol_o = \left(\frac{D_o}{2}\right)^2 \pi (3.486) = 10.782$ IN³ = .006239 ft³

$Vol_s = \frac{274.93}{(2.67)(453.6)(62.4)} = .003663$

$Vol_v = .002576$

$\gamma_d = 274.93/(453.6 \times .006239) = $ **97.2 PCF**

$e_o = (.002576)/(.003663) = $ **0.703**

RD = (.967 − .703)/.381 = **78%**

(from end of sample volume) V_{air} = 0 or S = 100% ← ASSUMED

WT SOIL = **274.93 gm** $\quad$ VOL SOIL = .003663 ft³

(SPLIT W/C = 24.46%) $\quad Vol_{WATER}$ = (SPLIT W/C)(TOTAL WT.) + DRAINAGE

$Vol_{VOIDS} = Vol_{WATER}$ = (.2446)(274.93) + 4.99 = **72.24 cc**

VOLUME TOTAL = $V_{VOIDS} + V_{SOIL}$ = 72.24 + (274.93)/2.65 = **175.99 cc**

$\gamma_d = \frac{274.93}{175.99}(62.4) = $ **97.5 PCF** $\quad e = \frac{72.24(2.65)}{274.93} = $ **.696** $\quad RD = \frac{1.090 - .696}{.488} = $ **79%**

FIGURE B4

VOLUME CHANGES AT IMPORTANT STAGES IN SAMPLE HISTORY

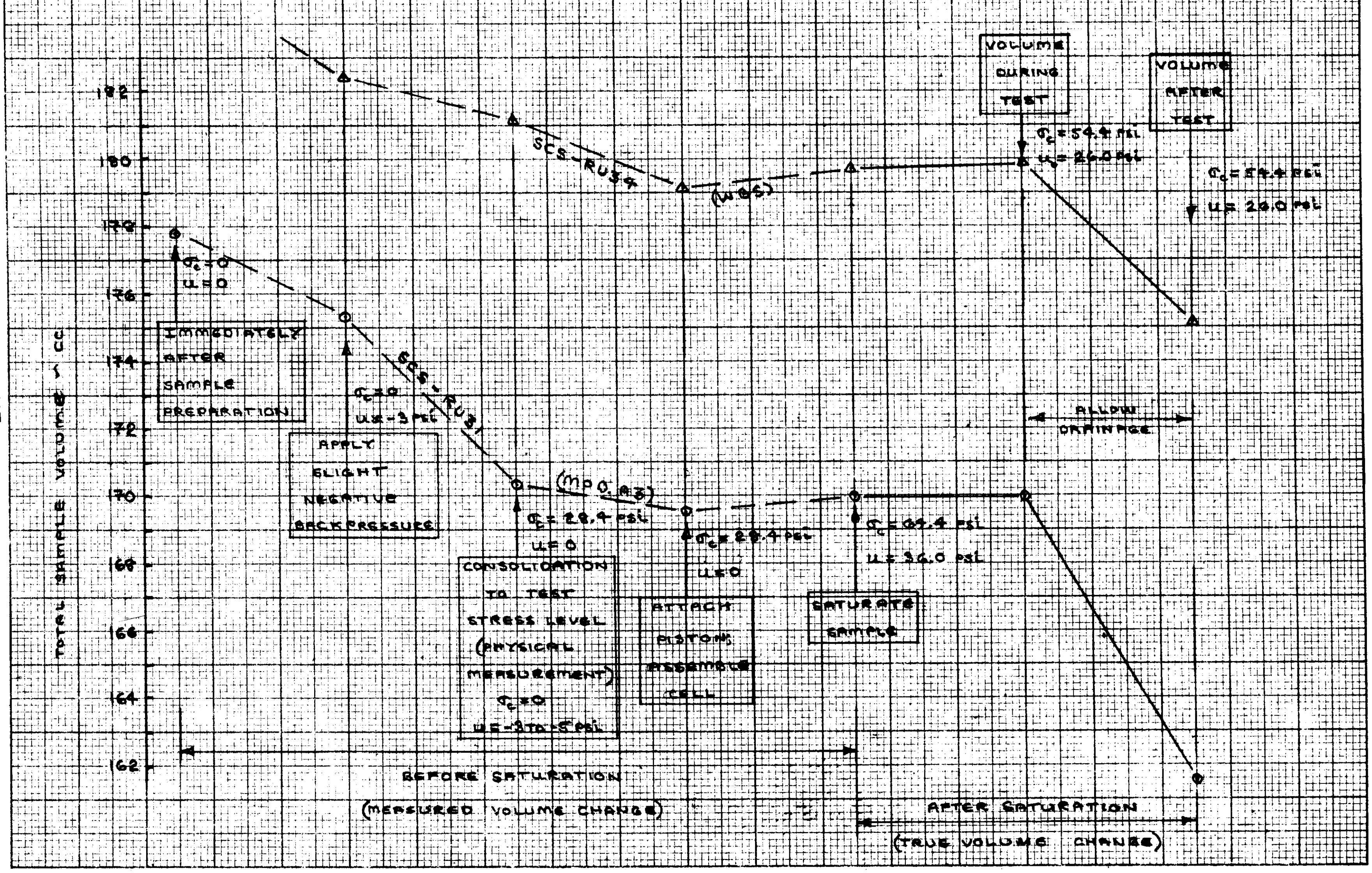

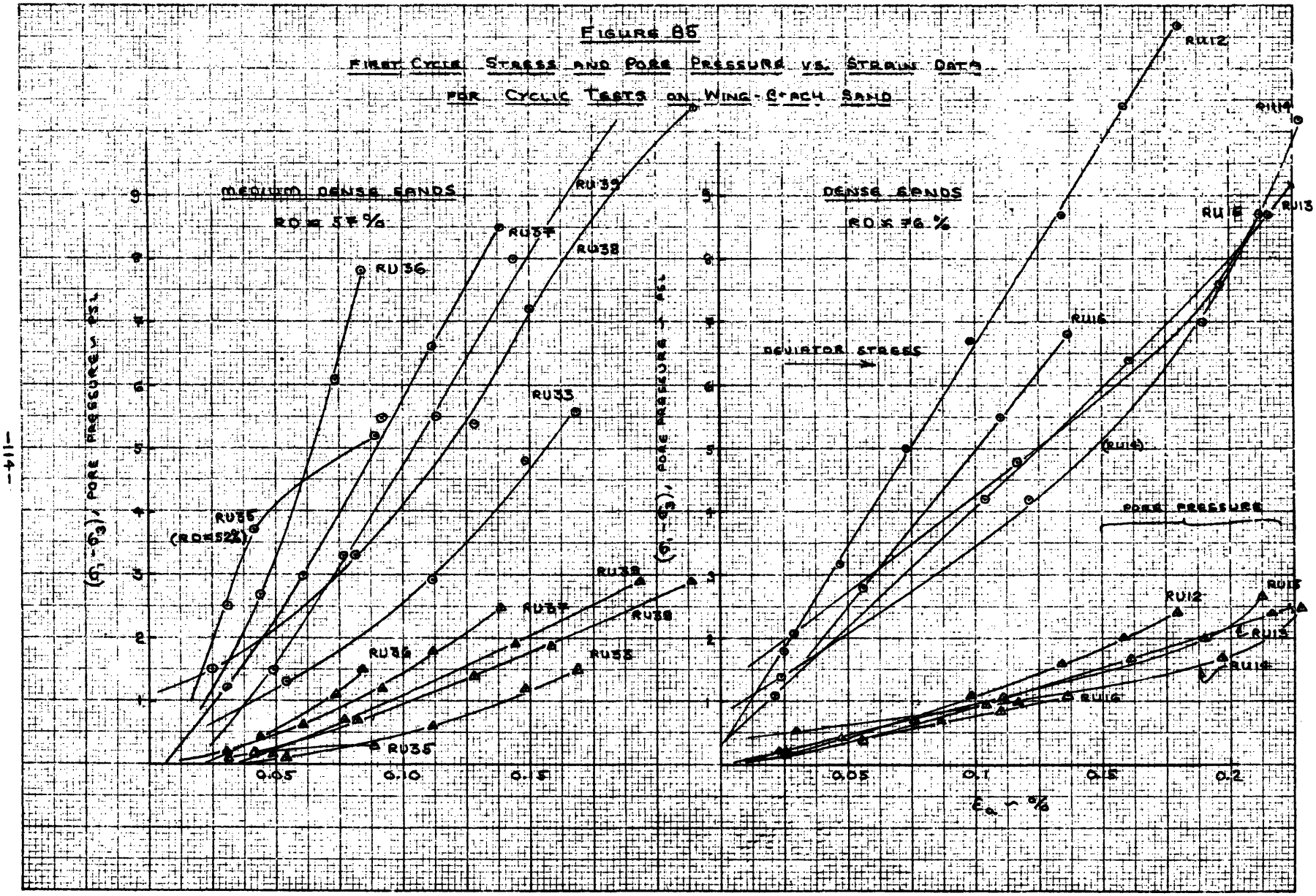
FIGURE 85
FIRST CYCLE STRESS AND PORE PRESSURE VS. STRAIN DATA
FOR CYCLIC TESTS ON WING-CATCH SAND
MEDIUM DENSE SANDS
RD = 57 %
DENSE SANDS
RD = 76 %
RU39
RU37
RU38
RU36
RU33
RU35
(RD=52%)
RU32
RU34
RU12
RU14
RU13
RU16
(RU16)
DEVIATOR STRESS
PORE PRESSURE
(σ1-σ3)/ PORE PRESSURE, tsf
(σ1-σ3), PORE PRESSURE, tsf
εa - %
0.05
0.10
0.5
0.1
0.2

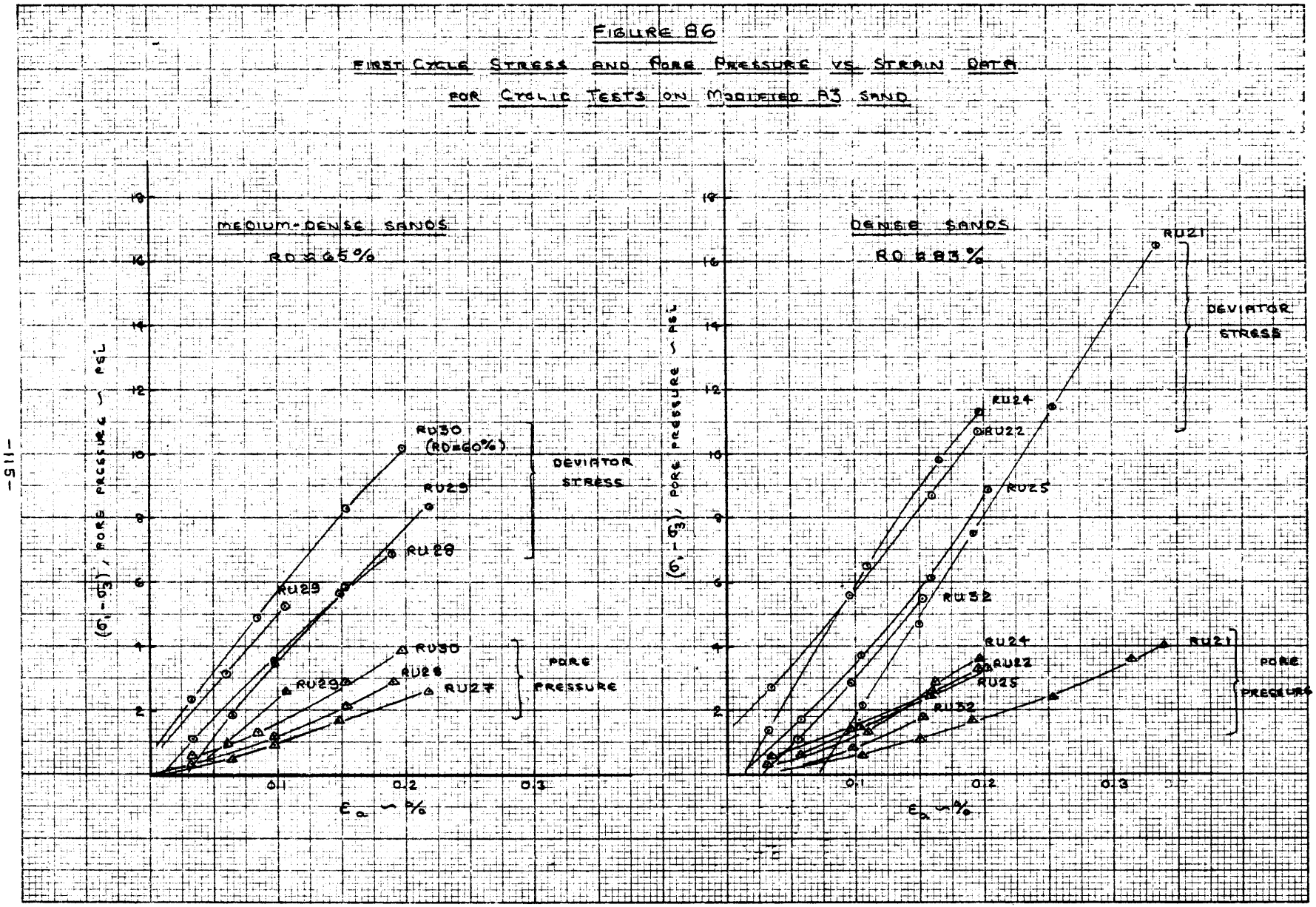

FIGURE B6

FIRST CYCLE STRESS AND PORE PRESSURE VS. STRAIN DATA FOR CYCLIC TESTS ON MODIFIED A3 SAND

APPENDIX C

VOLUME MEASUREMENTS

Sample volume (density) is of critical concern in these tests because most comparisons are made on a basis of relative density. Two methods of determining volume were used in this program and have been described in Appendix B. They are 1) physical measurements after initial consolidation and 2) computation of water volume after testing. Both methods were used when possible as a check against "losing" the relative density of the test. Without knowing this relative density, a test is only useful to show characteristic liquefaction behavior.

Results of this study into volume measurements are plotted in Figure C-1. In this figure "difference in measured density" is plotted against pore pressure response. Complete agreement of the two methods is represented by a data point falling on the dashed zero-difference line.

Several interesting results can be drawn from this statistical representation. The first is that there is very good agreement between the two methods. Secondly, neither method is consistantly higher of lower than the other, a good indication that the same thing is being measured. Several other patterns are also apparent, although not drawn from so much statistical data as the first two conclusions.

Of four samples where small voids were noted after preparation, all four had physically measured volumes larger than those measured at the end of testing. This is, of course, reasonable because a physical measurement ignores the void and overestimates volume by that amount. A more surprising result is that even with the assumption of 100 percent

saturation there is fairly good agreement at pore pressure responses of 75 to 80 percent. It would be expected that if actual saturation was less than 100 percent its overestimation would indicate an end-of-test-volume less than the measured volume. Put another way, an overestimation of S in the equation Gw = Se would indicate smaller void ratios than actually exist. There should be a trend toward points falling above the axis as pore pressure resonse decreases, an indication of partial saturation. Tests RU18 (S ≈ 69%, response = 6%) and RU19 (S ≈ 84%, response = 5%) confirm this by overpredicting density by 14.5 and 7.1 PCF respectively.

Four conclusions are then drawn from this study into sample measurements.

1. Density determination on consolidated saturated sand samples by careful physical measurement and by water volume measurement can agree very closely.
2. Neither method consistently predicts a density too high or too low when compared with the other method.
3. Small voids in a sample can easily result in a physically measured density of 1.0 to 2.5 PCF lower than that value determined by volume measurement.
4. A "low" pore pressure response of 75 to 80 percent in nearly saturated sands does not produce significant disagreement between the two sample volume measurement methods. However, samples saturated at 84 percent with a pore pressure response of 5 percent may cause overprediction of density by 7.1 PCF if complete saturation is assumed.

FIGURE C-1

COMPARISON OF TWO METHODS USED TO COMPUTE DRY DENSITY

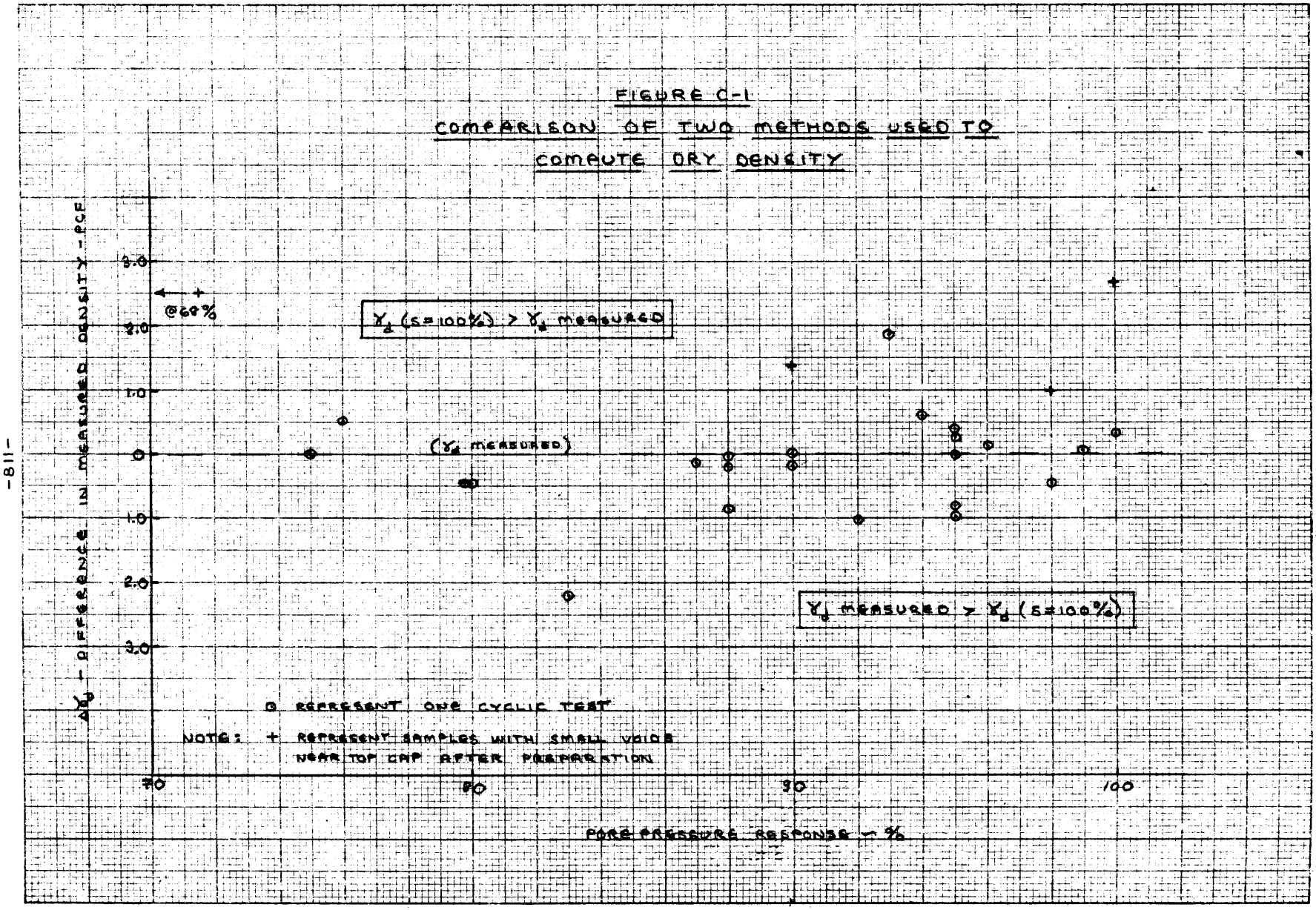

NOTE: ○ REPRESENT ONE CYCLIC TEST

\+ REPRESENT SAMPLES WITH SMALL VOIDS NEAR TOP CAP AFTER PREPARATION

APPENDIX D

TEST DATA

Figures D-1 through D-12 present results from cyclic tests plotted in terms of pore pressure and strain versus number of cycles. Pertinent information for each test is included for ease in reference. Tests SCS-RU13, 14, 15, 19, 21, 22, 26, 29, 30, 32, 33, 37, and 38 are plotted in these figures. Test SCS-RU26 and 30 are plotted on the same axis in Figure D-7. Similar data is presented in Figures 33 to 35 for tests SCS-RU12, 17 and 20. Pore pressure and strain data for other tests are summarized and also shown in main text figures.

The tests not plotted on an individual basis include the initial test series on dense Wing-Beach sand (SCS-RU1 to RU11), tests which did not liquefy, partially saturated tests, and duplications of plotted tests. Plotted tests are from the four major test series at low, medium and high N_i values. They are meant to give an indication of strain and pore pressure behavior over that range.

Each test has pore pressures plotted at both extension and compression phases of a cycle. Enough data points are shown to determine behavior of these values throughout the test. It is noted that a different pore pressure scale is used in tests SCS-RU26, 29, 30, 32, 33, 37, and 38. "Number of cycles" is shown arithmetically in Appendix D and logarithmically in main text summary plots.

Vertical strain is plotted in the lower half of each figure. Strain in extension and compression is separated and plotted, in most cases, until necking occurs. Double amplitude strains are shown on another

scale beneath compressive values. Significant values of initial liquefaction, 5%, 10%, 15%, 20% and 25% strain are marked. It is noted that looser samples consistantly reached 30% double amplitude strain before necking. Most of the denser sands had not reached 15% strain when necking occured.

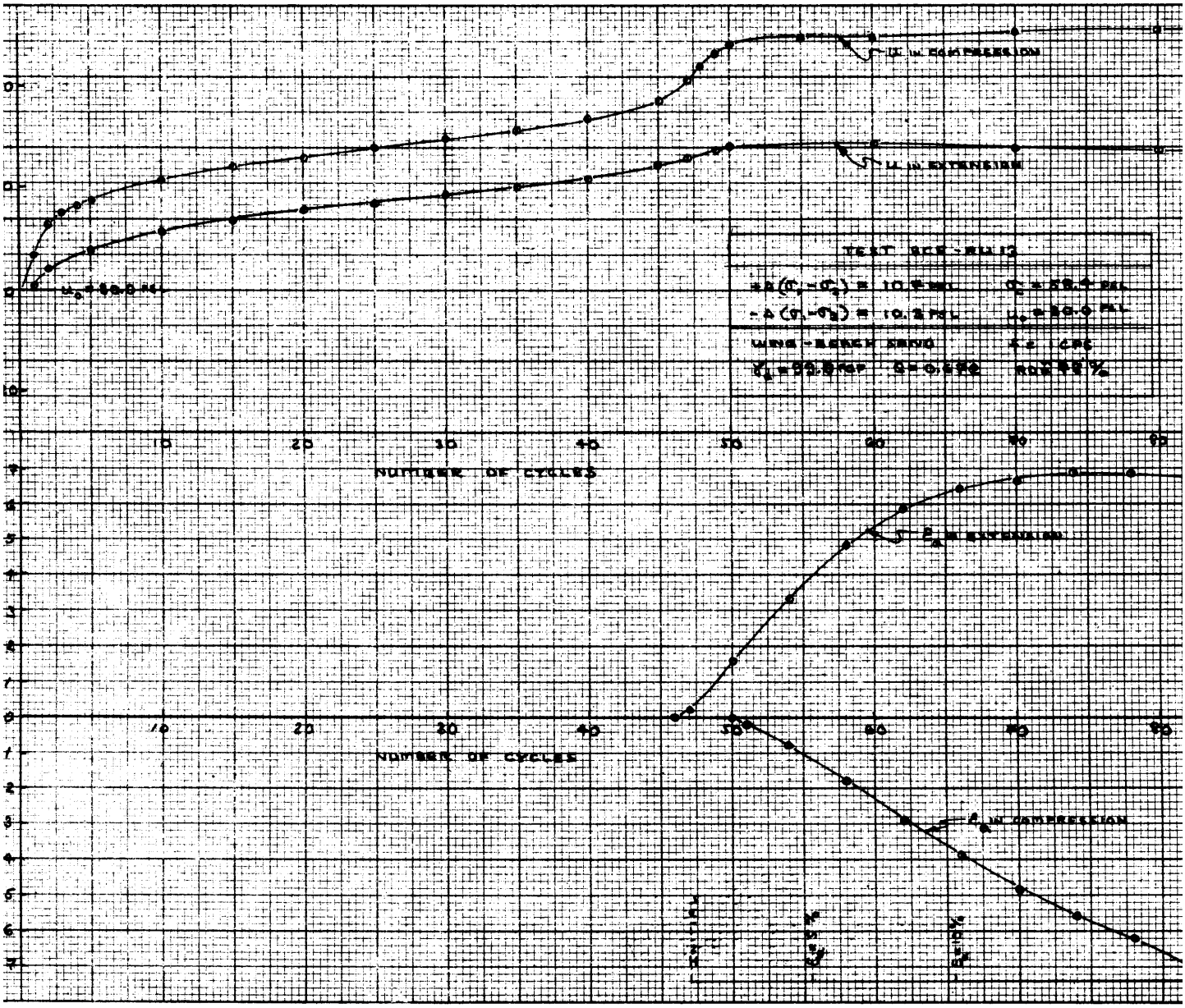
NUMBER OF CYCLES
NUMBER OF CYCLES

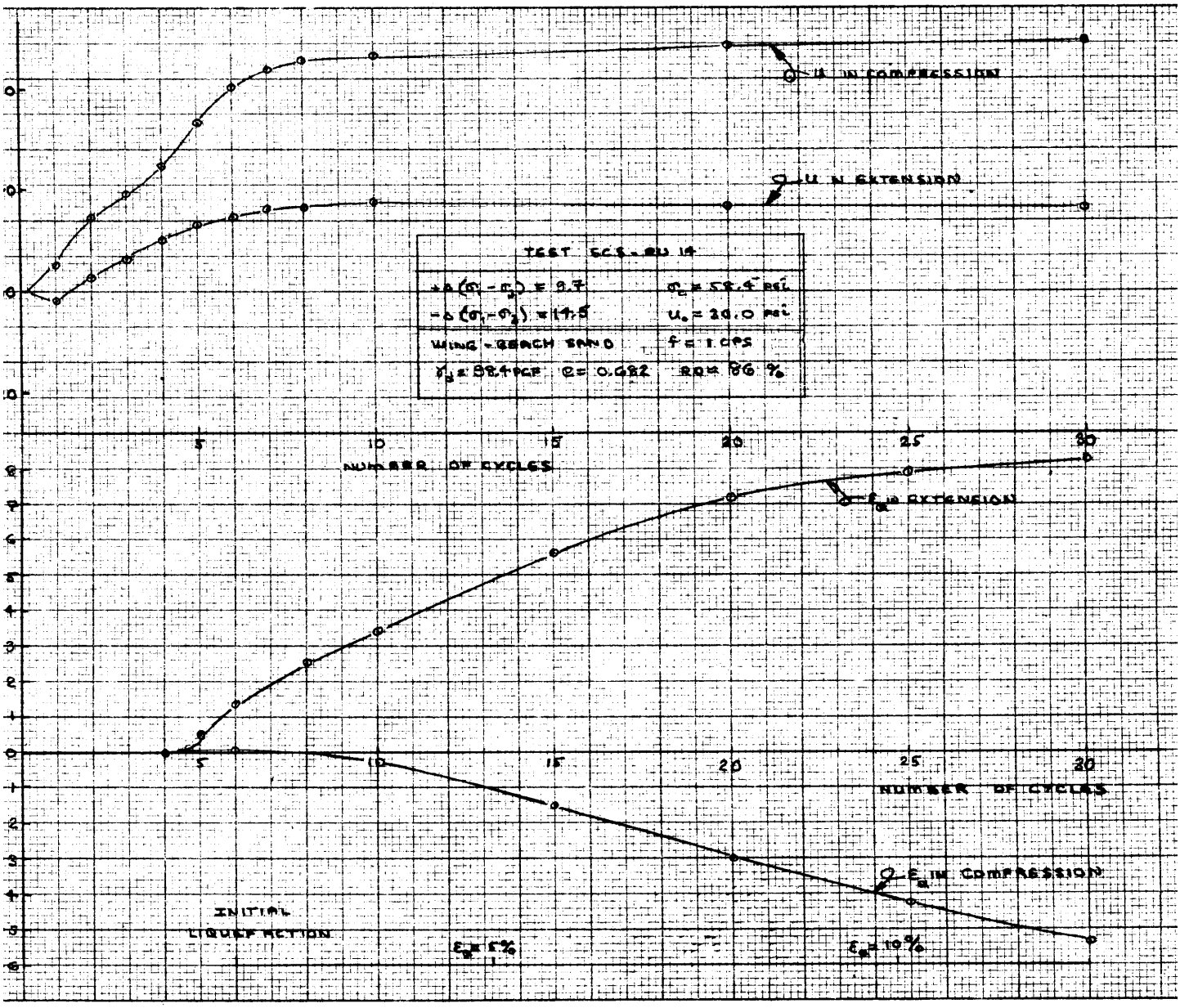
TEST SCS-BU 14
+Δ(σ1-σ3) = 9.7
-Δ(σ1-σ3) = 11.5
σc = 58.4 psi
uo = 30.0 psi
WILMINGTON SAND
f = 1 cps
γd = 98.4 pcf
e = 0.682
RD = 86 %
U IN COMPRESSION
U IN EXTENSION
NUMBER OF CYCLES
εa IN EXTENSION
εa IN COMPRESSION
INITIAL LIQUEFACTION
εa = 5%
εa = 10%
NUMBER OF CYCLES

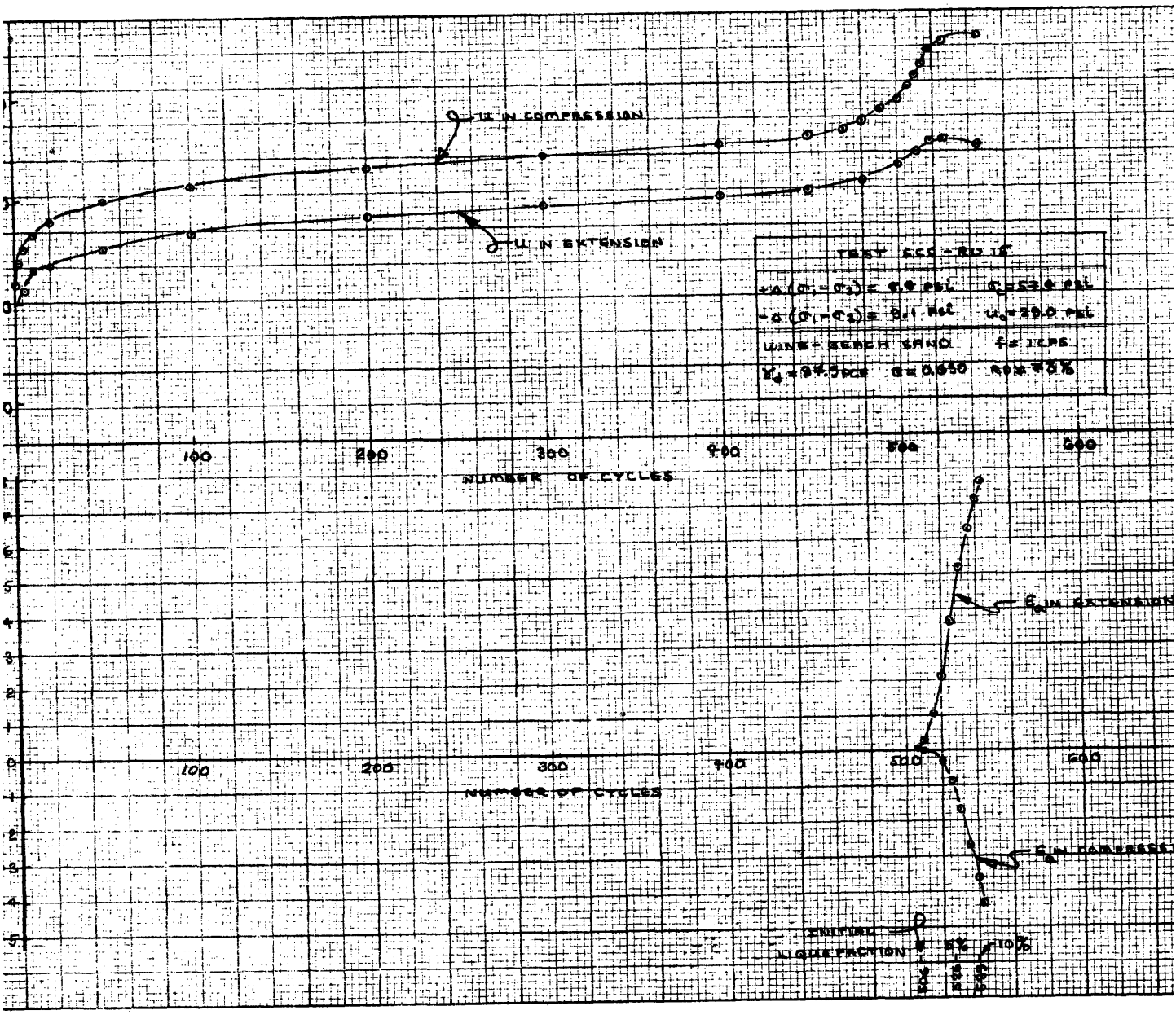
ε IN COMPRESSION
ε IN EXTENSION
TEST SCS-RD 18
+Δ(σ1-σ3) = 9.9 PSI
-Δ(σ1-σ3) = 9.1 PSI
σ3 = 5.0 PSI
ud = 29.0 PSI
DUNES BEACH SAND
f = 1 CPS
γd = 94.5 PCF
e = 0.850
ROM 95%
100
200
300
400
500
600
NUMBER OF CYCLES
100
200
300
400
500
600
Number of cycles
ε IN EXTENSION
ε IN COMPRESS
LIQUEFACTION
5%
10%

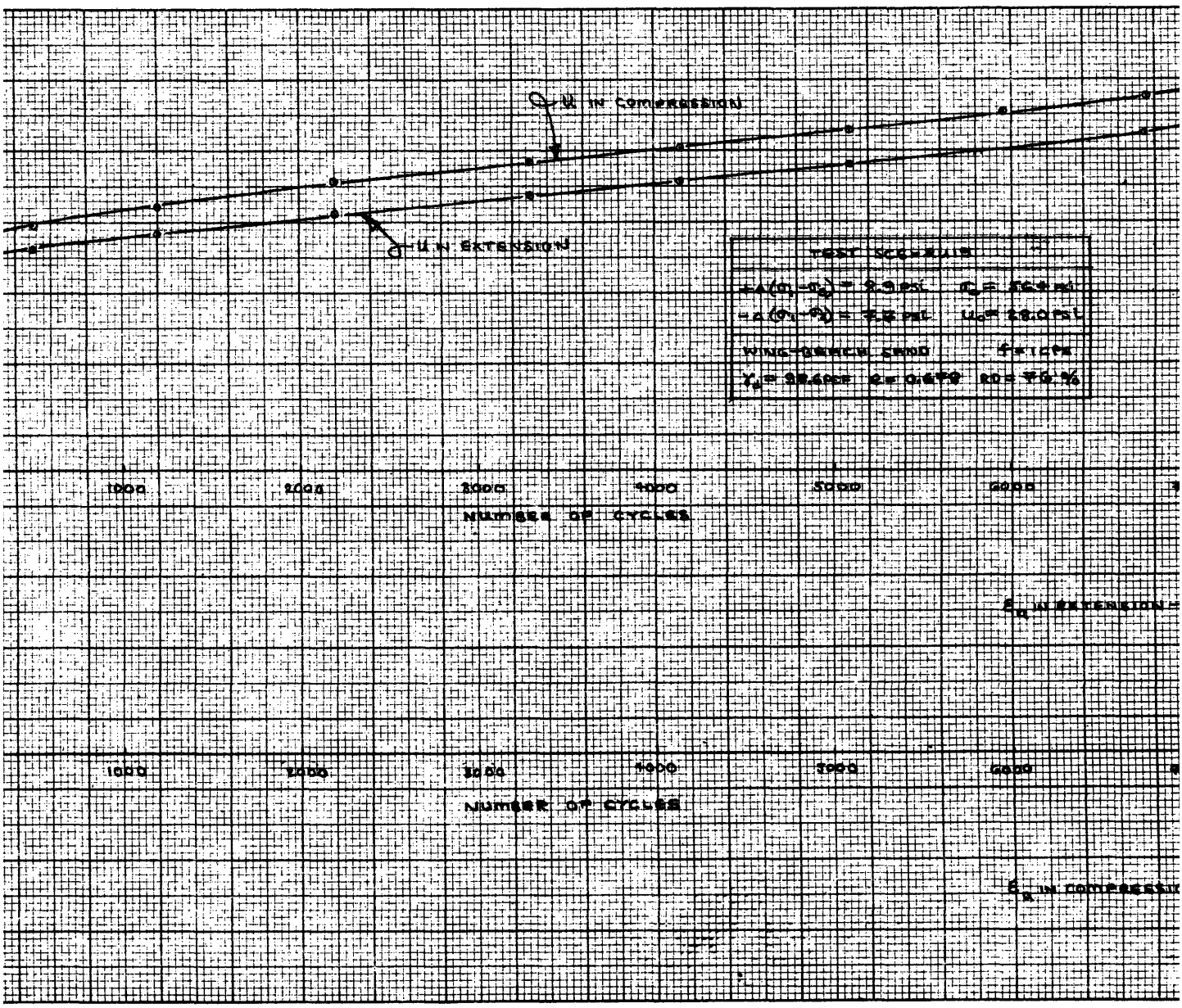
W in compression
W in extension
1000
2000
3000
4000
5000
6000
Number of cycles

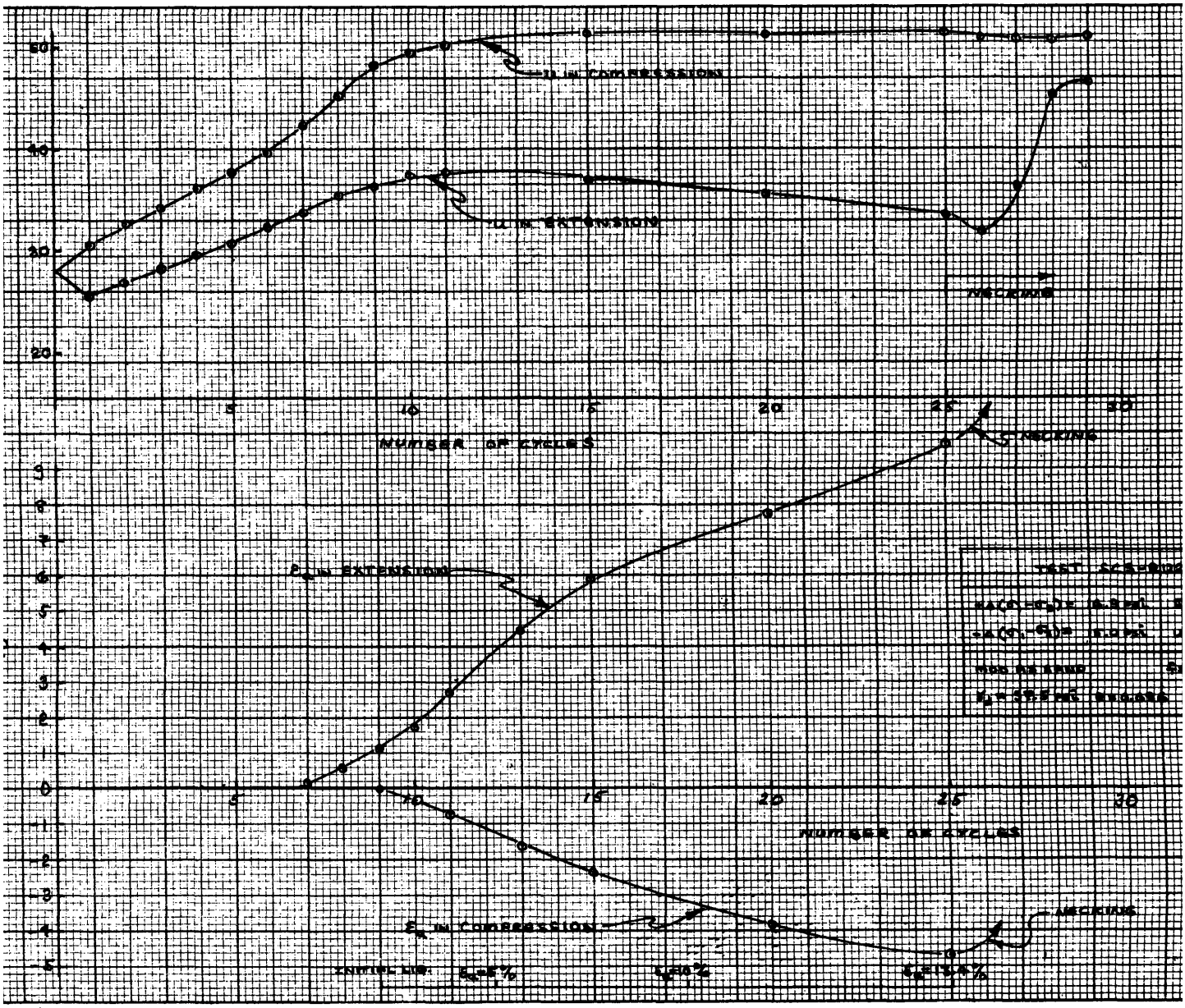
60
40
20
0
-1
-2
-3
-4
-5
5
10
15
20
25
30
NUMBER OF CYCLES
ε_{11} IN COMPRESSION
ε_{11} IN EXTENSION
NECKING
ε_{22} IN EXTENSION
ε_{22} IN COMPRESSION
NECKING
NUMBER OF CYCLES
INITIAL VAL. ε_{11}=5%
ε_{11}=10%
ε_{11}=15%

FIGURE D6

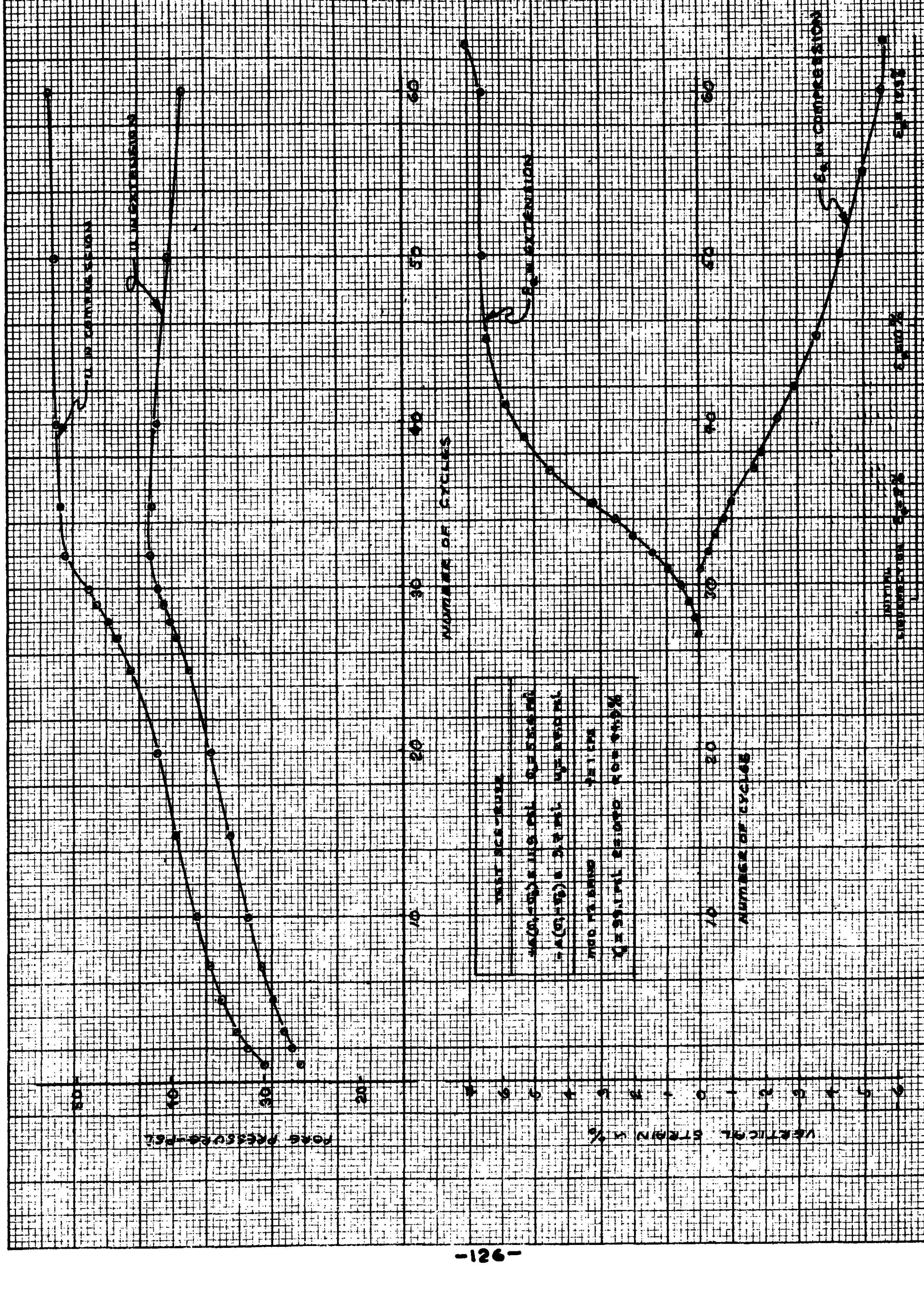
NUMBER OF CYCLES
VERTICAL STRAIN %
PORE PRESSURE-PSI
10
20
30
40
50
60

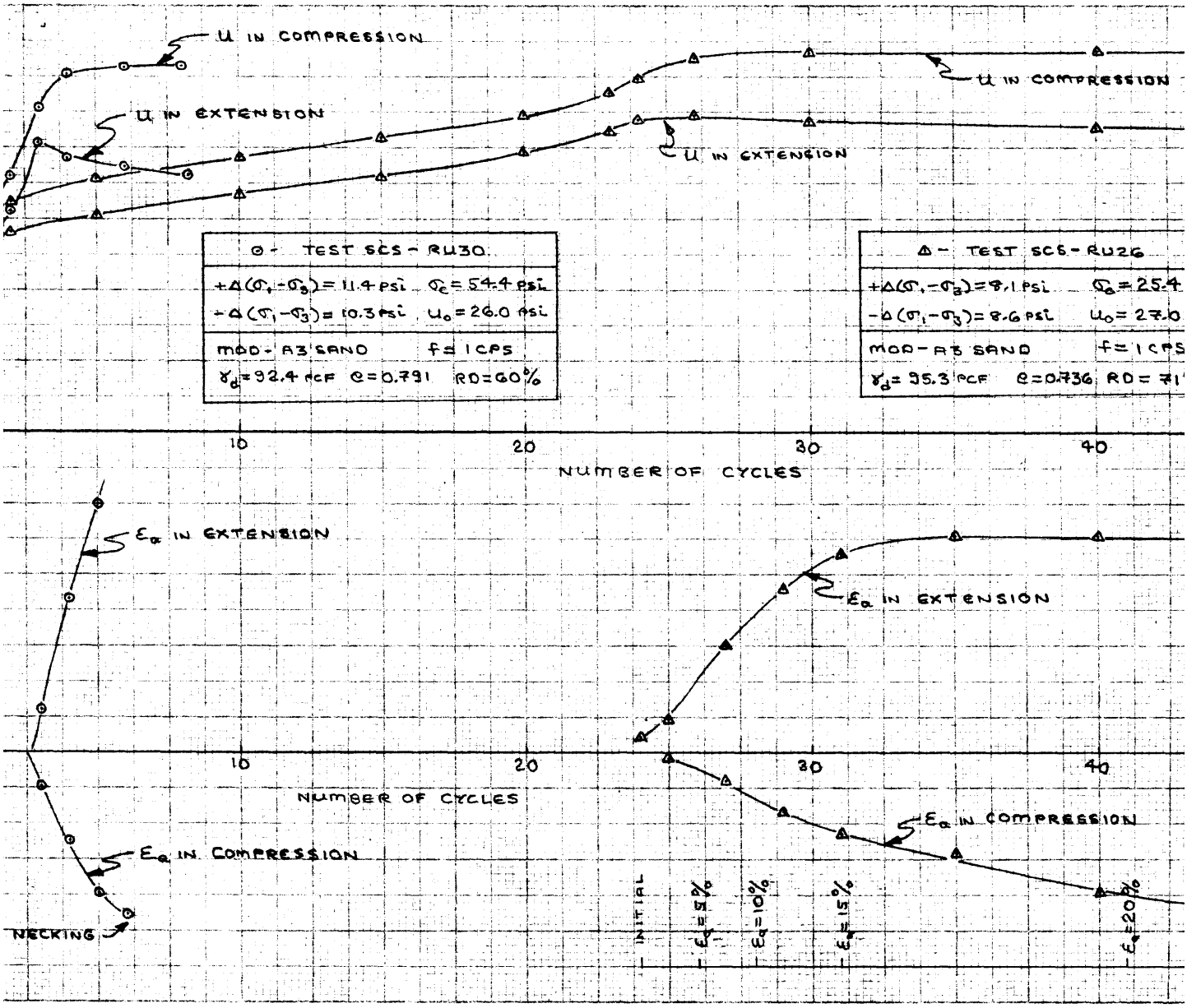
u IN COMPRESSION
u IN EXTENSION
u IN COMPRESSION
u IN EXTENSION
⊙ - TEST SCS - RU30.
+Δ(σ1-σ3)= 11.4 psi σc= 54.4 psi
-Δ(σ1-σ3)= 10.3 psi u0= 26.0 psi
MOD - A3 SAND f= 1 CPS
γd= 92.4 pcf e=0.791 RD=60%
Δ - TEST SCS - RU26
+Δ(σ1-σ3)=8.1 psi
-Δ(σ1-σ3)= 8.6 psi u0= 27.0
MOD - A3 SAND f= 1 CPS
γd= 95.3 pcf e=0.736 RD= 71
10
20
30
40
NUMBER OF CYCLES
εa IN EXTENSION
εa IN EXTENSION
10
20
30
40
NUMBER OF CYCLES
εa IN COMPRESSION
εa IN COMPRESSION
NECKING
INITIAL
εa=5%
εa=10%
εa=15%
εa=20%

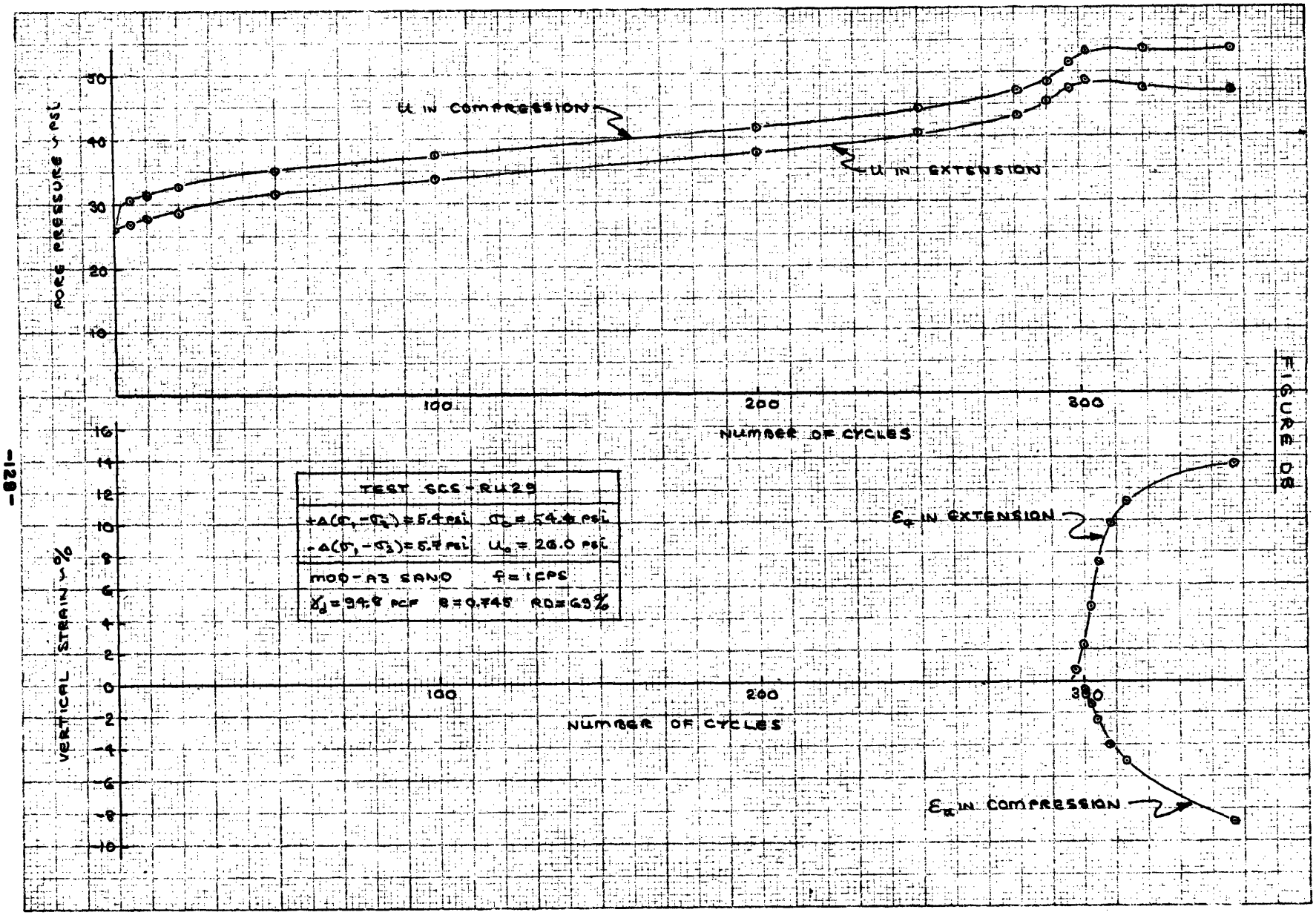
PORE PRESSURE, psi
50
40
30
20
10
u_c IN COMPRESSION
u_e IN EXTENSION
100
200
300
NUMBER OF CYCLES
TEST SCS-RU29
$+\Delta(\sigma_1-\sigma_3)=5.4$ psi $\sigma_c=54.4$ psi
$-\Delta(\sigma_1-\sigma_3)=5.7$ psi $u_o=26.0$ psi
MOD-A3 SAND f=1 CPS
$\gamma_d=99.8$ PCF B=0.745 RD=69%
VERTICAL STRAIN, %
16
14
12
10
8
6
4
2
0
-2
-4
-6
-8
-10
100
200
300
NUMBER OF CYCLES
ε_v IN EXTENSION
ε_v IN COMPRESSION

FIGURE 28

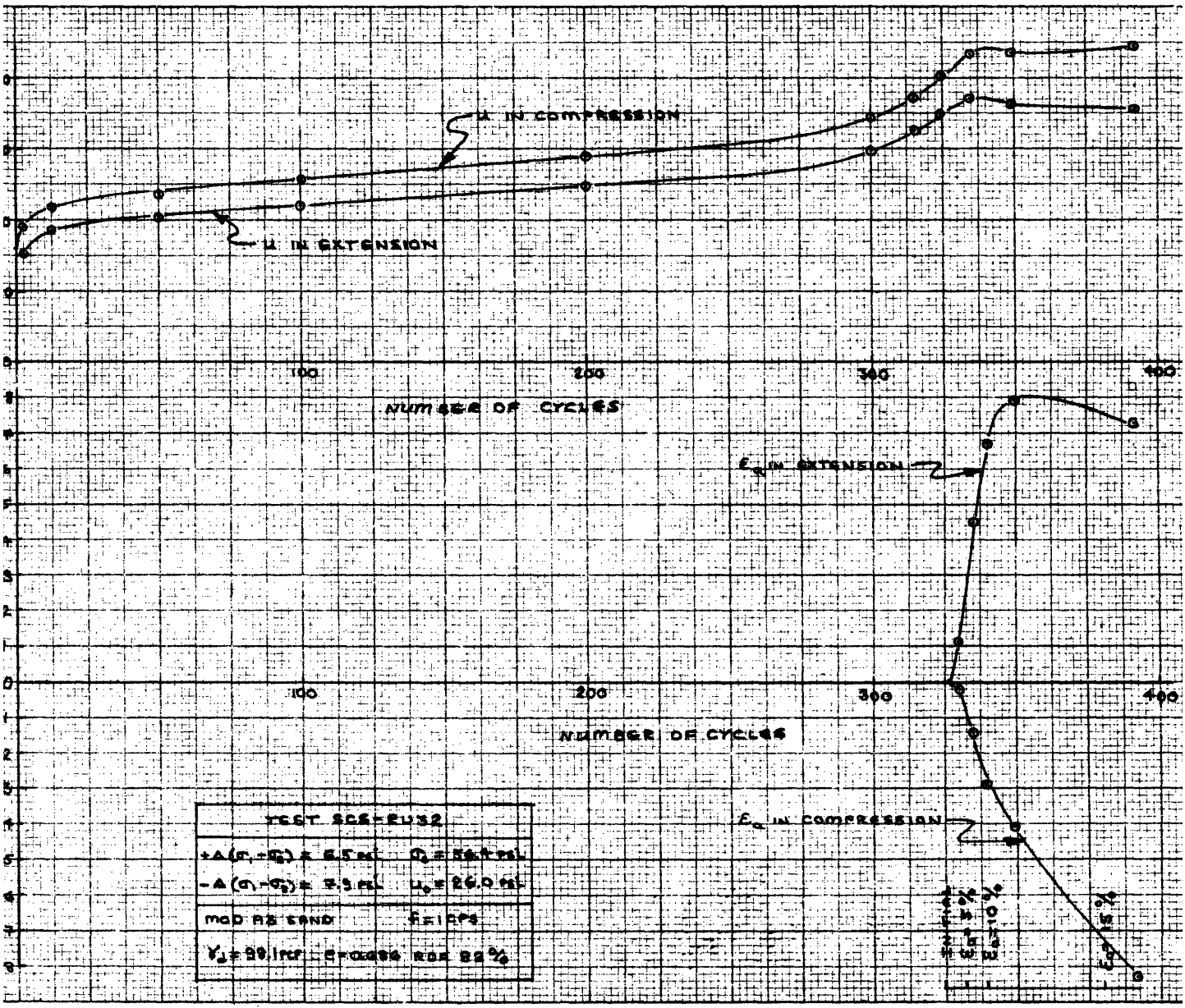
u IN COMPRESSION
u IN EXTENSION
100
200
300
400
NUMBER OF CYCLES
ϵ_a IN EXTENSION
ϵ_a IN COMPRESSION
100
200
300
400
NUMBER OF CYCLES
TEST SCS-EU32
$\pm A(\sigma_1-\sigma_3) \pm$ 6.5 psi
σ_3 = 13.4 psi
$-A(\sigma_1-\sigma_3) \pm$ 7.5 psi
u_b = 26.0 psi
mod RS sand
f = 1 cps
γ_d = 99.1 pcf
RD = 82 %

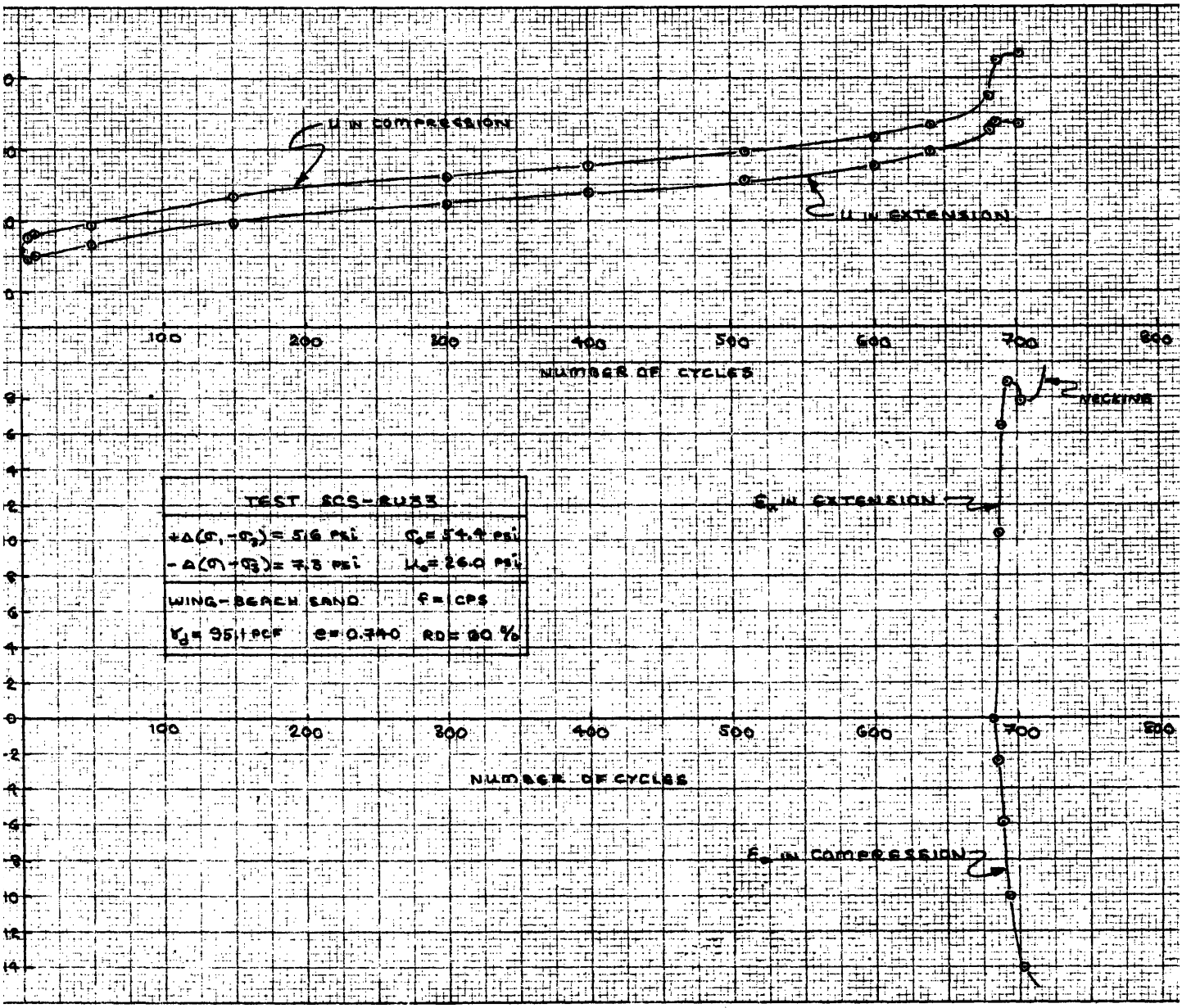
U IN COMPRESSION
U IN EXTENSION
NUMBER OF CYCLES
NECKING
ε_a IN EXTENSION
ε_a IN COMPRESSION
NUMBER OF CYCLES
TEST SCS-RU33
$+\Delta(\sigma_1-\sigma_3)$ = 5.6 psi
σ_c = 54.9 psi
$-\Delta(\sigma_1-\sigma_3)$ = 7.8 psi
U_c = 26.0 psi
WING-BEACH SAND
f = cps
γ_d = 95.1 pcf
e = 0.740
RD = 80 %

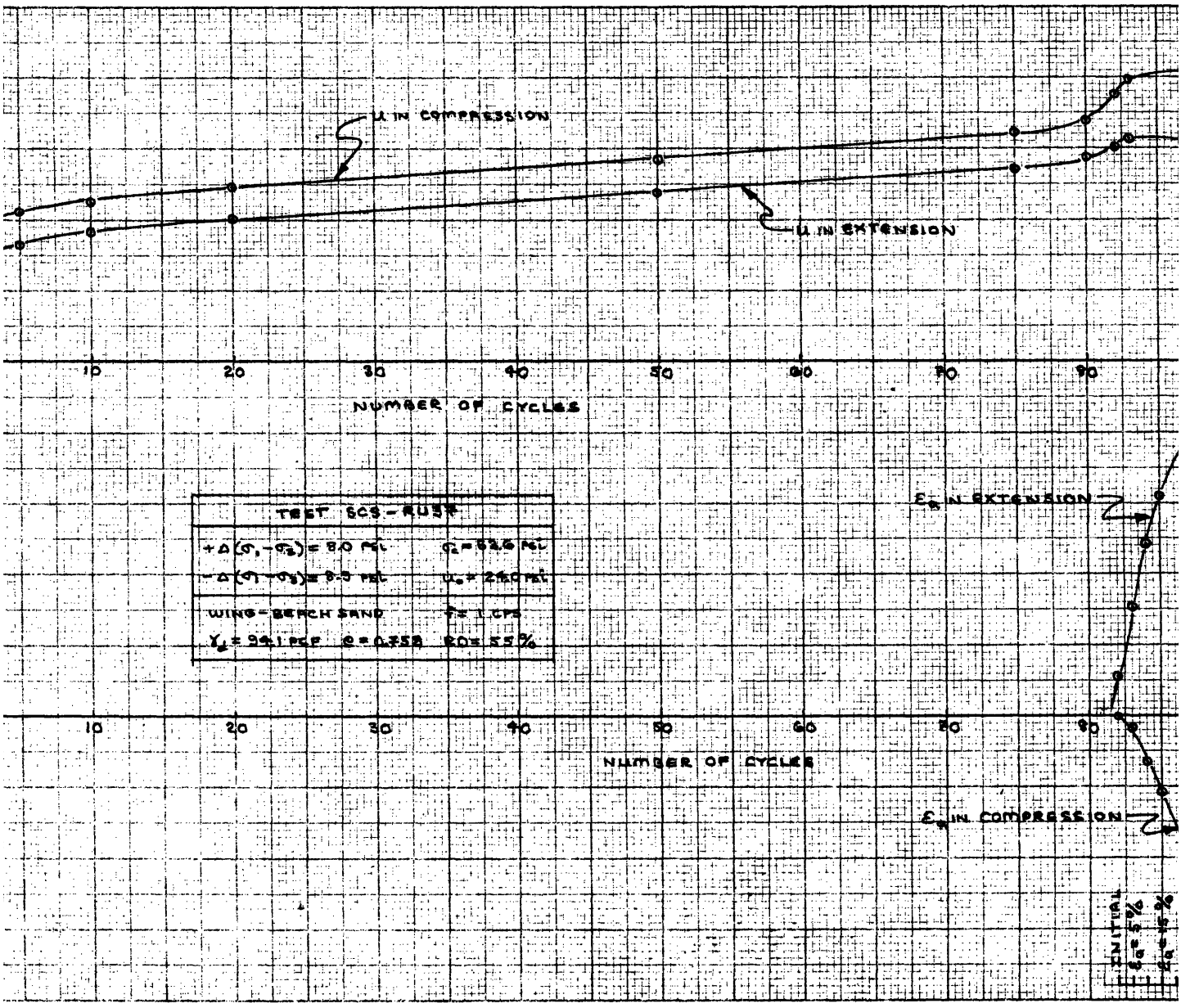
u IN COMPRESSION
u IN EXTENSION
10
20
30
40
50
60
70
80
NUMBER OF CYCLES
TEST SCS - RUST
+Δ(σ1-σ3) = 8.0 PSI
σ3 = 52.6 PSI
-Δ(σ1-σ3) = 8.0 PSI
u0 = 24.0 PSI
WING-BENCH SAND
f = 1 CPS
γd = 99.1 PCF
e = 0.758
RD = 55%
10
20
30
40
50
60
70
80
NUMBER OF CYCLES
εa IN EXTENSION
εa IN COMPRESSION
INITIAL
εa = 5%
εa = -5%

FIGURE 012

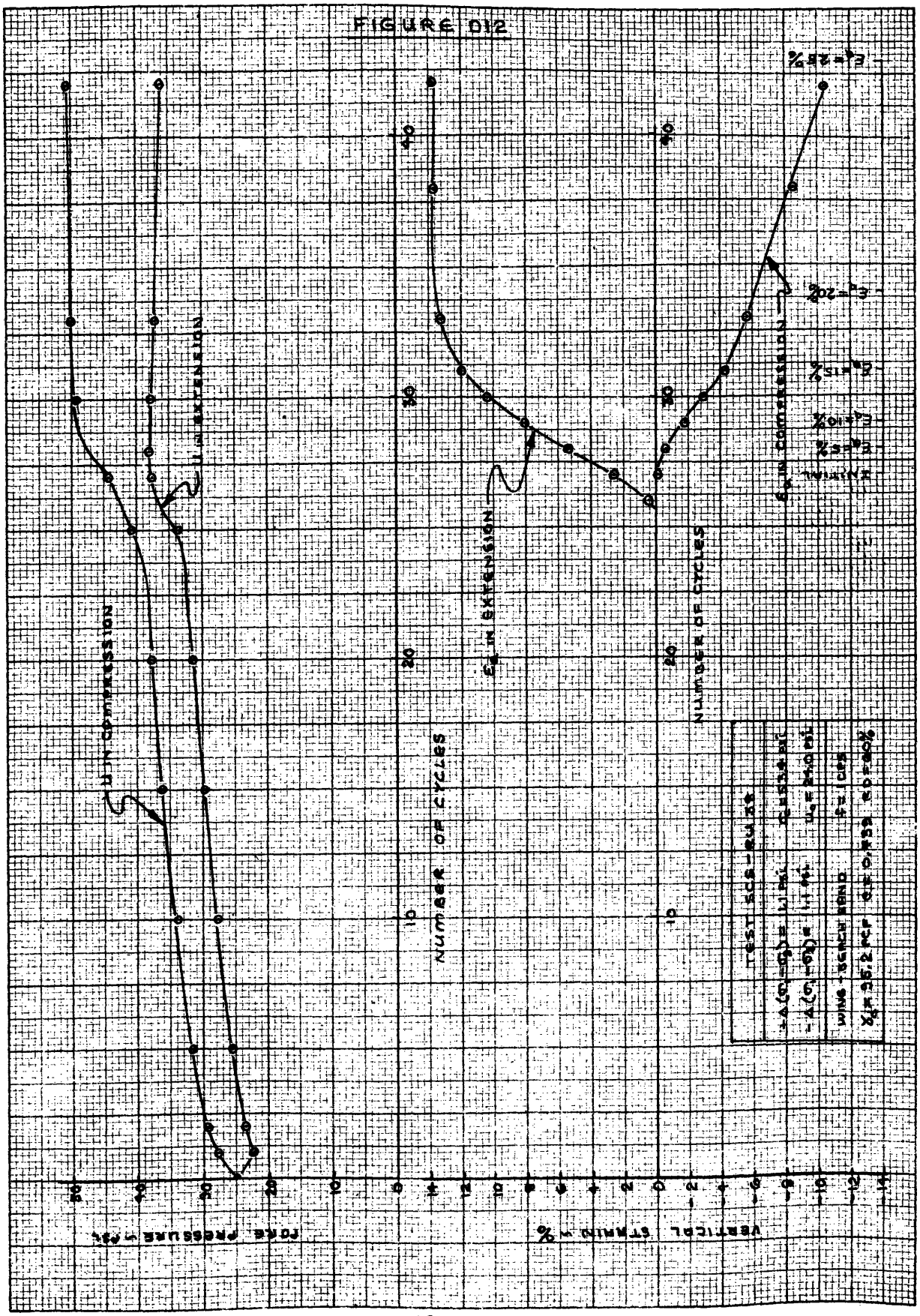
VERTICAL STRAIN - %
FORCE PRESSURE - #s
IN COMPRESSION
IN EXTENSION
NUMBER OF CYCLES
ε_a IN EXTENSION
ε_a IN COMPRESSION
$\varepsilon_a = 2.5\%$
$\varepsilon_a = 2.0\%$
$\varepsilon_a = 1.5\%$
$\varepsilon_a = 1.0\%$
$\varepsilon_a = .5\%$
INITIAL
TEST SEQUENCE
$+\Delta\sigma_3 - \sigma_3 = 1$ PSI
$-\Delta\sigma_3 - \sigma_3 = 1$ PSI
WIRE - SCRATCH BOND
$\sigma_3 = 15.2$ PSI
$\sigma_3 = 30.2$ PSI
$\sigma_3 = 60.2$ PSI
CYCLES

APPENDIX E

LIST OF SYMBOLS

TEST SCS-RU6	refers to triaxial cyclic shear test, undrained with stress reversal, number six
TEST SD-3	refers to triaxial compressive shear test, drained, number 3
C_u	coefficient of uniformity
D_{50}	diameter of average (by weight) soil grain
e	void ratio immediately prior to testing
e_{max}	maximum void ratio for a given sand
e_{min}	minimum void ratio for a given sand
E_a	axial strain (+ is compression)
g	acceleration of gravity
N	number of cycles
N_i	number of cycles to initial liquefaction
$\bar{p}$	average of vertical and horizontal confining stress, equal to $\frac{\bar{\sigma}_v + \bar{\sigma}_h}{2}$
q	average difference of vertical and horizontal confining stress, equal to $\frac{\bar{\sigma}_v - \bar{\sigma}_H}{2}$
RD	relative density
SG	specific gravity
u	pore pressure
ϕ	sample diameter
H	sample Height
C	sample circumference

γ_d	dry unit weight
α	maximum angle drawn to peak of stress path $\tan \alpha$ = sin (angle of internal friction)
σ_1	major principal stress
σ_3	minor principal stress
σ_V	vertical stress
σ_H	horizontal stress
$\Delta(\sigma_1 - \sigma_3)$	deviatoric stress
$\overline{\sigma}_{co}$	initial effective confining stress
$\overline{\sigma}_1$, $\overline{\sigma}_3$, $\overline{\sigma}_V$, $\overline{\sigma}_H$	effective stress condition (i.e., $\overline{\sigma}_3 = \sigma_3 - u$)